ISAS - INTERNATIONAL SCHOOL FOR ADVANCED STUDIES

From Self Organized Criticality to Patterns Formation. Theoretical Aspects, Occurence in Nature.

Thesis submitted for the degree of
"Doctor Philosophiæ"

CANDIDATE

Guido Caldarelli

SUPERVISORS

Prof. Amos Maritan

Prof. Attilio L. Stella

October 1996

SISSA - SCUOLA INTERNAZIONALE SUPERIORE DI STUDI AVANZATI
TRIESTE
Strada Costiera 11

TRIESTE

Symbols and Acronyms used

s = Size of an avalanche.

t = Duration time of an avalanche.

d = Euclidean dimension of the embedding space.

D = Fractal dimension of the avalanche.

D_{sur} = Fractal dimension of the boundary avalanche.

P_i = Mean field probability to have height i on a site.

$P(s)$ = Size avalanche probability distribution $\propto s^{tau}$.

$P_{sur}(s)$ = Boundary size avalanche probability distribution $\propto s^{-\tau_{sur}}$.

$P'(s)$ = Integrated size avalanche probability distribution $= \int_0^s P(s')ds' \propto s^{1-tau}$.

$P'_{sur}(s)$ = Integrated boundary size avalanche probability distribution $= \int_0^s P(s')ds' \propto s^{1-tau_{sur}}$.

$Q(t)$ = Time avalanche probability distribution $\propto t^y$.

$Q_{sur}(t)$ = Boundary time avalanche probability distribution $\propto t^{y_{sur}}$.

$Q'(t)$ = Integrated time avalanche probability distribution $= \int_0^t P(t')dt' \propto t^{1-y}$.

$Q'_{sur}(t)$ = Integrated boundary time avalanche probability distribution $= \int_0^t P(t')dt' \propto t^{1-y_{sur}}$.

SOC = Self Organized Criticality

ASM = Abelian Sandpile Model

BS = Bak & Sneppen (model)

BM = Born Model

MF = Mean Field

AE = Acoustic Emission

Table of Contents

Table of Contents iii

List of Figures vi

List of Tables ix

Introduction 1

1 S.O.C. Models 5

1.1 Some sandpile models 5

1.1.1 Critical Height Model (CHM) 6

1.1.2 Critical Slope Model (CSM) 7

1.1.3 Critical Laplacian Model (CLM) 7

1.2 A biological model 8

1.3 Comparison with usual critical phenomena 9

1.4 Mean Field for Sandpiles 11

1.5 Mean Field and Markov Processes 13

2 Inhomogeneities in Self–Organized Systems 17

2.1 Abelian Sandpiles 18

2.1.1 Numerical Data 18

2.1.2 Mean Field Theory for Abelian Sandpiles 24

2.2 Biological Models and Boundary Effects 25

2.2.1 Numerical Data 26

2.2.2 Branching Process Theory 28

3 External Field and Self–Organized Systems **35**

3.1 Temperature Sandpile Model 35

3.2 Mean Field Approach 36

3.3 Very Hot Sandpiles and Random Walks 40

3.3.1 Probability Distribution of Exit Times 41

4 Self–Organization and Breakdown in Elastic Media. **45**

4.1 Introduction 45

4.2 Theory of Elasticity 46

4.2.1 Strain Tensor 46

4.2.2 Stress Tensor 47

4.2.3 The Thermodynamics of Deformation 48

4.2.4 Hooke's law 49

4.3 The Standard Born Model 51

4.4 Acoustic Emission and Annealed Disorder 53

4.5 Numerical Data 56

4.6 Results 58

5 Landscape Evolution in River Networks **61**

5.1 Introduction 61

5.2 Geomorphology of River Networks 64

5.2.1 Basic Phenomenology 64

5.2.2 Hack's law 65

5.2.3 Digital Elevation Map Method 65

5.2.4 Drainage Area and Threshold Erosion: Feedback between Channelling and Hillslope Evolution 69

5.3 The model 71

5.4 Results 72

5.4.1 Landscape evolutions 72

5.4.2 Area and length exponents 73

5.5 Geological constraints and Quenched Random Pinning 76

5.6 Conclusions 80

Bibliography 84

List of Figures

1.1 The reaction diagram and the explicit form of the reaction equations 12

1.2 (a) Profile of a real sandpile that justify our hypothesis (in (b)) on the θ behavior with respect to the distance from the boundaries. 14

1.3 P_2 versus h for $\epsilon = 10^{-3}$. 16

2.1 The layer considered for the statistics. On the right side the microscopical effect of such a boundary 18

2.2 One process that cannot occur on the boundary of a system. 19

2.3 On the left data collapse for $P'(s,L) = \int_1^s P(s',L)ds'$. P' is scaled by $L^{D(\tau-1)} = L^{0.42}$, corresponding to $\tau = 1.21 \pm 0.01$ and $D = 2$. A direct estimate of D based on log–log fitting radius of gyration data versus s gives $D \simeq 1.96 \pm 0.06$. On the right data collapse for $P'_{sur}(s,L) = \int_1^s P_{\rm sur}(s',L)ds'$. P'_{sur} is scaled by $L^{D(\tau_{sur}-1)} = L^{1.02}$, corresponding to $\tau_{sur} = 1.51 \pm 0.05$ and $D = 2$. This value different from the bulk one signales the presence of a different boundary exponent. 21

2.4 On the left data collapse for $Q'(t,L) = \int_1^t Q(t',L)dt'$. Q' is scaled by $L^{z(y-1)} = L^{0.41}$, corresponding to $y = 1.33$ and $z = 1.26 \pm 0.05$. On the right data collapse for $Q'_{sur}(t,L) = \int_1^t Q_{\rm sur}(t',L)dt'$. Q'_{sur} is scaled by $L^{z(y_{sur}-1)} = L^{1.04}$, corresponding to $y_{sur} = 1.81$ and $z = 1.26 \pm 0.05$. 21

2.5 On the left data collapse for $P'(s,L) = \int_1^s P(s',L)ds'$. P' is scaled by $L^{D(\tau_{sur}-1)} = L^{0.62}$, corresponding to $\tau_{sur} = 1.31$ and $D = 2$. A direct estimate of D based on log–log fitting radius of gyration data versus s gives $D \simeq 1.97 \pm .03$. On the right data collapse for $P'_{sur}(s,L) = \int_1^s P_{\rm sur}(s',L)ds'$. P'_{sur} is scaled by $L^{D(\tau_{sur}-1)} = L^{1.20}$, corresponding to $\tau_{sur} = 1.60$ and $D = 2$. 23

2.6 On the left data collapse for $P'(s,L) = \int_1^s P(s',L)ds'$. P' is scaled by $L^{D(\tau_{sur}-1)} = L^{0.62}$, corresponding to $\tau_{sur} = 1.31$ and $D = 2$. A direct estimate of D based on log–log fitting radius of gyration data versus s gives $D \simeq 1.97 \pm .03$. On the right data collapse for $P'_{sur}(s,L) = \int_1^s P_{\rm sur}(s',L)ds'$. P'_{sur} is scaled by $L^{D(\tau_{sur}-1)} = L^{1.20}$, corresponding to $\tau_{sur} = 1.60$ and $D = 2$. 23

2.7 The fitness distribution for site belonging to the boundary. Within the error bars the sharp threshold occurs at the same value of the bulk case. 26

2.8 $Q(s) = \int_s^{s_{max}} P(s')ds'$ is the integrated distribution; the fitting form is $As^{1-\tau'} + C$ with $\tau' = 1.25 \pm 0.01$ ($N = 1000$). 27

2.9 *first* and *all* return times probabilities at boundary sites. Statistics refer to 10^9 mutations in the whole chain. 28

3.1 Reaction diagram of the process. The red transitions refer to thermal processes, that is they refer to all the topplings happening under the threshold. 38

3.2 Average height θ versus $e^{-\frac{1}{T}}$ as obtained on a 64×64 square lattice. 39

3.3 Probability distributions P(s) for different temperatures. 40

3.4 High temperature avalanche distribution. Crossover between different behaviors at a size s_c varies with T, provided that s_c/T is small enough. In the present case $T = 100$, $f(s) \propto s^{-1/2}$ and $g(s) \propto s^{-1.50}$. 41

4.1 Flow-chart of the algorithm used in the simulations. The loop over steps from 2 to 4 is repeated as long as new bonds are broken, and is what we define as an avalanche. The simulation ends when the sample is broken in two pieces. 54

4.2 Cumulated frequency distribution of the number of broken springs during an avalanche for different lattice sizes: 200 simulations for a 16×16 sites lattice; 100 simulations for a 32×32 sites lattice; 100 simulations for a 64×64 sites lattice. . . . 56

4.3 Cumulated frequency distribution of the normalized energy lost during avalanches for the simulations of FIG. ??. 57

4.4 Frequency distribution for the duration time of the avalanches for the simulations of FIG. 4.2 58

5.1 Satellite Image of Everest and Cho Oyu, November 3^{rd}1994 (courtesy of NASA). . . 62

5.2 Typical structure of a river from mountains to the sea 64

5.3 Drainage (sub)basin and relative longest stream. The Hack's law states $L \propto A^h$, $h \simeq 0.6$. 65

5.4 Relation between lengths and area of the Shenondah Valley subbasins (courtesy of Rodriguez-Iturbe and Rinaldo). 66

5.5 Relation between lengths and area of the different rivers in the world (courtesy of Rodriguez-Iturbe and Rinaldo). 66

5.6 An example of the DEM method on a sample elevation map. The mean height of the regions are in fictitious unit length and it is reported in the upper right corner. . 67

5.7 An example of the DEM method on a sample elevation map for the Fella river in the North of Italy. 68

5.8 In clockwise order a snapshot of the final landscape for Model A, Model B, Model D and Model C. Model A and C have a single outlet, Model B and D have multiple outlets. The initial condition is deterministic for A and B, while C (D) has a small random noise superimpose to A (B). 74

5.9 The network structure corresponding to the landscapes of the previous figure. Only sites with area ≥ 5 are shown for sake of clarity. 75

5.10 Log-Log plot of the area cumulated distribution $P(a, L)$ versus a for model A,B,C and D, in the same order as above. The full line has a slope corresponding to $\tau = 1.43$, $\tau = 1.50$, $\tau = 1.38$ and $\tau = 1.38$ respectively. 77

5.11 Scaling function $a^{1-\tau}P(a, L)$ versus a/L^{1+H} for model C. The used values to obtain the collapse were $\tau = 1.38$ and $H = 0.6$. 78

5.12 Log-Log plot of the upstream cumulated lengths $\Pi(l, L)$ versus l for model C. The full line has a slope corresponding to $\gamma = 1.6$. 78

5.13 Scaling function $l^{1-\gamma}\Pi(l, L)$ versus l/L^{d_l} for model C. The used values to obtain the collapse were $\gamma = 1.6$ and $d_l = 1.0$. 79

5.14 Comparision between the evolution of two identical initial configurations of model C with size $L = 100$ without (left) and with pinning (right). The pinning diluition was 5%. 80

5.15 Log-Log plot of the area distribution $P(a, L)$ vs. a (left) and corresponding collapse plot (right) for model C with a 5% dilution. 81

List of Tables

1.1 Values of the exponents τ and y for the models described. 8

2.1 Determination of avalanche exponent via direct estimate and collapse fit 22

2.2 Determination of avalanche exponent via direct estimate and collapse fit 24

5.1 Scaling relations: all the exponents can be determined in terms of d_l in the fractal case and H in the self-affine case. 81

5.2 Summary of the results for the four models considered in the text. Here we show the sets of critical scaling exponents τ and γ obtained from the various simulations after suitable ensemble averaging. 82

Introduction

Critical Phenomena play a fundamental role in the modern physics. Critical behavior is characterized by the absence of any characteristic scale for the physical quantities. Developing a tools describing these properties had represented a formidable challenge for the theoretical physicists. At the critical point the system fluctuates strongly at all wavelengths and no perturbation theory can be builted up. A more useful approach can be found in the K. G. Wilson Renormalization Group that bases its rules directly on scale invariance properties of a critical system. This new kind of approach to physical phenomena can be related to another conceptual revolution due to B. Mandelbrot (Mandelbrot (1982)). In his work he has pointed out that natural landscapes are by the most part composed by scale invariant (selfsimilar) objects and that in Nature the euclidean regularity is an exception. Furthermore with the fractal geometry tools one is able to manage with very different phenomena in such a way to consider complexity as a self standing object. "Clouds are not spheres, mountains are not cones, coastlines are not circles, bark is not smooth nor does lightnings travel in a straight line..." and from this point of view all these patterns show the same scale invariant properties of ordinary critical phenomena. Also in this case, in fact, one deals with systems characterized by an infinite correlation length. Despite of this fact a very deep difference exists between these two classes of physical processes: while the critical point in liquid-vapour transition is reached by a tuning of the system parameters (pressure and temperature), this seems not the case for the pattern formation in Nature. In this last case one deals with systems that are intrinsically irreversible and no hamiltonian treatment can be developed. The story of the whole process is necessary to describe the relative occurrence probability of a given configuration and therefore it cannot be ignored. As it will be pointed out in the following the scale invariance by itself does not imply a critical condition. The system may arrange in a fractal form and remain stable with respect to external perturbation. Sometimes one can observe that this widespread occurence is related to the fact that the critical state is an attractor for the dynamics of the system.

The term Self Organized Criticality (SOC) refers to this last case in which a stationary critical state is approached spontaneously by the system. No tuning of external parameters is required to reach a critical state. To visualize the concept of SOC Bak Tang and Wiesenfeld (Bak, Tang and Wiesenfeld (1987)) have introduced a class of cellular automata whose dynamics is inspired by sandpiles. Throwing sand in a box small mountains will appears until a critical slope is reached;

further addition can produce local or more general rearrangements and eventually bring material outside the box. When a stable configuration is reached the addition of new sand brings again to the critical slope and the process lasts forever with a slope mean average value around the critical one. This stationary state is characterized by the scale invariant space and time distributions of the rearrangements (avalanches).

Due to for the different nature of the criticality a direct comparison can not be made with ordinary critical phenomena. However we have studied a formal comparison between these two class of systems, regardless the different causes of criticality. With the tools of the standard theory of critical phenomena we have analyzed many different situations and we have been able to fully clarify new phenomena explicitly noted by numerical data (Stella, Tebaldi and Caldarelli (1995), Caldarelli, Maritan and Vendruscolo 1996, Caldarelli, Tebaldi and Stella (1996)a, Caldarelli 1996). A satisfactory approach to the evolution towards the critical state (that is also able to describe some properties of the critical state itself) has also been obtained using the Dynamically Driven Renormalization Group (Pietronero, Vespignani and Zapperi (1994), Vespignani, Zapperi and Loreto 1996) recently developed, and whose application to some topics of this thesis is still in progress (Caldarelli, Tebaldi and Stella 1996b, Caldarelli, Loreto, Ivaskevic and Vespignani 1996). The result at this stage of the work is that these cellular automata seem robust enough with respect to changes in their rules. Nevertheless the same robustness is only related to their qualitative behavior, the precise value of the critical exponents fluctuate with respect to the particular choice of the model. In this sense it is clear the paradigmatic meaning of the sandpile model. These cellular automata are only an example for a wide range of phenomena differing only by the values of this critical exponents. This "non universality" may be considered a weak point of this approach, with respect to the ordinary critical phenomena. Nevertheless a theory that pretends to explain the variety of landscapes and patterns in Nature has to show this property to unify in a unique framework a plenty of different quantitative behaviors. To fully clarify the basic idea of self-organization it is, therefore, necessary and vital to address directly to some "physical" problems.

This has been the starting point of the second part of the work. We have applied all the concepts developed in the first part to models more closely related to some physical situation as for example the solid breakdown and the erosion processes occurring in fluvial evolution. In this two cases it is clear that the process of landscape formation cannot last forever and a final state has to be reached in the evolution. Strictly speaking, in general, in this case the SOC approach makes no longer sense. What we have observed is that with models strictly inspired by the former one we had been able to reproduce the experimental situations. It is worth to note that organization to self-similarity (statical infinite correlation) is again present also in the case of no more criticality (when the response of the system to the external stress is not infinite, i.e. $\chi = \frac{\partial m}{\partial h} < \infty$ with obvious symbology). Furthermore at least in one case (for river network action in the sculpture of landscapes) the self-similarity arises from variational principles and a feedback process similar to the SOC one can be viewed as the evolution way for a dissipative system towards its statical minimum

point. It is remarkable that the same microscopical rules of many SOC models hold not only for the dynamical equilibrium of open systems but also for the transient state of many dissipative systems addressing the concept of self organization to the competition between optimization and disorder.

This thesis is designed in such a way that each chapter can be read as a self-standing work. At the beginning of each chapter there is a short summary of the basic concepts and of the basic phenomenology fully explained in the first chapter.

The work is so (self-) organized: In the first chapter there is a long part dedicated to the presentation of the basic automata model and to the theoretical tools used in the following chapters.

In the second chapter the boundary effects for such systems are discussed. While the third chapter is dedicated to the role of an external field. The purpose of this research is to test the robustness of the SOC definition to study if these simple cellular automata can describe properly the robustness in Nature landscapes.

Chapter four contains the first application of the concepts previously introduced to a directly accessible physical case: the breakdown of media. A description inspired to the previous cellular automata it is able to reproduce qualitatively the behavior of Acoustic Emission also if in this case no critical state exists and our analysis apply to the transient state.

In the fifth chapter a long analysis is dedicated to the River Networks. Also in this case the starting point is inspired by sandpiles model and also in this case we find a self organization in the evolution and a stable one final state.

1 S.O.C. Models

1.1 Some sandpile models

There are several examples of sandpile automata models showing SOC properties. Most of them and all those presented here have a common structure.

They are defined over a finite box Λ in the d–dimensional hypercubic lattice; for any site i an integer variable $z_i = 1, 2, 3...$ is assigned, representing the height of the sand present. Selecting randomly a site, one grain of sand is added, that is the variable z_i is increased by one. A function of this height z_i is then defined: for example the height itself, the difference of height between nearest neighbours (the first discrete derivative of the height), or the discrete laplacian operator of height (the second discrete derivative) and so on. Until such function on the site i is below a certain threshold value the configuration is stable. As soon as this condition is not fulfilled, the column of sand "topples" on the nearest neighbours (n.n), that is

$$z_i \rightarrow z_i - \Delta_{ki} \tag{1.1}$$

where,

$$\Delta_{ki} = \begin{cases} 2d & k = i \\ -1 & k, \text{nearest neighbor of } i \\ 0 & \text{otherwise.} \end{cases} \tag{1.2}$$

This process is called *toppling*.

The particle number is preserved for toppling in the interior sites. For topplings on the boundary sites ($i \in \partial\Lambda$) some grains fall outside from the box and never come back. After a long time, the rate of input (grain addition) and of output (drop through the boundary) are equal on the average and the system reaches a critical state. In this state the average sand height fluctuates around its average.

A site can increase its height either by external addition or by toppling of a nearest neighbour. In this last process one site can reach the threshold for toppling. It becomes critical and topples, making critical the sites around. Due to the loss of particles from system, this process will stop

after a certain time and can be repeated adding sand from exterior. All the toppling processes between two sand additions are said to form an *avalanche.*

One can define both a size and a characteristic time for an avalanche. The size of an avalanche can be evaluated, for instance, as the total number of toppling sites (one site can topple more than once) or the total number of topplings (it is clear that these two definitions give results more and more similar as the dimension of space increases) [1].

If the two following steps are regarded as a unit time:

- list of critical sites;
- toppling process for every site of the list, and updating of neighbours heights,

the lifetime of an avalanche can be defined as the number of unit step between two sand additions.

The size s and the lifetime t of avalanches obey power law distributions

$$P(s) \sim s^{-\tau} \tag{1.3}$$

$$Q(t) \sim t^{-y} \tag{1.4}$$

The quantities $P(s)$ and $Q(t)$ are directly accessible by computer simulations. $P(s)$, for example, is the total number of avalanches of size s as the number of grain additions goes to infinity.

To reduce noise in the numerical simulations where of course the number of grain addition is finite, these distributions are integrated over increasing bin lengths of s and t. In this way one deals with the two integrated distributions:

$$P'(s) = \int_1^s P(s')ds' \sim s^{1-\tau} \tag{1.5}$$

$$Q'(t) = \int_1^t Q(t')dt' \sim t^{1-y}. \tag{1.6}$$

Plotting these over logarithmic scales one can easily find the values of exponents.

To give a brief review of the state of art about the various models we list them with their most significant properties. A summary of the exponent values is shown in Table 1.1.

1.1.1 Critical Height Model (CHM)

In this model the stability of a sand column depends on a preassigned value of the sand height itself h_c. The instability condition is then

$$z \geq z_c \qquad (\text{usually } z_c = 2d). \tag{1.7}$$

[1] In the following section a special case will be shown in which the two definitions are equivalent, that is one site can topple only once during an avalanche.

In the steady state each site has an equal height on the average except from the boundaries where this value is lower.

This is a particular case of the general Abelian Sandpile Model (ASM). Indeed the steady state does not depend on the sequence of toppling processes. Introducing a state function for the state of the system, the grain addition can be viewed as the action of site operators (whose matrix elements are expressed in eq.(1.2)) on this function. These operators follow a commutative operator algebra allowing to determine exactly some of the properties of the model (Majumdar and Dhar (1992), Dhar (1990)). Besides this theoretical approach, the ASM has been studied also by a Renormalization Group approach(Pietronero et al. (1994)). From the largest realized computer simulations (Manna (1990), Manna (1991), Grassberger and Manna (1990)), one gets the exponent values: $\tau = 1.22 \pm 0.01$ and $y = 1.32 \pm 0.01$.

1.1.2 Critical Slope Model (CSM)

In this model a sand column topples when the local slope in any of the four direction reaches a preassigned value. That is

$$z_i - z_j \geq \Delta z_c \qquad \forall j \quad n.n.\ i. \tag{1.8}$$

It is now necessary to fix a value for the height at the boundary of the box. For example one can kept them at zero height.

This model is not an Abelian one, in fact, now the stability condition (1.8) of two column depends one from each other and so the toppling of one of them can destroy the instability of the other. The average height depends on the value of critical slope, and in any case the shape of the pile of sand in the box is not uniform on the average as in the previous model, but the whole systems arrange itself in a pyramidlike structure. It is to be noticed that in $d = 2$, if the value of local slope is chosen lesser or equal to three the steady state is composed by columns with negative height. That is some avalanches dig a hole in the box throwing grains outside from the boundaries. This behavior disappears by increasing Δz_c. Even if this model (for high values of Δz_c) resembles in a clear way the behavior of real sand piles, it was not extensively studied. This is due to the absence of an evident scaling property in the distribution function.

1.1.3 Critical Laplacian Model (CLM)

In this model a sand column topples when the local laplacian operator, defined in d dimension as

$$l_i = (2d)z_i - \sum_{<i'n.n.i>} z_{i'} = \sum_{<i'n.n.i>} (z_i - z_{i'}) \tag{1.9}$$

is greater than or equal to a fixed (threshold) value l_c.

Since the laplacian operator is directly related to the loss of gravitational energy in a toppling process (considering the grain mass and the force strength equal to unity), this model seems to

	CHM ($z_c = 4$)	CLM ($l_c = 9$)	Restricted CLM ($l_c = 8$, $z_c = 4$)
τ	1.22 ± 0.01	1.30 ± 0.01	1.288 ± 0.002
y	1.32 ± 0.01	1.57 ± 0.01	1.508 ± 0.003

Table 1.1: Values of the exponents τ and y for the models described.

be more satisfying than others with respect of real sandpiles. In particular SOC arise under the effect of gravity every time internal friction between grains stop the grain rolling along the profile (Frette, Christensen, Malthe-Sørensen, A., Feder, Jøssang, T. and Meakin (1996)).

It has to be noticed that this model is not Abelian, since the stability of a column depends on the others. Furthermore, as in CSM, holes are present in $d = 2$ if the condition $l_c \leq 8$ is verified.

Contrary to the case of CSM one can see a clear scaling behaviour with $\tau = 1.30 \pm 0.01$ and $y = 1.57 \pm 0.01$. This regime becomes more clear if one studies a "restricted " version of model in which the toppling happens when $l_i \geq l_c$ and $z_i \geq z_c$. Note that in this case it is not possible to dig holes in a toppling process: the average height is always positive.

This restricted model is believed to belong to the same universality class of the CLM and it is introduced in order to simulate very large systems (computer simulations converge more rapidly to steady state). Moreover, as previously noted, the power law behaviour of this restricted CLM enables a more precise extimate of the exponents than in CLM case. One finds $\tau = 1.288 + .002$ and $y = 1.508 \pm 0.003$.

1.2 A biological model

The SOC properties can be present not only in sand piles real or modelized, but also in processes like biological evolution. In fact, the evolution of an ecology of interacting species consists in intermittent bursts of activity separating relatively long periods of quiescence, rather than gradual mutations (Gould and Eldredge (1993), Gould and Eldredge (1977)). Furthermore the presence of power law has been notated for the number of genera with s species, $N(s) \propto s^{-\tau}$, with $\tau \simeq 2$. A similar scaling behaviour exists across the taxonomics hierarchy, i.e. for species within genera, families within orders ecc. also giving the same exponent $\tau \simeq 2$ (Burlando (1990), Burlando (1993)). Similarly, the distribution of life times t, of fossil generation (Raup (1986)), can be described by a power law $P_life(t) \propto 1/t^{\tau_life}$, where again the exponent is about 2. As observed (Gould and Eldredge (1993), Gould and Eldredge (1977)) , when viewed at sufficiently large time scales, the pace of extinction itself is episodic with long periods of stasis interrupted by sudden bursts of mass extinction. Punctuated equilibrium with scale-free extinctions has been attributed to the

self–organized critical dynamics of strongly interacting species, without the need for catastrophic exogenous causes as meteorites. The punctuated equilibrium process governing large scale evolution may be sufficiently robust or universal to be captured by an astract mathematical model.

For example, it has been demonstrated (Bak, Chen and Creutz (1989)) that the Game of Life (a cellular automaton simulating a community of living organisms) when driven by random mutations operates at the critical state.

A more sophisticated model that attempts in explaining many of the properties of biological evolution, even with great simplifications with respect to real life, is the Bak–Sneppen (BS) model (Bak and Sneppen (1993), Flyvbjerg, Sneppen and Bak (1993)).

It is defined by the four following steps:

- N species are arranged on a one dimensional line with e.g. periodic boundary conditions.
- A random barrier is assigned to each species (it consists of a random variable η_i uniformly distributed in the interval $[0, 1]$).
- The site with the lowest barrier and its site nearest neighbors (n.n) are updated and other random value are extracted in the same interval .

The basic idea is to link the height of barrier with the genetic code of species. The higher is the barrier the longer is the time between two modifications of the genetic code. If the barrier is low, the species can mutate and evolve. The updating of nearest neighbours takes into account that species are linked together (for example, they can be in the same food chain). This the mutation of one species induces mutations in the n.n species. In this way, the system self–organizes to a critical "steady state" in which almost all the barrier are uniformly distributed over a certain threshold value $\eta_c = 0.67$. The avalanches in this model are defined as the sequence of mutations of barriers below a certain fixed value η. In this way the size of avalanche is uniquely defined as the number of these mutations. For η close below the global self–organized threshold η_c the avalanche distribution displays a power law with an exponent $\tau = 1.1$. Of course this model can be easily generalized to an higher number of dimension to simulate more correlations between the species.

1.3 Comparison with usual critical phenomena

To better understand SOC phenomena we have been guided by the analogy that one can settle with a class of more extensively studied phenomena. The models presented above show long range space (and time) correlations, as the usual critical phenomena. One can make a close comparison between (for example) ferromagnetic systems and SOC models. In sand pile models the external grain addition can be viewed as the action of an external field over the system. In this case it is clear that all the avalanche processes can be viewed as the response of the system to this field.

The analogy with ordinary critical phenomena is related to the behavior of the system with respect to the average height θ. In fact if θ is very small (below a "critical value" θ_c) no activity occurs in the system without external flux of sand. If the system is kept at θ sufficiently large (above θ_c) also without external additions one observes a "spontaneous" flux of sand. We remark here, that the condition to ensure this criticality (i.e. the value of θ) cannot be fine tuned from exterior, but is determined by the story and the evolution of the system. Notwithstanding this difference, one can try to identify this quantity with the temperature in ordinary critical phenomena. In the same way one can also introduce the quantities j, h to represent respectively the flux of sand inside SOC systems and the amount of sand injected from exterior. Schematically,

- θ can be considered the temperature for SOC systems;
- the external sand addition h plays the role of an external field (e.g. the magnetic field);
- the flow j of sand (that is essentially proportional to the number of lattice size whose $\theta > \theta_c$) is the control parameter (e.g. the magnetization);
- The correlation length ξ in this case is the cutoff in the avalanche below the critical threshold.

Since the quantity directly accessible in computer simulations is the cluster size s of an avalanche, it holds

$$s_{co} \propto \xi^D \tag{1.10}$$

Where s_{co} is the cutoff cluster size and D the fractal dimension of the cluster. The criticality is reached when the response of the system to an external infinitesimal field diverges. That is when

$$\chi = \frac{\partial j}{\partial h}|_{h=0} \to \infty \tag{1.11}$$

One expects the usual behaviors near the critical region

$$j \propto (\theta - \theta_c)^{-\beta} \tag{1.12}$$

$$j \propto h^{1/\delta} \tag{1.13}$$

$$\xi \propto (\theta - \theta_c)^{-\nu} \tag{1.14}$$

$$s_{co} \propto (\theta - \theta_c)^{-1/\sigma}. \tag{1.15}$$

$$\chi \propto (\theta - \theta_c)^{-\gamma}. \tag{1.16}$$

Since χ is simply the average cluster size caused by sand injection just below θ_c it holds:

$$\chi = \int_0^{s_{co}} sP(s)ds = s_{co}^{2-\tau} \propto (\theta - \theta_c)^{-\frac{2-\tau}{\sigma}} \propto (\theta - \theta_c)^{-\gamma}. \tag{1.17}$$

Furthermore, since the dynamics is essentially diffusive at the stationary state, each extra unit of sand will need L^2 steps to diffuse away (on the average) in a box of linear size L.

For cluster limited by L^D sizes the stationarity condition becomes

$$\int_0^{L^D} sP(s)ds = L^{D(2-\tau)} \propto L^2. \tag{1.18}$$

From these considerations follow the scaling relations

$$\gamma = \frac{2-\tau}{\sigma} \tag{1.19}$$

$$D = \frac{1}{\sigma\nu} \tag{1.20}$$

$$D\gamma\sigma = \frac{\gamma}{\nu} = 2 \tag{1.21}$$

1.4 Mean Field for Sandpiles

Following the ideas exposed in the previous section, now we introduce the concepts of the Mean Field (MF) analysis for Sandpiles Model (specifically the Abelian one) that will be used in the next sections.

One supposes to deal with a $d = 1$ system, generalization to higher dimension being straightforward. According to the previous rules a site will topple at height 2. We define *active* sites those with 2 or more grains, *inactive* the others. In this one dimensional system one can consider only four different states. That is, a site is empty or it is filled with one, two or three grains of sand. The total fraction of sites whose height is n will be denoted with P_n. In MF P_n can be also viewed as the probability for a certain site to be at height n.

The probability to be active is $P_A = P_2 + P_3$, and the probability to be inactive is $P_I = 1 - P_A = P_0 + P_1$.

The state 0 will change to state 1 during the next time step with probability $1 - h$ if one of its neighbors is active and the other inactive, and with probability h f both of them are inactive. This process can be schematized by the following equation

$$0 \xrightarrow{2(1-h)P_AP_I+hP_I^2} 1 \tag{1.22}$$

Similar considerations hold for the other states and one can obtain the reaction diagram of FIG.1.1.

Imposing the stationarity condition on the rate flows into a state and out of the state (e.g. $0_{in} = 0_{out}$), the following mean field equation hold.

$$P_2(1-P_2)^2 - hP_2 = 2P_0P_2(1-P_2) + 2P_0P_3 + hP_0 + P_0P_2^2 - 2hP_0P_2 \tag{1.23}$$

$$\begin{aligned} &2P_0P_2(1-P_2) + 2P_0P_3 + hP_0 + 2P_2^2 + P_3 + hP_2 - 4hP_0P_2 \\ &\quad = 2P_1P_2(1-P_2) + 2P_1P_3 + hP_1 + P_1P_2^2 - 2hP_1P_2 \end{aligned} \tag{1.24}$$

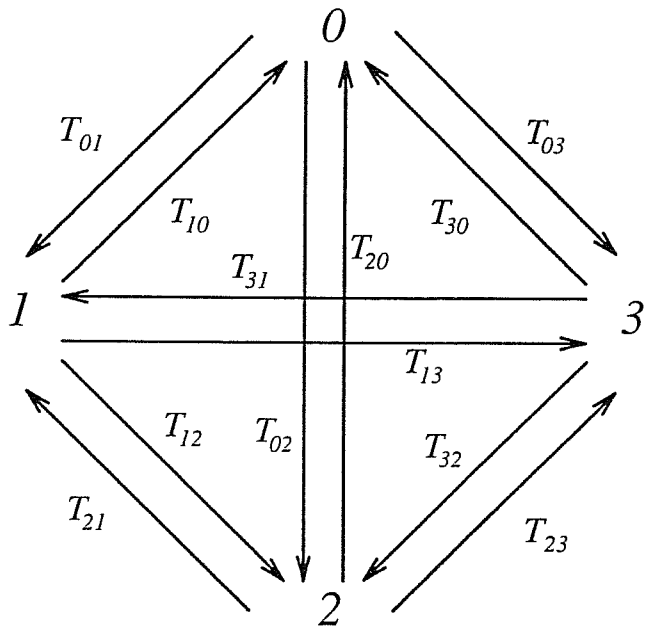

$$T_{01} = 2(1\text{-}h)P_A P_I + hP_I^2$$
$$T_{02} = (1\text{-}h)P_A^2 + 2hP_A P_I$$
$$T_{03} = hP_A^2$$
$$T_{10} = 0$$
$$T_{12} = 2(1\text{-}h)P_A P_I + hP_I^2$$
$$T_{13} = (1\text{-}h)P_A^2 + 2hP_A P_I$$
$$T_{20} = (1\text{-}h)P_I^2$$
$$T_{21} = 2(1\text{-}h)P_A P_I + hP_I^2$$
$$T_{23} = hP_A^2$$
$$T_{30} = 0$$
$$T_{31} = (1\text{-}h)P_I^2$$
$$T_{32} = 2(1\text{-}h)P_A P_I + hP_I^2$$

Figure 1.1: The reaction diagram and the explicit form of the reaction equations

$$2hP_0P_2 - 4hP_1P_2 + 2P_1P_2(1 - P_2) + 2P_1P_3 + hP_1 + P_0P_2^2 = P_2 \tag{1.25}$$

$$P_1P_2^2 + 2hP_1P_2 = P_3 \tag{1.26}$$

Those equations are obtained in the hypotheses of h small (1 grain for site) and $j = P_A = P_2 + P_3$ small, that define the critical region.

From the fourth equation (1.26) $P_3 \propto P_2^2$ follows. Since in previous hypotheses P_2 must be small, the contribution of P_3, in the critical region can be neglected, since it is an infinitesimal of the second order.

From the first two equations (1.23), (1.24) substituting $P_3 = P_1P_2$ one gets respectively (in the limit $h \to 0$)

$$P_0 = \frac{1}{2} - P_2 + O(P_2^2) \tag{1.27}$$

$$P_1 = P_0 + P_2 + O(P_2^2) = \frac{1}{2} + O(P_2^2) \tag{1.28}$$

Thus, the average height θ defined by $\sum_{i=0,3} iP_i$ assumes, at the stationary state near the critical region, the value $\theta_c \simeq P_1 \simeq \frac{1}{2} + O(P_2^2)$.

The set of P_i's satisfies the normalization condition $\sum_{i=0}^{3} P_i = 1$. Since in the above hypotheses at $h = 0$ P_2 is zero (in this case the equation for P_2 gives $0 = 0$), eq.(1.25) could be used to obtain the dependence of the order parameter P_2 with respect to h. In this case θ is an unknown function of h and must be treated as an indipendent variable. In this sense eq.(1.25) only links the unknown

average height to the external field. Introducing the quantity θ one has from this equation

$$4P_2^2 + (1 - 2\theta - 2h)P_2 - h\theta = 0. \tag{1.29}$$

At the first significant order one gets the first critical exponent

$$P_2 = \frac{1}{2}(\theta - \theta_c) \Rightarrow \beta = 1. \tag{1.30}$$

After differentiation of the (1.29) with respect to h one obtains

$$8P_2\chi + 2P_2 + (1 - 2\theta)\chi - \theta = 0. \tag{1.31}$$

From which one gets

$$\chi = \frac{1}{4}\frac{1}{(\theta - \theta_c)} \Rightarrow \gamma = 1. \tag{1.32}$$

Thus, at the critical point χ diverges. Since at the critical point $\theta = \theta_c = 1/2$ after substitution in equation (1.29) one obtains

$$4P_2^2 + 2hP_2 - \frac{h}{2} = 0. \tag{1.33}$$

From which it follows

$$P_2 = (\frac{h}{8})^{1/2} \Rightarrow \delta = 2. \tag{1.34}$$

Those are the results and the formulation introduced by C.Tang and P.Bak (Tang and Bak (1988)b, Tang and Bak (1988)a).

1.5 Mean Field and Markov Processes

Since the main characteristic of SOC systems is to describe non equilibrium dynamical properties we think that a master equation approach is more suitable to describe the phenomenon. To do that one can consider the Markovian process described by the following equations

$$\begin{aligned}
P_0(t+1) &= P_0(t) + P_1(t)T_{10}(t) + \\
&\quad P_2(t)T_{20}(t) + P_3(t)T_{30}(t) - \\
&\quad P_0(t)(T_{01}(t) + T_{02}(t) + T_{03}(t)) \\
P_1(t+1) &= P_1(t) + P_0(t)T_{01}(t) + \\
&\quad P_2(t)T_{21}(t) + P_3(t)T_{31}(t) - \\
&\quad P_1(t)(T_{10}(t) + T_{12}(t) + T_{13}(t)) \\
P_2(t+1) &= P_2(t) + P_0(t)T_{02}(t) + \\
&\quad P_1(t)T_{12}(t) + P_3(t)T_{32}(t) - \\
&\quad P_2(t)(T_{20}(t) + T_{21}(t) + T_{23}(t))
\end{aligned}$$

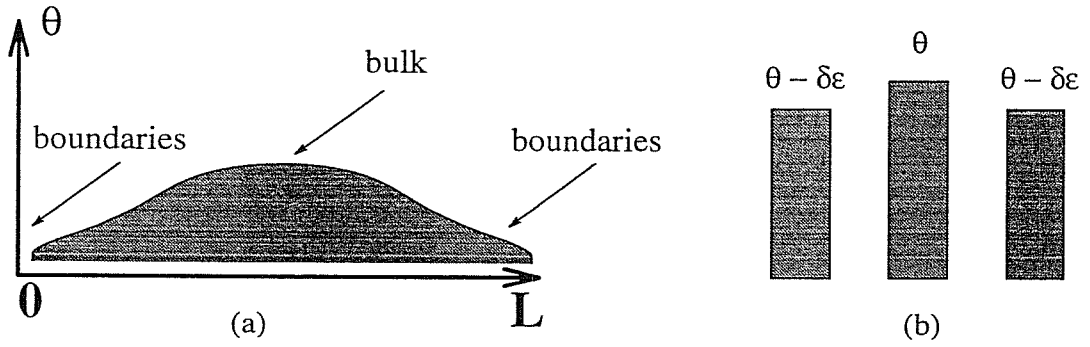

Figure 1.2: (a) Profile of a real sandpile that justify our hypothesis (in (b)) on the θ behavior with respect to the distance from the boundaries.

$$\begin{aligned} P_3(t+1) &= P_3(t) + P_0(t)T_{03}(t) + \\ &\quad P_1(t)T_{13}(t) + P_2(t)T_{23}(t) - \\ &\quad P_3(t)(T_{30}(t) + T_{31}(t) + T_{32}(t)) \end{aligned} \tag{1.35}$$

The transition rates T_{mn} between states m, n are displayed in the FIG.1.1. Now, the mean field solutions for the P_i's has to be recovered as the fixed points of the above iterations. It turns out from a simple analysis that the fixed point solution $P_z(\infty)$ differs from the exact solution previously introduced. In fact

- in the case of $h = 0$, the fixed points $P_n = P_n(\infty)$ depend dramatically from the initial conditions $P_n(0)$.
- in the case of $h \neq 0$, the fixed points $P_n(\infty)$ are $P_0 = 0, P_1 = 0, P_2 = 0, P_3 = 1$.

Because of the presence of the external field h, the system accumulates more and more energy (sand) until saturation if dissipative boundaries are absent. Then the presence of boundaries in the system is an essential ingredient to ensure the correct result. Otherwise the result of the iterations of eqs.(1.35) brings trivially to $P_3(\infty) = 1$ and the other $P_z(\infty)$'s equal to 0.

A very rough but efficent way to introduce the dissipation is to consider tails in the height profile (see FIG.1.2). Due to the loss of sand. on the average, a certain amount of sites near the boundaries are lowered. Precisely, if the site under consideration is characterized by θ, the height (*i.e. the activity*) of the nearest neighbor sites it is lowered by an infinitesimal amount $\delta\epsilon$.

This correspond to introduce a new set of probabilities Q_z such that

$$\begin{aligned} Q_0 &= P_0(1-\epsilon) + \epsilon/2 \\ Q_1 &= P_1(1-\epsilon) + \epsilon/2 \\ Q_2 &= P_2(1-\epsilon) \\ Q_3 &= P_3(1-\epsilon) \end{aligned} \tag{1.36}$$

where $\epsilon = \delta\epsilon/(\theta - 1/2)$. In terms of the Q_z's now the correct results are recovered. in the limit $\epsilon \to 0$. Another way to see this is to consider that with a probability $\epsilon \propto 1/L^d$ an active site can be on the border. Since toppling processes in such a case does not preserve the total number of active sites, a factor proportional to the number of boundary sites must be introduced to normalize P_2 and P_3.

It is important to notice that the $\epsilon \to 0$ limit does not commute with the ordinary (slow driving) $h \to 0$ limit. So for all *physical* systems there exists an upper critical value for the external field related to the capability of such a system to dissipate energy (sand).

If one wants explicitely to write down the MF equation for the Q_i's set (for example for the transition from the state 0 to the state 1) one will deal with transition rates of the following form:

$$T_{01} = P_0 \left(2(1-h)P_A(Q_i)P_I(Q_i) + hP_I(Q_i)^2\right), \quad i = 0,1,2,3 \tag{1.37}$$

This brings to this new set of equations for the P_i's

$$\begin{aligned}
&\text{l.h.s. eq.(1.23)} + (2P_2(1-P_0-P_1)(P_0+P_1))\epsilon = \\
&\text{r.h.s. eq.(1.23)} + P_0(2(P_2+P_3)(1-2P_0-2P_1-P_2-P_3))\epsilon && (1.38)\\
&\text{l.h.s. eq.(1.24)} + (2(P_0+P_2)(1-2P_0-2P_1)(P_2+P_3)+2P_3(P_0+P_1)(1-P_0-P_1))\epsilon = \\
&\text{r.h.s. eq.(1.24)} + P_1((P_2+P_3)(1-2P_0-2P_1-P_2-P_3))\epsilon && (1.39)\\
&\text{l.h.s. eq.(1.25)} + \left(2(P_1+P_3)(1-2P_0-2P_1)(P_2+P_3)-2P_0(P_2+P_3)^2\right)\epsilon = \\
&\text{r.h.s. eq.(1.25)} + P_2(2(P_2+P_3)(1-2P_0-2P_1)+2(P_0+P_1)(1-P_0-P_1))\epsilon && (1.40)\\
&\text{l.h.s. eq.(1.26)} + \left(-2P_1(P_2+P_3)^2\right)\epsilon = \\
&\text{r.h.s. eq.(1.26)} + P_3(2(P_2+P_3)(1-2P_0-2P_1)+2(P_0+P_1)(1-P_0-P_1))\epsilon && (1.41)
\end{aligned}$$

where all the terms $\propto h\epsilon$ have been neglected.

The main effect of this substitution is in the equation written for the dependence of P_2 from h, in fact, now one has (in the limit of vanishing field)

$$4P_2^2 + \epsilon P_2 - h/2 = 0 \tag{1.42}$$

whose solution gives

$$P_2(h) = \frac{\epsilon}{8}\left(\sqrt{8h/\epsilon^2+1}-1\right) \simeq \frac{1}{2}\frac{h}{\epsilon}. \tag{1.43}$$

Now, the order parameter depends linearly from the applied field. We remark that it is not surprising to find for a real sandpile (i.e. $\epsilon \neq 0$) no more divergence in the response function. In fact now there exists an upper cutoff for the avalanche due to the size of the sample that is not a finite effect size, but *it is intrinsic* in the particular kind of phenomenon. The important thing is to notice that according the above formula since $\epsilon \propto 1/L^d$ $P_2(h) \propto L^d h$ as $\epsilon \to 0$. and the response

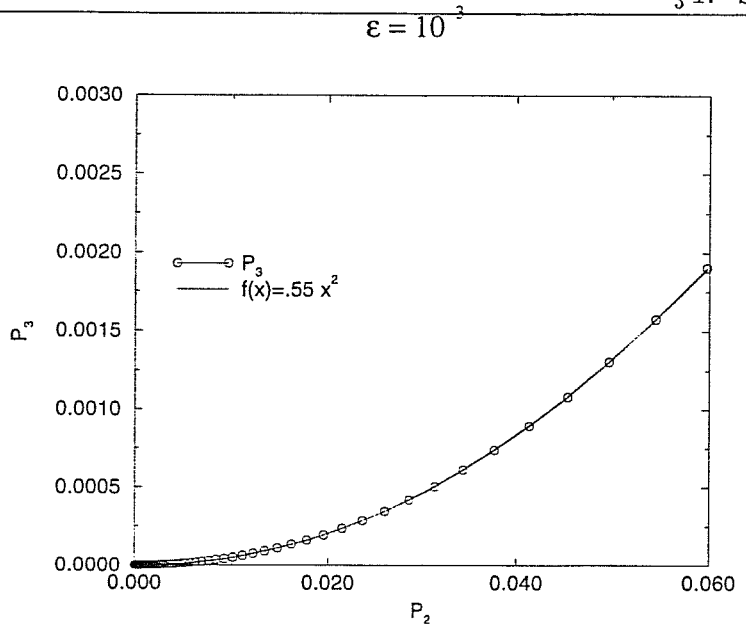

Figure 1.3: P_2 versus h for $\epsilon = 10^{-3}$.

function ($\chi \propto L^d$) diverges not in the limit of vanishing field but in the thermodynamic limit (i.e. for samples bigger and bigger one gets χ larger and larger but finite). This is the reason for which each direct measurement on experimental data gives results of the form $P_2(h) \propto a(L)h$ (Vespignani and Zapperi n.d.). The original result can be recovered only commuting the two limits $h \to 0$ and $\epsilon \to 0$.

We have also solved numerically the above MF equations (1.38-1.41) to verify the validity of our approximations. We found that in the limit $h \to 0$ (keeping ϵ fixed) the behavior is those represented in FIG.1.3. That is exists a clear linear dependence for P_2 from h. Tuning the value of the parameter ϵ the expected dependance on (h/ϵ) is recovered.

From this it is clear how much important boundaries are in the definition of SOC models. For this reason in the next chapter new boundaries scaling will be introduced and analyzed for such systems.

2 Inhomogeneities in Self–Organized Systems

In this chapter the role of the inhomogeneities in the system will be studied. The presence of a boundary does not destroy the self–organization, but gives rise to different universality classes for the critical exponents. This value difference as in the case of biological model can explain the different behavior in an ecology of species at the ends of a food chain. While in the case of usual sandpiles models represents the known stability properties of these aggregates for external perturbation acting on boundary.

Due to the topological properties of boundary (i.e. the absence of nearest neighbors for this layer of the system) all the properties presented here for the two prototype models (AS and BS) can be easily extended to the other self organized systems. In the case of AE, for example, the existence of different scaling behavior means that a failure on the surface of a uniform dilated medium has less chances to bring to the complete breakdown with respect to an internal failure. Similar considerations justify the interest in this particular kind of scaling. On the boundary in fact one deals with a simpler dynamics than in the bulk (as we shall see n the following all these processes are described by one wave of toppling). This allows to determine in a clearest way the properties of the system and this reason shows the great theoretical importance of a complete understanding of this class of phenomena. In the context of standard critical phenomena, inhomogeneities, of which a boundary surface is a typical example, are well known to produce exponents different from those describing bulk singularities(Binder (1993)). The boundary magnetization of a semi–infinite spin system, for example, responds to the bulk field with a susceptibility $\chi_1 \sim |\frac{T-T_c}{T_c}|^{-\gamma_1}$ for $T \to T_c$, with γ_1 different from the bulk susceptibility exponent.

In this chapter evidence is provided that one can clearly distinguish between bulk and surface scaling exponents in SOC systems, in the same way as in equilibrium spin models. In spite of the considerable recent activity on SOC, the general possibility of peculiar scalings at the boundary has not been appreciated. As shown below, it is indeed in avalanche and return time distributions that novel boundary scaling behavior is revealed.

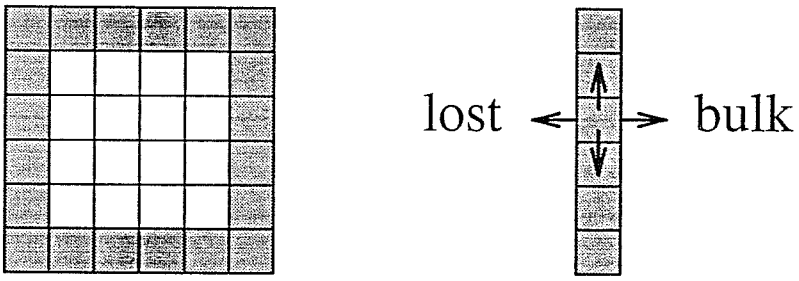

Figure 2.1: The layer considered for the statistics. On the right side the microscopical effect of such a boundary

2.1 Abelian Sandpiles

2.1.1 Numerical Data

An essential requirement of any sandpile model is the capability of dissipation at the borders, which allows the system to reach the critical state by elimination of the "sand" injected at random in the system. So far, in spite of the clear importance played by boundary conditions in SOC, very little attention has been paid to the possible consequences of the borders on critical behavior.

Consider a generic sandpile model, defined, as usual, on a finite box, Λ. For $j \in \partial\Lambda$, the boundary of Λ, the standard condition, allowing sand grains elimination, is of the Dirichlet form: $\Delta_{jj} = 2d$ for $j \in \partial\Lambda$. Of course, nothing prevents us from considering closed, Neumann boundary conditions (bc), i. e. $\Delta_{jj} = 2d - 1$ for j belonging to a subset of $\partial\Lambda$, e. g. one side or face. For such j's the stability condition becomes then $z_j \leq 2d - 2$. Closed bc alone do not allow sand elimination, which takes place through the other "Dirichlet faces".

So far, the determinations of τ, ν and D in the literature were all based on sampling avalanches starting anywhere in the whole system, and thus essentially in the bulk, but, as shown below, including surface contributions. This in sandpiles language means that we consider in our system all the phenomena related to sand injection in the first layer of our two dimensional system, that is the grey part ($\partial\Lambda$) in the left side of the FIG. 2.1. In this case the avalanche, started from the boundary will be considered in the boundary statistics. From the microscopical point of view the situation is represented in right part of FIG. 2.1, where the toppling is suffered only by three nearest neighbor of the considered site. It is worth to note that in this case all the toppling sites topple once in the avalanche. In fact, consider a process like those represented in FIG. 2.2; On the boundary, due to the absence of the fourth neighbor site, it can not occur. Furthermore, sites not belonging to $\partial\Lambda$ can not be the first to topple twice. Indeed, for them a second toppling would require that at least one of their 2d neighbors has already toppled at least twice. Since as previously seen this is not possible for sites belonging to $\partial\Lambda$, all site in the avalanche topple once. In a more figurative way one can describe this situation introducing the concept of "front wave". In this case all the avalanche are constituted by one front wave of toppling.

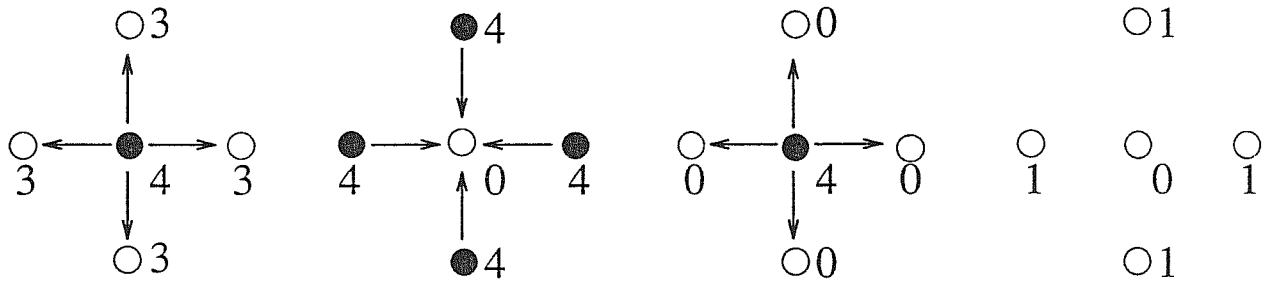

Figure 2.2: One process that cannot occur on the boundary of a system.

From numerical point of view it is easy to discover this mechanism. As previously introduced the long range space and time correlations are described by the two probability distributions $P(s) \propto s^{-\tau}$ and $Q(t) \propto t^{-y}$. In analogy with standard critical phenomena, we expect for boundary avalanches an appropriate $P_{\rm sur}(s, L)$, and $Q_{\rm sur}(s, L)$ with $\tau_{\rm sur}$ and $y_{\rm sur}$ possibly different from τ and y, respectively. Analogously, we shall define a $D_{\rm sur}$ and a $\nu_{\rm sur}$.

The quantities $P(s)$ and $Q(t)$ are directly accessible by computer simulations. $P(s)$, for example, is the normalized total number of avalanches of size s as the number of grain additions goes to infinity.

To reduce noise, these distributions are integrated over exponentially increasing bin lengths of s and t. In this way one deals with the two integrated distributions:

$$P'(s) = \int_1^s P(s')ds' \sim s^{1-\tau} \tag{2.1}$$

$$Q'(t) = \int_1^t Q(t')dt' \sim t^{1-y}. \tag{2.2}$$

Of course finite size effects are present, and they can be taken into account by considering size distribution $P'(s)$ in a box of linear size L, requiring that:

$$P'(s, L) = L^{-\rho_s} g_s(s/L^D) \tag{2.3}$$

ρ_s is a critical index and D is the fractal dimension of the avalanches. In this way L^D represents the natural unit measure for the avalanche sizes.

Note that in the limit $s/L^D \to 0$ (i.e. in the large scale limit), one requires that $P'(s, L)$ does not depend on L, that is

$$P'(s, L) \to P'(s). \tag{2.4}$$

SInce, in this limit the expected behavior is

$$P'(s, L) \propto s^{1-\tau}. \tag{2.5}$$

then

$$g_s(x) \propto x^{1-\tau}, \text{ and } \rho_s = D(\tau - 1). \tag{2.6}$$

Similar considerations holds for the time distribution too. In this case we have to consider the effect of finite size on the time distribution. If one introduces the dynamical exponent z that relates the size s of an avalanche with its duration trough the relation

$$t \propto s^z. \tag{2.7}$$

The value of z can be determined by noticing that, since

$$\int_0^{L^D} P(s)ds = \int_0^T Q(t)dt \tag{2.8}$$

substituting in this equation the relation of eq.(2.7) one obtains

$$L^{D(\tau-1)} \propto L^{z(y-1)} \tag{2.9}$$

and then

$$z = D\frac{(\tau-1)}{(y-1)}. \tag{2.10}$$

Since now the natural measure for duration avalanches is L^z, it holds

$$Q'(t,L) = L^{-\rho_t} g_t(t/L^z) \tag{2.11}$$

and the previous relation becomes:

$$\rho_t = z(y-1). \tag{2.12}$$

Where ρ_t and z are the counterpart of the ρ_s and D.

The exponent values can be determined numerically by collapsing curves related to different sizes in a plot of $P(s)L^{\rho_s}$ versus (s/L^D). Due to the avalanche compactness n $d = 2$ one can expect $D = 2$.

The collapse plot related to different sizes for the integrated size distribution probability $P'(s)$ is shown in FIG. 2.3 and for the duration time distribution $Q'(t)$ it is shown in FIG. 2.4. The main result is the presence of different scaling regimes for the boundary avalanche with respect to the bulk one. The values obtained in Dirichelet Boundary Conditions (DBC) are $\tau_{sur} = 1.51 \pm 0.05$ and $y_{sur} = 1.81 \pm 0.02$. with respect to the bulk values $\tau = 1.21 \pm 0.01$ and $y = 1.33 \pm 0.04$. This peculiarity arises also in higher dimensionality, for example in 3d systems, with respect to the bulk values $\tau = 1.40 \pm 0.05$ and $y = 1.61 \pm 0.04$ we obtain $\tau_{sur} = 1.73 \pm 0.05$ and $y_{sur} = 2.24 \pm 0.08$.

In boundary avalanches one deal with 1-front wave of toppling and this allow cleaner collapse plot, but it is worth notice that the dynamical properties of the phenomenon are not modified. In fact, on the basis of scaling arguments normally applied to the bulk, we expect $z_{\rm sur} = D(\tau_{\rm sur}-1)/(y_{\rm sur}-1) = 1.26 \pm 0.08$, where $z_{\rm sur}$ is the exponent relating the duration of border avalanches with their linear range. Our determination of $z_{\rm sur}$ is consistent with the estimated (Manna (1990), Manna (1991), Grassberger and Manna (1990))($z/D = 0.607 \pm 0.040$) and conjectured (Majumdar and Dhar (1992)) bulk values ($z = 5/4$). This consistency can be understood as follows. Indeed, in $d = 2$ the

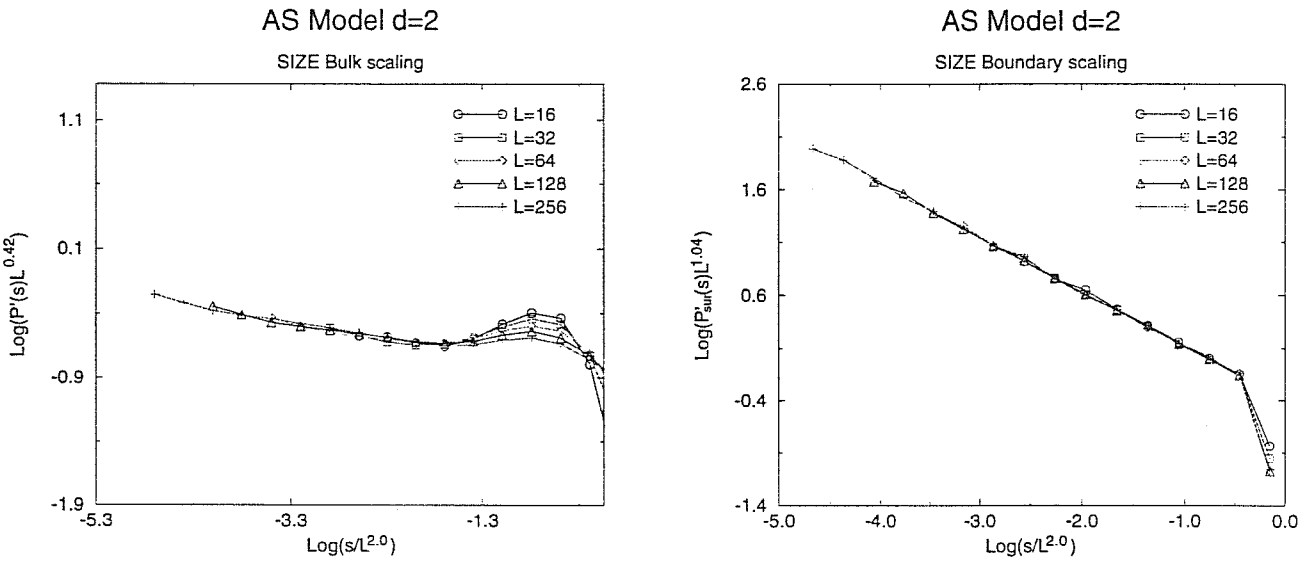

Figure 2.3: On the left data collapse for $P'(s,L) = \int_1^s P(s',L)ds'$. P' is scaled by $L^{D(\tau-1)} = L^{0.42}$, corresponding to $\tau = 1.21 \pm 0.01$ and $D = 2$. A direct estimate of D based on log–log fitting radius of gyration data versus s gives $D \simeq 1.96 \pm 0.06$. On the right data collapse for $P'_{sur}(s,L) = \int_1^s P_{\rm sur}(s',L)ds'$. P'_{sur} is scaled by $L^{D(\tau_{sur}-1)} = L^{1.02}$, corresponding to $\tau_{sur} = 1.51 \pm 0.05$ and $D = 2$. This value different from the bulk one signales the presence of a different boundary exponent.

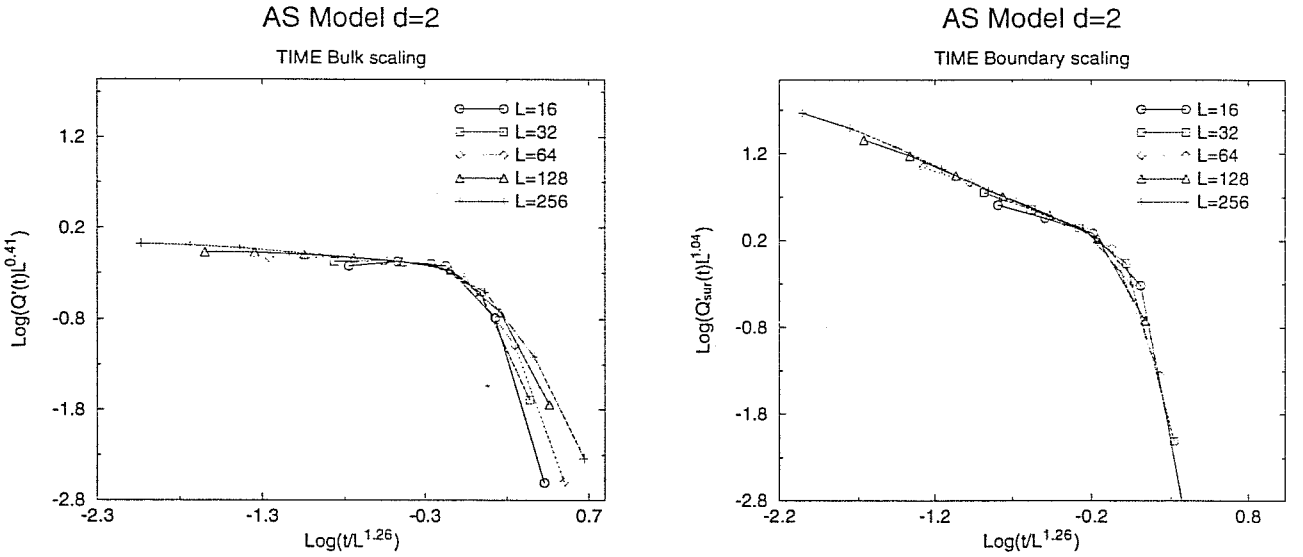

Figure 2.4: On the left data collapse for $Q'(t,L) = \int_1^t Q(t',L)dt'$. Q' is scaled by $L^{z(y-1)} = L^{0.41}$, corresponding to $y = 1.33$ and $z = 1.26 \pm 0.05$. On the right data collapse for $Q'_{sur}(t,L) = \int_1^t Q_{\rm sur}(t',L)dt'$. Q'_{sur} is scaled by $L^{z(y_{sur}-1)} = L^{1.04}$, corresponding to $y_{sur} = 1.81$ and $z = 1.26 \pm 0.05$.

Abelian Sandpile Model d=2				
		τ	y	D
Bulk values		1.21 ± 0.01	1.33 ± 0.04	1.96 ± 0.03
Surface values	NBC	1.27 ± 0.05	1.41 ± 0.05	1.97 ± 0.03
	DBC	1.51 ± 0.05	1.81 ± 0.02	1.96 ± 0.06
Abelian Sandpile Model d=3				
		τ	y	D
Bulk values		1.41 ± 0.03	1.62 ± 0.02	2.9 ± 0.1
Surface values (DBC)		1.70 ± 0.05	2.24 ± 0.08	2.9 ± 0.1

Table 2.1: Determination of avalanche exponent via direct estimate and collapse fit

bulk value of z is expected to coincide with the fractal dimension of red bonds(Coniglio (1989)) in the 0–state Potts spanning clusters(Dhar (1990)). Such dimension might remain unaltered whether or not the cluster backbone is supposed to connect points on the boundary(Coniglio (1982)).

To stress the difference between the behavior of boundary and bulk avalanche we have also introduced system with *reflecting boundaries* or Neumann Boundary Conditions (NBC). In this case one deals with probability distributions similar to the bulk case. In fact there are more similarities now in the microscopical process of toppling on the reflecting boundary and in the bulk. For example also the boundary avalanche are composed by different front waves also if their toppling threshold is lowered by one. We find for the exponents value $\tau_{sur} = 1.27 \pm 0.03$ for the size distribution and $y_{sur} = 1.42 \pm 0.04$ for the time one, which are consistent with the bulk scaling. The complete series of result is present in Table 2.1.

Obviously the above mentioned microscopic effect takes place irrespective of the particular kind of sandpile model considered. We here consider also the Restricted Critical Laplacian (RCL) Model. Also for this model, where toppling at site i requires that both z_i and the Laplacian $(\nabla^2 z)_i = \sum_j^{2d} z_j - 2dz_i$ simultaneously exceed thresholds a similar behavior occurs when one introduces dissipative Von Neumann conditions. The size probability distribution is shown in FIG. 2.5. FIG. 2.6 shows the behavior of $Q'(t)$

While in the bulk one gets $\tau = 1.31 \pm 0.04$ and $y = 1.48 \pm 0.03$ on the boundary with dissipative and reflecting boundary conditions, one has $\tau_{sur} = 1.60 \pm 0.06$, $y_{sur} = 1.97 \pm 0.03$ and $\tau_{sur} = 1.40 \pm 0.06$, $y_{sur} = 1.55 \pm 0.05$ respectively.. Also in this case all the final results are summarized in Table 2.2.

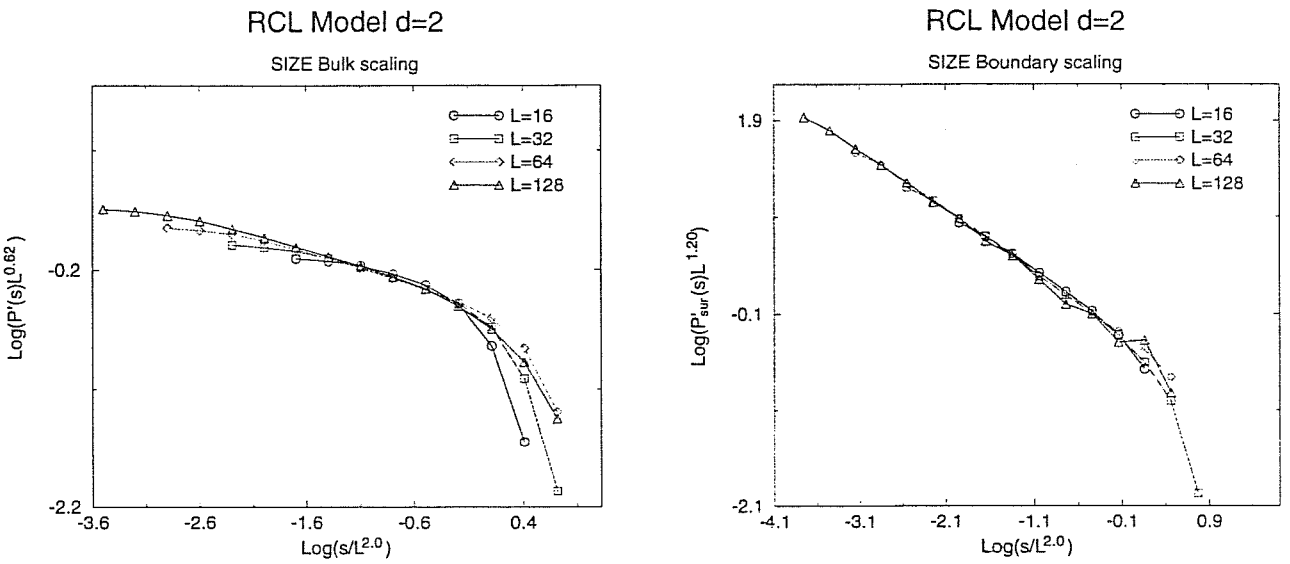

Figure 2.5: On the left data collapse for $P'(s,L) = \int_1^s P(s',L)ds'$. P' is scaled by $L^{D(\tau_{sur}-1)} = L^{0.62}$, corresponding to $\tau_{sur} = 1.31$ and $D = 2$. A direct estimate of D based on log–log fitting radius of gyration data versus s gives $D \simeq 1.97 \pm .03$. On the right data collapse for $P'_{sur}(s,L) = \int_1^s P_{\rm sur}(s',L)ds'$. P'_{sur} is scaled by $L^{D(\tau_{sur}-1)} = L^{1.20}$, corresponding to $\tau_{sur} = 1.60$ and $D = 2$.

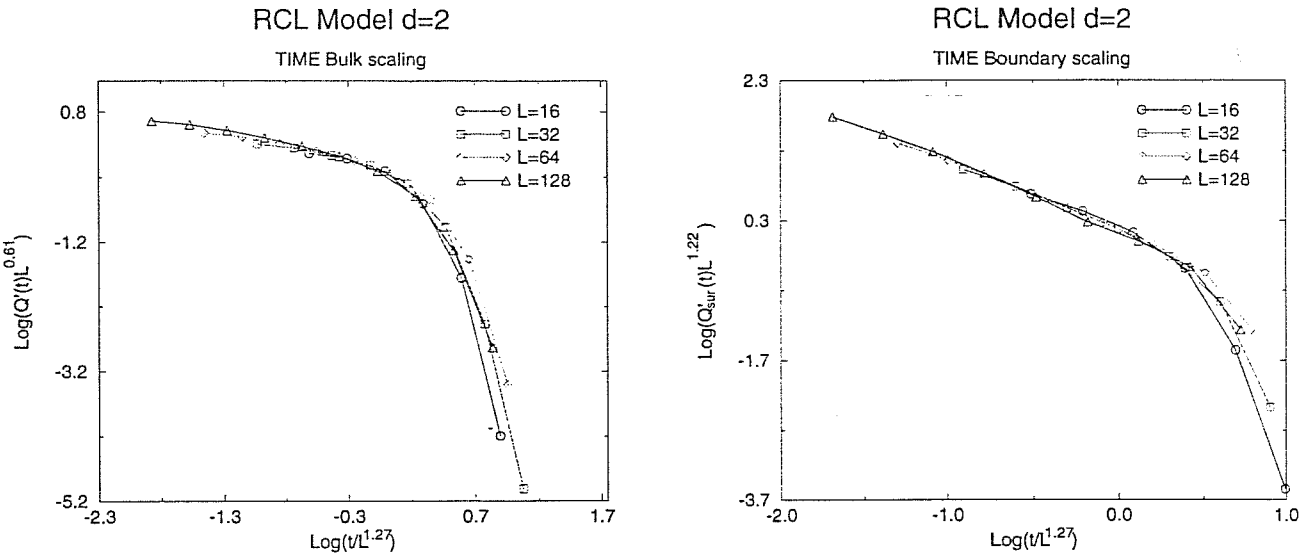

Figure 2.6: On the left data collapse for $P'(s,L) = \int_1^s P(s',L)ds'$. P' is scaled by $L^{D(\tau_{sur}-1)} = L^{0.62}$, corresponding to $\tau_{sur} = 1.31$ and $D = 2$. A direct estimate of D based on log–log fitting radius of gyration data versus s gives $D \simeq 1.97 \pm .03$. On the right data collapse for $P'_{sur}(s,L) = \int_1^s P_{\rm sur}(s',L)ds'$. P'_{sur} is scaled by $L^{D(\tau_{sur}-1)} = L^{1.20}$, corresponding to $\tau_{sur} = 1.60$ and $D = 2$.

Restricted Critical Laplacian Model 2d			
	τ	y	D
Bulk values	1.31 ± 0.04	1.48 ± 0.03	1.97 ± 0.03
Surface values (NBC)	1.40 ± 0.06	1.55 ± 0.05	1.97 ± 0.03
Surface values (DBC)	1.62 ± 0.06	1.97 ± 0.03	1.97 ± 0.03

Table 2.2: Determination of avalanche exponent via direct estimate and collapse fit

2.1.2 Mean Field Theory for Abelian Sandpiles

We shall now consider the mean field theory previously introduced regarding the boundary situation as a perturbation of the bulk stationary state. To do that we shall introduce an explicit dependence of the physical quantities from the position in the system. We consider a sem finite chain where an index i numbers sites starting from the origin. P_k^i represents the probability that $z_i = k$. Reaction rate equations can then be written as in the translationally invariant case. The order parameter also in this case is the toppling probability at site i, P_2^i, while the mean average is $\theta = \theta_c = 1/2$. To leading order in P_2^i one can put

$$P_0^i = \frac{1}{2} + \alpha_0^i P_2^i \tag{2.13}$$

$$P_1^i = \frac{1}{2} + \alpha_0^i P_1^i. \tag{2.14}$$

where α's are suitable coefficients, and $P_3^i = O((P_2^i)^2)$.

At the origin of the chain one gets

$$P_2^0 = \frac{1}{2}P_2^1 + (\theta - \frac{1}{2} - 2P_2^0)P_2^1 + h(\theta - 2P_2^0) - \frac{h}{2}P_2^1 \tag{2.15}$$

and for $i \geq 1$,

$$\begin{aligned} P_2^i = & -\frac{1}{2}P_2^{i-1}P_2^{i+1} - \frac{h}{2}(P_2^{i-1} + P_2^{i+1}) + (\theta - 2P_2^i)(P_2^{i-1} + P_2^{i+1}) + \\ & \frac{1}{4}P_2^i(P_2^{i-2} + P_2^{i+2}) + h(\theta - 2P_2^i) + \frac{h}{4}(P_2^{i-2} + 2P_2^i + P_2^{i+2}), \end{aligned} \tag{2.16}$$

where the α's have been eliminated by use of $\alpha_0^i + \alpha_1^i + 1 \simeq 0$ (probability conservation), and $\theta \simeq 1/2 + \alpha_1^i P_2^i + 2P_2^i$.

By disregarding eq.(2.15), and turning to standard notations, a translationally invariant solution of eq.(2.16) (true deeper inside in the bulk), with $P_2^i \equiv P_2$, satisfies

$$4(P_2)^2 + (1 - 2\theta + 2h)P_2 - h\theta = 0$$

which is easily seen to imply

$$P_2 \sim (1/2)(\theta - \theta_c)^{-1}, \quad \theta \geq \theta_c \Rightarrow \beta = 1, \tag{2.17}$$

$$\chi \equiv \partial P_2/\partial h \sim (1/4)(\theta - \theta_c)^{-1} \Rightarrow \gamma = 1. \tag{2.18}$$

Inhomogeneous solutions of eqs.(2.15),(2.16) are most easily discussed in terms of

$$\chi_i \equiv \partial P_2^i/\partial h|_{h=0}. \tag{2.19}$$

One finds a solution of the form

$$\chi_n = \chi + \delta \exp[-nq] \tag{2.20}$$

with $q \sim |\theta - \theta_c|^{1/2}$ and $\chi_0 \sim |\theta - \theta_c|^{-1/2}$. Thus $\gamma_0 = 1/2 \neq \gamma$ in MF, while the behavior of the reciprocal "penetration length" q, reveals directly the expected $\nu = 1/2$ (Tang and Bak (1988)b).

Since $D = 4$ in MF (Tang and Bak (1988)b), we conclude that

$$\tau_{\rm sur} = 2 - \gamma_0/\nu D = 7/4, \tag{2.21}$$

to be compared with the bulk $\tau = 3/2$.

A similar calculation gives γ_0 with Neumann bc at site 0. In this case P_1^0 replaces P_2^0 everywhere and eq.(2.15) is suitably modified. Again a solution of the form (2.20) is found, this time with $\chi_0 \equiv \partial P_1^0/\partial h|_{h=0} \sim |\theta - \theta_c|^{-1}$. Thus, in MF closed conditions give $\gamma_1 = \gamma = 1$. MF calculations can of course be carried on also in higher d, yielding the same γ_1's.

2.2 Biological Models and Boundary Effects

Bak and Sneppen (BS) (Bak and Sneppen (1993), Flyvbjerg et al. (1993)) introduced a SOC model describing an ecology of interacting species evolving by mutation and selection. This model provides an illustration of the mechanisms determining intermittency (punctuated equilibrium (Eldredge and Gould (1988))) and scaling (Raup (1986)) in the evolutionary activity. Below we show that such intermittency and scaling have a richer structure than appreciated so far. Indeed, at the level of universal properties, it is possible to draw a clear cut distinction between evolutionary activities occurring in the "bulk" and at the "boundary" of an ecology. Bulk and boundary refer to different locations of a given species within the network of interactions with other species conditioning its evolution.

In a coarse grained, simplified description, BS associate to the i-th species of an ecology a single fitness parameter, x_i, $(0 < x_i < 1)$. x_i represents the ability of species i to survive: the higher x_i, the higher the barrier to overcome in order to switch a mutation in the species. A genetic mutation changes the barrier of the species and modifies also the barriers of the other species interacting directly with it. This interaction should represent the fact that two species, take part in the same food chain. Sites of a lattice can be used to represent the species: in this case nearest neighbor (n.n.) species can be assumed as directly related biologically, and thus interacting.

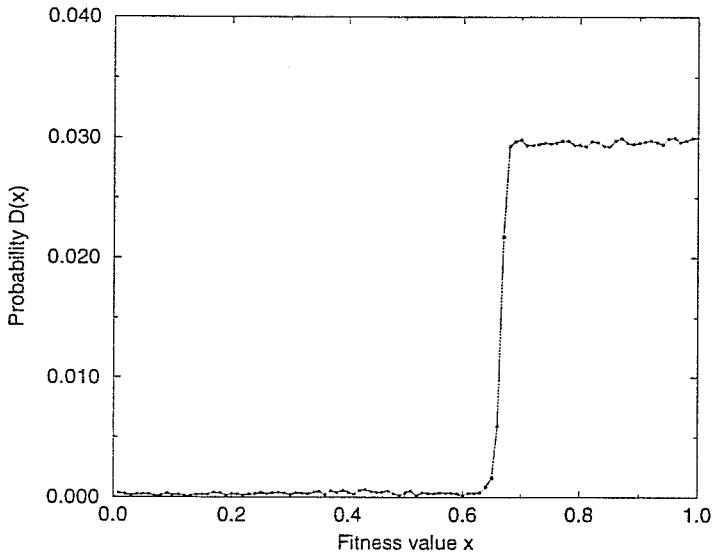

Figure 2.7: The fitness distribution for site belonging to the boundary. Within the error bars the sharp threshold occurs at the same value of the bulk case.

An avalanche corresponds to a sequence of mutations of events causally related to the mutation of a given ancestor $x_{i_{min}}$ The probability P that an avalanche involves s mutations is expected to vary asymptotically as $P(s) \propto s^{-\tau}$ in the SOC state.

The dynamical evolution rules of the original model are as follows. Starting from an initial fitness landscape, the site i with lowest x, i_{min}, is selected to undergo a mutation and its fitness $x_{i_{min}}$ is modified: a new random number in the interval $[0, 1]$ is chosen with uniform probability distribution. Due to the interaction, also some neighbors of i_{min} get modified fitnesses, as effect of the previous mutation. For a linear chain with n.n. interactions this implies that $x_{i_{min}-1}$ and $x_{i_{min}+1}$ are replaced by new randomly chosen x's always with the same distribution as before. In this class of models the study of the boundary refers to the study of extremal species in the food chain. We expect a different behavior for the species that are only predator and not prey and viceversa.

2.2.1 Numerical Data

In order to identify boundary scaling beyond MF, we performed systematic simulations with open, n.n. BS chains of different lengths ($N \leq 10^3$). First we verified that the distribution of boundary x's in the stationary state is essentially unaltered with respect to that of the periodic, bulk case, and displays the same sharp threshold at $x_c = 0.665 \pm 0.015$ (Bak and Sneppen (1993)). This test is shown in FIG. 2.7.

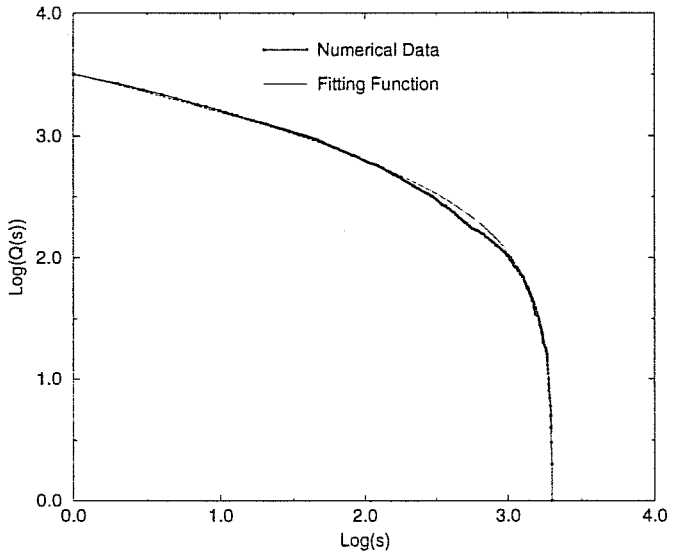

Figure 2.8: $Q(s) = \int_s^{s^{max}} P(s')ds'$ is the integrated distribution; the fitting form is $As^{1-\tau'} + C$ with $\tau' = 1.25 \pm 0.01$ ($N = 1000$).

By selectively sampling avalanches starting near the boundaries or in the interior of the chains, we extrapolate a boundary exponent $\tau' = 1.25 \pm 0.01$ (see FIG. 2.8).

This value is clearly different from the bulk one $\tau \simeq 1.08$ (de Boer, Jackson and Wettig (1995)). So, also in the n.n. model boundary avalanches have a probability decaying more rapidly at large s, than in bulk. A further characterization of boundary scaling is given by the distribution of first return times of activity (x taking the minimum value) at the same boundary site. These times are distributed as $t^{-\tau'_{first}}$, with $\tau'_{first} = 1.35 \pm 0.01$, different from the bulk value $\tau_{first} = 1.58$ (Maslow, Paczuski and Bak (1994)). By recording the times of all subsequent returns of activity one can also obtain a distribution $\propto t^{-\tau'_{all}}$, with $\tau'_{all} = 0.65 \pm 0.01$, again distinct from $\tau_{all} = 0.42$ in bulk (Maslow et al. (1994)). Such boundary exponents are consistent with a scaling relation $\tau'_{first} + \tau'_{all} = 2$, already satisfied in the bulk (Maslow et al. (1994)). Since the validity of such relation should not depend on the position considered along the chain, the above consistency is further indication of the good quality of our determinations. Data concerning these exponents are shown in FIG. 2.9. We conclude that at the boundaries activity has a different pattern of intermittency. First returns are shifted towards longer time scales. On the other hand, once the boundary has been reached, activity remains more easily trapped there, giving rise to concentrated sequences of returns. In applications of the BS model, the choice of a more or less regular network of interactions remains to some extent arbitrary, and should not matter for universal properties, unless the long-range limit of a random neighbor model is assumed. However, the distinction elucidated above between bulk and boundary species, appears to have important consequences, affecting the universal scaling

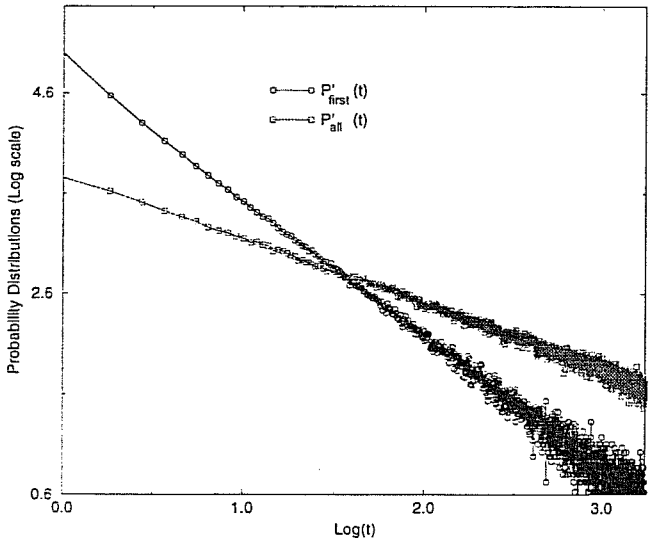

Figure 2.9: *first* and *all* return times probabilities at boundary sites. Statistics refer to 10^9 mutations in the whole chain.

features of evolution. Thus, boundary scaling offers additional, deeper insight into the properties of biological models and widens the context of their possible comparison with paleontological data. We showed here that within the framework of punctuated equilibrium there exists a well defined boundary scaling in addition to the bulk one.

2.2.2 Branching Process Theory

Branching processes (BP) occur in many fields of physics and biology, ranging from nuclear reactors, to polymers and population dynamics (Harris (1963)). Within the context of self–organized criticality (SOC), BP, or correlated versions of them, are expected to underlie the physics of many models, describing sandpiles (Bak et al. (1987), Alstrøm (1988), Pietronero et al. (1994), Vespignani, Zapperi and Pietronero (1995)), earthquakes (Olami, Feder and Christensen (1992)), river networks (Rodriguez-Iturbe and Rinaldo in press (1996), Scheidegger (1967)) or species mutations (Bak and Sneppen (1993)). Avalanches are often believed to be described in terms of critical BP in the mean field (MF) limit. We now, introduce and solve an inhomogeneous generalization of the standard BP. This allows us to determine peculiar scaling properties of BP at boundaries. In a unifying perspective, such properties provide a substantial extension of previous MF descriptions of SOC models. In a standard MF description, on the other hand, the notion of position is completely lost and one can, e.g., choose to replace the fitnesses of a certain number, $K-1$, of other species selected at random, besides i_{min}. This random neighbor (r.n.) model is the only one for which a MF treatment of avalanches could be set up so far (Flyvbjerg et al. (1993), de Boer, Derrida,

Flyvberg, Jackson and Wettig (1994)). However, the lack of any meaning for distance in this MF is a quite strong limitation, to the extent that the very notion of SOC can be legitimately questioned (de Boer et al. (1995)). Avalanches correspond to sequences of mutations in which the minimal x species is always found among those resulting from genetic changes in previous stages. Consider to start from a given ancestor mutation for which $x_{i_{min}} = \lambda$. Since λ was the minimal x value in the system, according to the previous definition, every x does not exceed λ for the whole duration of the avalanche. The probability P that an avalanche involves s mutations is expected to vary asymptotically as $P(s) \propto s^{-\tau}$ in the SOC state, in which for all avalanches λ attains the value x_c, the sharp threshold of the stationary x-distribution (Flyvbjerg et al. (1993)).

So far, in models like the n.n. chain, τ and similar exponents have always been discussed as bulk quantities (de Boer et al. (1995), Boettcher and Paczuski (1996)), i.e. considering statistics of avalanches starting everywhere within large, periodic systems. Compared to those in the bulk, a species at one end of an open chain (e.g., main predator, or basic level of microscopic life) has less species directly or indirectly connected to it. The paths through which dynamical correlations can propagate starting from an initial mutation on the boundary are also reduced. In this way, e.g., in semi-infinite geometry, boundary avalanches could be characterized by peculiar exponents, different from the bulk ones. Demonstrating boundary scaling in models like the BS one is a challenge, especially at the analytical level. Indeed, in the context of SOC with extremal dynamics, exact results are essentially limited to the above mentioned MF treatment (de Boer et al. (1994), Boettcher and Paczuski (1996)). Consideration of boundary effects or other inhomogeneities clearly requires a meaningful notion of distance. We achieve this within a novel MF description of the BS model with n.n. interactions, generalizing the standard BP studied in probability theory (Harris (1963)).

The BP description can be obtained regarding the probability to "generate" $0, 1, 2...$ species as the bifurcating probability to generate $0, 1, 2...$ sons. The root of the tree is the species ancestor in the avalanche. The criticality is ensured as soon as the probability to get an infinite tree becomes different from 0.

We now introduce the standard BP theory (Harris (1963), Feller (1971)), we consider all the species able to produce new particles

- a single particle forms the original $0-$th generation, whose size is S_0=1;
- every particle has probability $p_k(k = 0, 1, 2, 3, 4...)$ to produce k new particles;
- We call *generating function* $G(z)$ the sum

$$G(z) = p_0 + p_1 z + p_2 z^2 + ... \tag{2.22}$$

  if $G(z)$ converges in some interval $\{-z_0 < z < z_0\}$ for the given $\{p_0, ..., p_n, ...\}$ sequence of real numbers.

- Consider $\mu = \frac{dG}{dz}|_{z=1}$. $\mu = \sum_{k=0}^{\infty} k p_k$ = expected number of directed descendants.

- if $\mu \leq 1$ the process dies out
- if $\mu > 1$ exist a finite probability to have infinite process

Those present are the basic concepts in the BP theory. Now we want to point out the relation of BP with respect to the avalanche size in BS. To deal with the analogous of the avalanche one has to introduce the total number of descendants $Y_n = S_0 + S_1 + S_2 + ... + S_n$, at the n^{th} generation, where the random variable Y_n is related to the event S_i =the size of the i^{th} generation is equal to S_i

An avalanche can be identified with a tree, where nodes represent species mutating within the avalanche. From each node as many branches depart, as there are species undergoing genetic change directly due to a mutation taking place at that node. The same species can act as node more than once within an avalanche. *The complex structure of correlations of the BS model is simplified in MF by assuming that, at each node, well defined, independent probabilities exist for all branchings compatible with the dynamical rules.* Avalanches are generation trees, whose distribution in number of generating individuals, s, is given by P. The existing MF approach clearly can not address exponents for diverging lengths, as defined, e.g., in a Landau approach to standard criticality. We introduce a characteristic length within MF through boundaries breaking translation invariance and leading to a position dependence of the BP description. Standard BP theory deals with the discrete transform

$$\tilde{P}(z) = \sum_{s=1}^{\infty} P(s) z^s, \tag{2.23}$$

on which the scaling of $P(s)$ produces singular behavior of the form

$$\tilde{P}(z) = 1 - c(1-z)^{\tau-1} + \textit{less singular terms} \tag{2.24}$$

for $z \to 1^-$. In eq.(2.24) c is a suitable positive constant and the last term on the r.h.s. indicates regular or subleading singular terms. Without making reference to relative locations of the species along the chain, the standard BP assumes that well defined probabilities, p_i $(i = 0, 1, 2, ...K)$, apply to the events in which a given species undergoing mutation triggers subsequent genetic changes, in the same avalanche, in i species, possibly including itself. Independence of branchings leads to validity of Watson's functional equation (Harris (1963))

$$\tilde{P}(z) = zG(\tilde{P}(z)) \tag{2.25}$$

In fact, the probability to have $n+1$ events can be written as

$$P(n+1) = \sum_{i=1}^{k} p_i \sum_{\{n_j\}:\sum_{j=1}^{i} n_j = n} \prod_{j=1}^{i} P(n_j) + \delta_{n0} p_0 \tag{2.26}$$

Using the definition (2.23) of discrete transform we get

$$\tilde{P}(z) = \sum_{n=0}^{\infty} z^{n+1} P(n+1) = z \sum_{i=1}^{k} p_i \sum_{\{n_j\}:\sum_{j=1}^{i} n_j = n} \prod_{j=1}^{i} z^{n_j} P(n_j) + z p_0 \tag{2.27}$$

and we are able to find eq.(2.25) since the above expression becomes

$$\tilde{P}(z) = \sum_{n=0}^{\infty} z^{n+1} P(n+1) = z \sum_{i=1}^{k} p_i \sum_{n_1=0}^{\infty} .... \sum_{n_i=1}^{\infty} \prod_{j=1}^{i} z^{n_j} P(n_j) + z p_0 \tag{2.28}$$

$$= z \sum_{i=0}^{k} P_i (\tilde{P}(z))^i = z G(\tilde{P}(z)) \tag{2.29}$$

with $G(y)$ previously defined (see eq.(2.22). Eq.(2.25) imposes a constraint on the p_i's consistent with a singularity of the form (2.24). Such constraint reads $G'(1) = 1$ and automatically fixes $c = \sqrt{2/G''(1)}$ and $\tau = 3/2$ as the only compatible exponent (a condition analogous to our $G'(1) = \sum_i i p_i = 1$, is also at the basis of the RG approach to sandpiles (Pietronero et al. (1994)) where it enforces energy balance).

In fact, from eqs.(2.24)-(2.25) it follows $1 = \tilde{P}(1) = G(1)$. Expanding in the neighborhood of 1 one get $z = 1 - \delta z$ and $\tilde{P} = 1 - \delta \tilde{P}$. Substituting in the previous equation one gets

$$\delta \tilde{P} = G'(1)\tilde{P} + \delta z - \frac{G''(1)}{2} \delta \tilde{P}^2 + O(\delta \tilde{P} \delta z) \tag{2.30}$$

Thus at the leading order

- $G'(1) < 1 \Longrightarrow \delta \tilde{P} = \frac{\delta z}{1 - G'(1)}$. It has to be noticed that if $P(n) = z_0^n A$ where $z_0 < 1$ ($P(n)$ vanishes exponentially) then $A = \frac{1-z_0}{z}_0$, $\sum_{n=1}^{\infty} P(n) = 1$, and $\tilde{P}(z) = z \frac{1-z_0}{1-z_0 z} \overset{z \cong 1}{=} 1 - \frac{\delta z}{1-z_0} + O(\delta z^2)$. From that one gets $z_0 = G'(1)$.
- $G'(1) = 1 \Longrightarrow \delta \tilde{P} = -\sqrt{\frac{2}{G''(1)}} (\delta z)^{1/2}$, from which it follows $c = \sqrt{2/G''(1)}$ and $\tau = 3/2$ if $\tau < 2$.

This result for τ is largely universal with respect to different choices of the parameters p_i and only relies on the analyticity of G. A natural choice is $p_i = \binom{K}{i} x_c^i (1 - x_c)^{K-i}$. In fact the x distribution is fermilike with the threshold equal to x_c. Then p_i can be regarded as the probability to have only i species under the threshold.

In the random neighbor model $x_c = 1/K$ (Flyvbjerg et al. (1993)), implying $G'(1) = 1$. Replacing x_c by $\lambda < x_c$ would amount to consider off-critical avalanches ($G'(1) < 1$), with $x_c - \lambda$ playing the role of temperature-like field. Let us consider now a semi-infinite sequence of species on a chain. To each species is associated an integer coordinate $j = 0, 1, 2, ...$ In a n.n. model the presence of the boundary requires to allow for a j-dependence of the avalanche size distribution: thus, $P_j(s)$ or $\tilde{P}_j(z)$ will describe avalanches starting at site j along the chain. This situation can still be analyzed within what we call here inhomogeneous BP. Since, as a consequence of a mutation at $j \geq 1$, at most 3 species can be further involved in the avalanche ($K = 3$ for the n.n. case), probabilities p_0, p_1, p_2, and p_3 will describe the possible outcomes of such a mutation. For convenience, and consistently with the above expressions of the p_i's in terms of x_c, one can

further assume that with probability p_0, no further mutation takes place in the avalanche; with probabilities $p_1/3$ and $p_2/3$ the avalanche propagates, respectively, in any one and any two of the species in the set $\{j-1, j, j+1\}$; finally, p_3 is the probability that the avalanche involves all three species. In the MF spirit it is also sensible to assume j-independence for the p_i's as long as $j \geq 1$. Of course, there should be different probabilities p'_i for $j = 0$, where the boundary imposes $p'_3 = 0$. A possible choice made below is to assign $p'_0 = p_0 + \frac{1}{3}p_1, p'_1 = \frac{2}{3}p_1 + \frac{2}{3}p_2$ and $p'_2 = \frac{1}{3}p_2 + p_3$ at $j = 0$, again implying equivalence of $j = 0$ and $j = 1$ with respect to single branch outcomes.

With the above positions, eq.(2) is replaced by a full hierarchy of equations:

$$\begin{aligned}
\widetilde{P}_0(z) &= z\left(p'_0 + \frac{p'_1}{2}\left(\widetilde{P}_0(z) + \widetilde{P}_1(z)\right) + p'_2\left(\widetilde{P}_0(z)\widetilde{P}_1(z)\right)\right) \\
\widetilde{P}_j(z) &= z\left(p_0 + \frac{p_1}{3}\left(\widetilde{P}_{j-1}(z) + \widetilde{P}_j(z) + \widetilde{P}_{j+1}(z)\right) + \frac{p_2}{3}\left(\widetilde{P}_{j-1}(z)\widetilde{P}_{j+1}(z) + \right.\right. \\
&\quad \left.\left. \widetilde{P}_j(z)\widetilde{P}_{j+1}(z) + \widetilde{P}_{j-1}(z)\widetilde{P}_j(z)\right) + p_3\left(\widetilde{P}_{j-1}(z)\widetilde{P}_j(z)\widetilde{P}_{j+1}(z)\right)\right);\ j \geq 1. \qquad (2.31)
\end{aligned}$$

$\widetilde{P}_j(z)$ should converge to the bulk solution of eq.(2.25), for j approaching infinity. Thus, it is advantageous to adopt the following ansatz:

$$\tilde{P}_j(z) = \tilde{P}(z) + \Delta(z)e^{-q(z)j} + l.s.t. \qquad (2.32)$$

where q is an inverse length and $\tilde{P}$ is the solution of eq.(2.25). As shown below, the assumed j-independence of Δ and q is consistent, as corrections to it would only involve subleading singular terms for $z \to 1^-$. By substituting eq.(2.32) into eqs.(2.31) one can deduce singular behaviors of $\tilde{P}_0$ and q. For $z \to 1^-$, we expect $\Delta(z) \sim (1-z)^\alpha$ and $q(z) \sim (1-z)^\beta$, with α and β suitable exponents. After substitution in eqs.(2.31) for $j \geq 1$ one gets

$$1 = \frac{z}{3}(1 + 2\cosh q(z))\left(G'\left(\tilde{P}(z)\right) + \frac{\Delta(z)}{2}G''\left(\tilde{P}(z)\right)\right) + l.s.t. \qquad (2.33)$$

Taking into account that $\tilde{P}$ has the form (2.24) with $\tau = 3/2$, the leading singular terms in eq.(2.33) give:

$$\frac{q(z)^2}{3G''(1)} + \frac{1}{2}\Delta(z) = a(1-z)^{1/2} + l.s.t.; \qquad (2.34)$$

where $a = c$ of eq.(2.24). The same kind of substitution in the first of eqs.(2.31) leads to

$$\Delta(z) = a(1-z)^{1/2} - b\Delta(z)q(z) + l.s.t. \qquad (2.35)$$

with $b = 1$. Eq.(2.34) and eq.(2.35) determine both α and β above. In particular $\tilde{P}_0(z)$ takes the form

$$\tilde{P}_0(z) = \tilde{P}(z) + \Delta(z) + l.s.t. = 1 - b(1-z)^{3/4} + l.s.t. \qquad (2.36)$$

In general $b = \frac{p'_1/2+p'_2}{2(p'_1/2+p'_2)-1}$ and the results (2.34) and (2.36) make sense for $\sum ip'_i < 1$. This condition is satisfied by our choice of p'_i's, which further acquire the form $p'_i = \binom{K-1}{i} x_c^i(1-x_c)^{K-1-i}$, if the p_i's are expressed in terms of x_c as discussed above. Thus, the threshold x_c for the distribution of

x values at the borders in the stationary state is assumed to be the same as in the bulk. According to eqs.(2.24) and (2.36)

$$P_0(s) \sim s^{-7/4} \tag{2.37}$$

Thus, in our MF description the BS SOC state is characterized by a boundary scaling with an exponent $\tau' = 7/4$ different from the bulk one. Boundary avalanches of course suffer more rapid extinction and their distribution decreases faster for large s. It is interesting to note that, by exploiting analogies with magnetic systems, $\tau' = 7/4$ has been predicted recently within a MF approach to border avalanches in Abelian Sandpile Models (ASM) with Dirichelet boundary conditions (Stella et al. (1995)). This lends further support to the idea that in ASM a BP description underlies the statistics of avalanches in the MF limit, for which also $\tau = 3/2$ is expected (Tang and Bak (1988)b). A further consequence of eqs.(2.34), (2.35) is the singularity:

$$q(z) \sim (1 - z)^{1/4}. \tag{2.38}$$

Thus, the penetration length of the border disturbance, q^{-1}, diverges for $z \to 1^-$. In MF treatments of inhomogeneous equilibrium models, quantities like q^{-1} show the same divergence with temperature as classical correlation lengths. By interpreting z as a standard fugacity for a polymer, one deduces from eq.(2.38) a correlation length exponent $\nu = 1/4$. This is indeed the classical ν of branched polymers (Harris and Lubensky (1981)). Of course the definition of ν for a SOC system requires one to identify physically meaningful parameters describing the approach or the departure from criticality. For BS avalanches such a parameter is the temperature-like deviation $x_c - \lambda$. By introducing λ-dependent p_i's and p_i''s in our equations, the result (2.38) can be converted into $q(\lambda, z = 1) \sim (x_c - \lambda)^{1/2}$, which implies $\nu = 1/2$. Remarkably enough, this is the classical ν exponent expected for ASM (Tang and Bak (1988)b). This and the above mentioned coincidence of τ' strongly support the idea that BP fully underlie also the MF description of ASM avalanches.

3 External Field and Self–Organized Systems

In this chapter we shall analyze the role of an external field as for example a temperature field-like parameter in the physics of Sandpiles. As previously noted, the Sandpiles model and the BS model are deterministic cellular automata. Our purpose is to introduce the randomness in the dynamics linking the toppling process to the energy released by the presence of an external field. The aim of this research is to test the robustness of such models with respect to external perturbations. It is an important issue to investigate how robust are the critical steady states of these sandpile models under changing of the dynamical rules which define them. For example it has been pointed out (Hwa and Kardar (1992)) that conservation laws are essential to ensure a critical steady state (see also (Cafiero, Loreto, Pietronero, Vespignani and Zapperi (1995))). Here we shall investigate the role of a parameter T, analogous to the temperature, whose introduction will mild the sharp threshold always present in sandpiles models (Vergeles (1995)). Our result for the Sandpiles show the existence of a new critical state connected with the presence of the Temperature field. This is different from the behavior of BS Model in which the criticality disappears as soon as the external field is switched on. Also in this case we have performed a MF treatment of the phenomenon and we are able to produce the numerical data supporting our results.

3.1 Temperature Sandpile Model

The standard Abelian sandpile model (Dhar (1990)) is a cellular automaton on a box in the d-dimensional hypercubic lattice. At a given time t every site i stores column of $z_{i,t}$ grains of sand. The microscopic dynamics takes place according to the following simple rule.

If at time t, $z_{i,t} \geq z_c = 2d$, the site i topples, giving one grain of sand to each of its $2d$ nearest neighbors. Thus, at time $t+1$. $z_{i,t+1} = z_{i,t} - 2d$ and $z_{i+\delta,t+1} = z_{i+\delta,t} + 1$, where δ runs over the nearest neighbours of i.

As an implication of this rule, the new updated sites may topple at time $t+1$. A chain of s sequential toppling processes is called an avalanche of size s. When an avalanche stops, a new grain

of sand is added to the system from outside on a randomly chosen site.

In our hot sandpile *also a site i with height below z_c can topple* at time t with probability

$$\rho(i,t) \propto e^{-(z_c - z_{i,t})/T} \tag{3.1}$$

if one of its nearest neighbours topples at time $t-1$ and the updating of toppling sites is performed in parallel. Here T is the "temperature" of the system. In this toppling process only $z_{i,t}$ nearest neighbours (randomly chosen) gain one sand grain. The avalanche stops at time t as soon as all sites have $z_{i,t} < z_c$ and no toppling occurs due to the temperature. It has to be noticed that at any time after the avalanche stops the state of the system is stable. In fact, we suppose that a kind of inertia keeps together the grains in states with $z_{i,t} < z_c$ for all i. The energy gain given by the presence of temperature can be used only if the site is on the front of an avalanche, that is if it "suffers" a toppling. In this way a site with $z_{i,t} < z_c$ has the possibility to topple only when the avalanche touches its neighbours. This rule keeps the sisytem stable with respect to the time evolution. In fact if there is no rain there is no external flow.

3.2 Mean Field Approach

In order to determine the influence of the "temperature" we have generalized the mean field approach of ref. (Tang and Bak (1988)b) to include the rule (3.1). In this paper, as well as in (Tang and Bak (1988)a), a formal analogy with ordinary critical phenomena is used. The role of the magnetic field h is played by the external flux of sand [1]. The flux of sand within the system is the toppling probability and can be viewed as the order parameter. Finally, the response of the system to the external field, that is the mean value of the avalanches size, is the susceptibility χ. These physical quantities allow to characterize the criticality of the system and, as usual (Tang and Bak (1988)b), calculation will be performed in one dimension ($d = 1$). generalization to higher dimensions being straightforward.

We define the probability A that a site is active, that is, it can topple. together with the probability $I = 1 - A$ to be inactive. Let P_z be the fraction of sites with an height variable z. which becomes the probability to find a site i with height $z_i = z$ for infinite size systems. The average height is defined as

$$\theta_A = \sum_z z P_z. \tag{3.2}$$

and will play a role similar to the temperature for ordinary critical phenomena (Tang and Bak (1988)b). In $d = 1$, a site whose height is two or more will certainly topple, whereas a site whose height is one will do that with a probability $\rho = e^{-1/T}$. Henceforth, the toppling probability A can

[1] The role of h in SOC models has been clarified in ref. (Hwa and Kardar (1992)). Here we will consider the $h \to 0$ limit only.

be expressed in terms of the P_z through the equation:

$$A = P_1 \rho A_C + P_2 + P_3 \tag{3.3}$$

and thus

$$I = P_0 + P_1(1 - \rho A_C). \tag{3.4}$$

The factor A_C is there to ensure a causal connection in the sequence of topplings. This term is not equal to $(1 - I^2)$ (the probability that at least one of the neighbors sites is active at the previous time), but considering all the possible incompatibilities it is equal to

$$A_C = 2(P_2 + P_3)(P_0 + P_1)(P_0 + P_2). \tag{3.5}$$

The probability to be inactive given in eq.(3.4) is obtained imposing the normalization condition $\sum_{i=0}^{3} P_i = 1$. This means that the probability to have heights larger than three is neglected (Tang and Bak (1988)b) in the stationary state.

We are interested in the small temperature behavior, i.e. $\rho \to 0$, and in the limit of small external flux, i.e. $h \to 0$. As a consequence in the stationary state P_2 and P_3 are small parameters. In fact, at a fixed value of h the effect of the temperature is to decrease P_2 and P_3, since topplings are more probable.

In this regime at the leading order we find:

$$\tilde{P}_A \simeq P_2 + P_3 + 2\rho P_1 P_0 P_2 + 0(\rho P_3) \tag{3.6}$$

$$\tilde{P}_I \simeq P_0 + P_1 - 2\rho P_1 P_0 P_2 + 0(\rho P_3). \tag{3.7}$$

We can write now the reaction diagram in FIG. 3.1 where all the possible processes of income and outcome in the state P_z are evaluated.

It is worth noticing that in the diagram $P_I = P_0 + P_1 - \rho P_1(P_2 + P_3)$ and $P_A = P_0 + P_1 - \rho P_1(P_2 + P_3)$ are the probabilities that a site nearest neighbors is respectively stable or critical

Following this reaction diagram we write the following MF equations for the stationary state

$$P_2(1 - P_2)^2 - hP_2 + 2\boldsymbol{\rho P_0 P_1^2 P_2} = 2P_0P_2(1 - P_2) + 2P_0P3 + hP_0 + P_0P_2^2 - 2hP_0P_2 \tag{3.8}$$

$$\begin{aligned} 2P_0P_2(1 - P_2) + 2P_0P_3 + hP_0 + 2P_2^2 + P_3 + hP_2 - 4hP_0P_2 - 4\boldsymbol{\rho P_0 P_1^2 P_2} &= \\ = 2P_1P_2(1 - P_2) + P_1P_3 + hP_1 + P_1P_2^2 - 2hP_1P_2 & \end{aligned} \tag{3.9}$$

$$2hP_0P_2 - 4hP_1P_2 + 2P_1P_2(1 - P_2) + 2P_1P_3 + hP_1 + P_0P_2^2 + 2\boldsymbol{\rho P_0 P_1^2 P_2} = P_2 \tag{3.10}$$

$$P_1P_2^2 + 2hP_1P_2 = P_3 \tag{3.11}$$

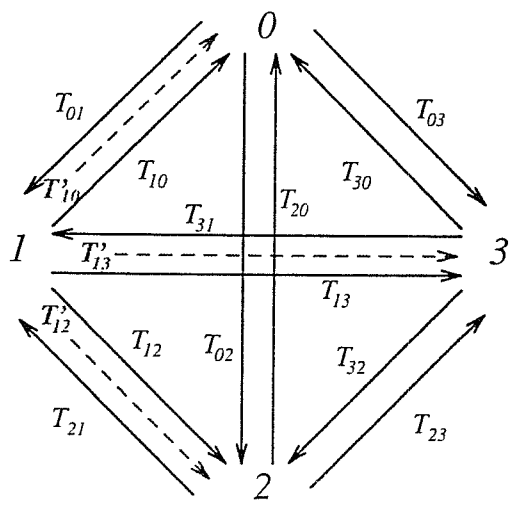

$T_{01} = 2(1\text{-}h)P_A P_I + hP_I^2$
$T_{02} = (1\text{-}h)P_A^2 + 2hP_A P_I$
$T_{03} = hP_A^2$
$T_{10} = 0$
$T_{12} = 2(1\text{-}h)P_A P_I + hP_I^2$
$T_{13} = (1\text{-}h)P_A^2 + 2hP_A P_I$
$T'_{10} = (1\text{-}h)P_I^2$
$T'_{12} = (1\text{-}h)P_A^2 + 2hP_A P_I$
$T'_{13} = hP_A^2$
$T_{20} = (1\text{-}h)P_I^2$
$T_{21} = 2(1\text{-}h)P_A P_I + hP_I^2$
$T_{23} = hP_A^2$
$T_{30} = 0$
$T_{31} = (1\text{-}h)P_I^2$
$T_{32} = 2(1\text{-}h)P_A P_I + hP_I^2$

Figure 3.1: Reaction diagram of the process. The red transitions refer to thermal processes, that is they refer to all the topplings happening under the threshold.

The solution in the MF approximations are

$$P_0 = \frac{1}{2} + \frac{\rho}{8} + O(P_2) \tag{3.12}$$

$$P_1 = \frac{1}{2} - \frac{\rho}{8} + O(P_2) \tag{3.13}$$

$$P_2 \simeq \sqrt{h} \tag{3.14}$$

$$\tag{3.15}$$

If we introduce θ_A the average height at the stationary state ($\theta_A \simeq P_1$), the first MF prediction is that θ_A decreases increasing the temperature. This behavior is confirmed by numerical simulations (Caldarelli, Maritan and Vendruscolo 1996).

To ensure the criticality to the system one has to to consider the response of the system. We define the susceptibility χ as the response of the order parameter $\tilde{P}_A$ to the external (vanishing) field h. One gets

$$\chi = \frac{\partial P_A}{\partial h}|_{h=0} = (1 + 2\rho P_0 P_1)\frac{\partial P_2}{\partial h} \tag{3.16}$$

From equation(3.10) one gets

$$\chi \propto \frac{\theta}{1 - 2\theta + 2\rho(\theta^3 - \theta^2)}. \tag{3.17}$$

One can also write at the most significant terms

$$\chi \propto \frac{\theta/2}{\theta - \theta_C}. \tag{3.18}$$

It is easy to verify

$$\theta_C = \frac{1}{2} - \frac{\rho}{8}. \tag{3.19}$$

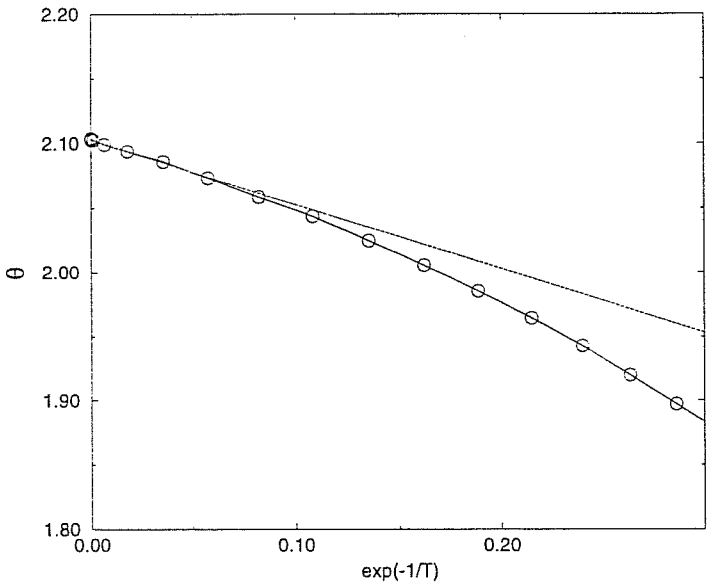

Figure 3.2: Average height θ versus $e^{-\frac{1}{T}}$ as obtained on a 64×64 square lattice.

Where θ_C is the height at which the susceptibility diverges and system is critical

The main result of this MF approach turns that $\theta_C = \theta_A$ so as θ approaches θ_A $\chi \rightarrow \infty$ with an exponent $\gamma = 1$. Also in this case as in 1.5 a more physical description of the MF can be obtained introducing dissipative boundaries in the system. The result are similar to the ordinary sandpile case, the two limits $h \rightarrow 0$ and $\epsilon \rightarrow 0$ has not to be interchanged to ensure correct result (see 1.5).

We now turn to the numerical results obtained in a square lattice at various T. The mean field prediction of eq. (3.19), i.e. θ_A decreases linearly in ρ, that might also be expected from an analytical dependence of θ_A on $e^{-\frac{1}{T}}$, has been also verified in a 2−dimensional square lattice of linear size $L = 64$ (see FIG. 3.2). The avalanche size distribution $P(s)$ in the stationary state has also been investigated. Due to very large relaxation times at $T \neq 0$ simulations have been performed up to linear sizes $L \leq 128$. Within the error bars in the range $T \leq 0.25$ ($\pi \simeq 1.8^{-2}$) we have found $P(s) \simeq s^{-\tau}$ with $\tau = 1.18 \pm 0.03$. which agrees with the BTW results (Bak et al. (1987)). Increasing the "temperature" we start noticing a different behavior. Without the presence of any cutoff (apart from finite size effects) signaling the loss of criticality (see FIG. 3.3) the critical exponent τ apparently changes continuously with T.

On the summary, it turns out that also in the presence of this external field the system self-organizes into a critical state. At this stage the presence of temperature is only a tuning of the average height and *does not destroy* the criticality of the system.

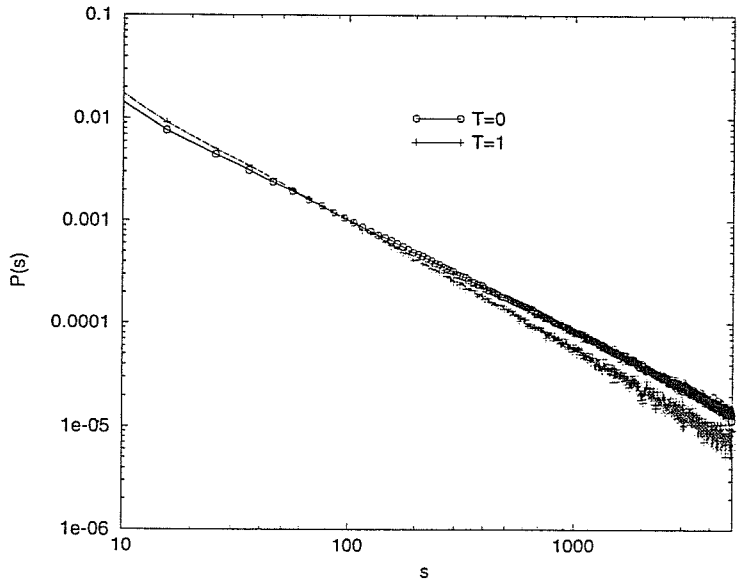

Figure 3.3: Probability distributions P(s) for different temperatures.

3.3 Very Hot Sandpiles and Random Walks

In order to understand if a characteristic avalanche size appears at least outside the small T limit of MF, we investigate the high temperature region. At infinite temperature the mean height is $1/L^2$ since in the system there is a single sand grain performing a random walk (RW). With the usual definition of toppling the avalanche size coincides with the number of steps necessary to a walker starting at a random point to reach a boundary. It is easy to see that in this case one gets:

$$P(s) \simeq s^{-\frac{1}{2}} \tag{3.20}$$

and thus, when $s/L^2 \ll 1$, even in the large temperature limit, there is no cutoff. The previous formula is demonstrated in the sequent subsection (3.3.1). In the state of high, but finite, temperature a smeared crossover is distinguishable between different regimes. At sufficiently small s the system behaves essentially as a pure RW where as the avalanche becomes larger and larger a grain can stop or excite another grain previously stopped and the behavior is essentially "BTW-like" with again a power law distribution for avalanche size with a T dependent exponent (see FIG. 3.4). We have tried scaling form of the type $P(s) = s^{-1/2} f(s/s_0)$ where $f(x) \sim x^{\frac{1}{2}-\tau}$ in the $x \to \infty$ limit. However due to the the large relaxation times and finite size effects the resulting collapse plots were not sufficiently good to support the above hypothesis.

In conclusion we have presented both analytical and numerical evidence that "hot" sandpiles are still critical with two different power law regimes for the avalanche size distribution and a possible

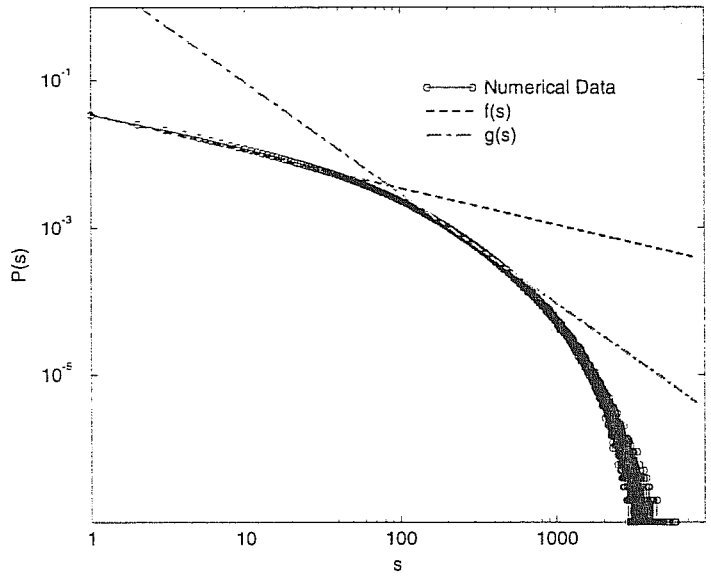

Figure 3.4: High temperature avalanche distribution. Crossover between different behaviors at a size s_c varies with T, provided that s_c/T is small enough. In the present case $T = 100$, $f(s) \propto s^{-1/2}$ and $g(s) \propto s^{-1.50}$.

T dependent critical exponent for the large size avalanches distribution.

3.3.1 Probability Distribution of Exit Times

We have to consider for random walks the probability distribution of exit time, for a 1-dimensional system with absorbing boundaries in 0 and L, generalization to higher dimensions been straightforward and presented at the end of this appendix.

Let us consider the quantity $P(x,t|x_0,0)$ that is the probability density for the walker to be at time t in x if at $t = 0$ it is in x_0. It holds, for absorbing b. c.:

$$P(x,0|x_0,0) = \delta(x - x_0) \tag{3.21}$$

$$P(x = 0,t|x_0,0) = P(x = L,t|x_0,0) = 0 \quad \forall t \tag{3.22}$$

$$\frac{\partial P}{\partial t} = \frac{\partial^2 P}{\partial x^2}. \tag{3.23}$$

This means that $\int_0^L P(x,t|x_0,0)dx$ represents the probability to be still in the system at time t and then the probability $\mathcal{P}(T \geq t)$ that the lifetime T at which the system is left is $\geq t$ (i.e. $\int_0^L P(x,t|x_0,0)dx = \mathcal{P}(T \geq t)$).

We can write without loss of generality

$$P(x.t|x_0,0) = \sqrt{\frac{2}{L}} \sum_{n=1}^{\infty} a_n(t) \sin\left(\frac{n\pi x}{L}\right) \tag{3.24}$$

where

$$\int_0^L dx \quad \sin\left(\frac{n\pi x}{L}\right) \quad \sin\left(\frac{m\pi x}{L}\right) = \frac{L}{2}\delta_{n,m}. \tag{3.25}$$

Notice that the b.c. (3.23) is automatically satisfied by eq.(3.24), making use of the eq.(3.23) we can write

$$\frac{\partial a_n(t)}{\partial t} = -\left(\frac{n\pi}{L}\right)^2 a_n(t) \Longleftrightarrow a_n(t) = e^{-\left(\frac{n\pi}{L}\right)^2 t} a_n(0) \tag{3.26}$$

From (3.25) it follows

$$\delta(x - x_0) = \sqrt{\frac{2}{L}} \sum_{n=1}^{\infty} a_n(0) sin\left(\frac{n\pi x}{L}\right) \tag{3.27}$$

and then $a_n(0) = \sqrt{\frac{2}{L}} sin\left(\frac{n\pi}{L}\right) x_0$. This allow to write in an explicit form the eq.(3.24)

$$P(x,t|x_0.0) = \frac{2}{L} \sum_{n=1}^{\infty} \sin\left(\frac{n\pi x}{L}\right) \sin\left(\frac{n\pi x_0}{L}\right) e^{-\left(\frac{n\pi}{L}\right)^2 t}. \tag{3.28}$$

What we are looking for is the average with respect to the starting point of $\mathcal{P}(T \geq t)$.

$$\langle \mathcal{P}(T \geq t) \rangle_L = \frac{1}{L} \int_0^L dx_0 \quad \mathcal{P}_{x_0}(T \geq t) = \tag{3.29}$$

$$\frac{2}{L^2} \sum_{n=1}^{\infty} e^{-\left(\frac{n\pi}{L}\right)^2 t} \left[\int_0^L dx \quad \sin\left(\frac{n\pi x}{L}\right)\right]^2 = \frac{8}{\pi^2} \sum_{n \quad odd} \frac{e^{-\left(\frac{n\pi}{L}\right)^2 t}}{n^2}. \tag{3.30}$$

Two distinct regimes are present

- $\frac{t}{L^2} \gg 1 \Rightarrow \mathcal{P}(T \geq t) \simeq \frac{8}{\pi^2} e^{-\left(\frac{\pi^2}{L^2}\right)^2 t} + O(e^{-\left(\frac{9\pi^2}{L^2}\right)^2 t})$
- $\frac{t}{L^2} \ll 1 \Rightarrow \mathcal{P}(T \geq t) \simeq 1 - \frac{4}{\sqrt{\pi}} \sqrt{\frac{t}{L^2}} + l.s.t.$

The second regime can be deduced as follows

$$\frac{\partial}{\partial t} \mathcal{P}(T \geq t) = \frac{8}{L^2} \sum_{n \quad odd} e^{-\left(\frac{n\pi}{L}\right)^2 t} \simeq \tag{3.31}$$

$$\simeq \frac{8}{L^2} \frac{1}{4} \int_{-\infty}^{\infty} dx \quad e^{-\frac{\pi^2 t x^2}{L^2}} \simeq \frac{2}{L\sqrt{\pi t}} \tag{3.32}$$

and we get

$$\mathcal{P}(T \geq t) \simeq 1 - \frac{4}{\sqrt{\pi}} \sqrt{\frac{t}{L^2}} + l.s.t. \tag{3.33}$$

The generalization at higher dimension is immediate: considering d dimension one has for absorbing boundary conditions $0 \leq x_i \leq L$, $i = 1, ..., d$.

$$P(\vec{x}, t|\vec{x_0}, 0) = \left(\frac{2}{L}\right)^d \sum_{n_1,n_2,...,n_d=1}^{\infty} \prod_{i=1}^{d} \sin\left(\frac{n_i \pi x_i}{L}\right) \sin\left(\frac{n_i \pi x_{0i}}{L}\right) e^{-\left(\frac{\vec{n}^2 \pi^2}{L^2}\right)t}. \tag{3.34}$$

where $\vec{n}^2 = n_1^2 + ... + n_d^2$. From this follows

$$\mathcal{P}_d(T \geq t) = \frac{1}{L^d} \int_{[0,L^d]} d^d x_0 \int_{[0,L^d]} d^d x \; P(\vec{x}, t|\vec{x_0}, 0) = \tag{3.35}$$

$$\left[\frac{8}{\pi^2} \sum_{n \; odd} \frac{e^{-\left(\frac{n\pi}{L}\right)^2 t}}{n^2}\right]^d = \left[\mathcal{P}_{d=1}(T \geq t)\right]^d. \tag{3.36}$$

At the leading order for each dimension, the probability to escape after t steps from an hyperbox of size L^d scales as $t^{-1/2}$.

4 Self–Organization and Breakdown in Elastic Media.

4.1 Introduction

In this chapter the basic ideas of SOC models are applied to an interesting physical problem, the media breakdown. In fact, statistical self-similarity is observed since a long time in seismic events (Carlson and Langer (1989)), as well as in energy release by material fracturing (Petri, Paparo, Vespignani, Alippi and Costantini (1994)) and many others different systems subjected to stress (Kramer and Lobkovsky (1995)). It is therefore very tempting to investigate the possibility that the same critical dynamics holds from the large scale of earthquakes down to the microscopic scale of the rheological properties of materials. In that case, as in usual critical phenomena, the detailed aspects of different structures would be irrelevant with respect to the critical properties.

In this work we try to specify the conditions under which self-organization takes place in stressed materials, and to which extent it can explain the intriguing experimental properties of the related Acoustic Emission (AE) that are far from understood (Petri et al. (1994)). In fact, the current understanding of dissipation in solids is largely phenomenological. A well known feature that determines the rupture process is the presence of disorder in the material. These inhomogeneities strongly influence the mechanical behavior of the material, and are responsible for the experimental patterns of AE, proving that energy dissipation occurs in avalanches, whose size ranges from the scale of microscopic perturbations to the large scale of the system size. Our purpose is to show that the onset of long range correlation in AE can be related to microscopical processes similar to those of simple SOC automata models. Specifically a *necessary condition* for the AE power law behavior turns out to be the presence of *annealed disorder* in the system.

Before describing the original work done in this thesis it is worth introducing the basic concepts of theory of elasticity (Landau and Lifshitz (1970)) to explain the fracture model used in the following sections.

4.2 Theory of Elasticity

4.2.1 Strain Tensor

If each point is identified by the vector $\vec{r} = (x_1, x_2, x_3)$ after a deformation the same point will have the coordinates $\vec{r}' = (x_1', x_2', x_3')$. To describe the deformation one introduces the *displacement vector*

$$\vec{u} = \vec{r}' - \vec{r} \Rightarrow u_i = r_i' - r_i, \quad \{i = 1, 2, 3\}. \tag{4.1}$$

Also the distance between two points wil be changed, in particular

$$dl = \sqrt{dx_1^2 + dx_2^2 + dx_3^2} \Rightarrow dl^2 = \sum_{i=1}^{3} dx_i^2 \tag{4.2}$$

$$dl' = \sqrt{dx_1'^2 + dx_2'^2 + dx_3'^2} \Rightarrow dl'^2 = \sum_{i=1}^{3} dx_i'^2. \tag{4.3}$$

Using $dx_i' = dx_i + du_i$, it follows $dl'^2 = \sum_{i=1}^{3}(dx_i + du_i)^2$.
If one writes $du_i = \sum_{k=1}^{3} \frac{\partial u_i}{\partial x_k} dx_k$ then interchanging the suffixes i, k:

$$dl'^2 = dl^2 + \sum_{i,k=1}^{3} \frac{\partial u_i}{\partial x_k} dx_i dx_k + \frac{\partial u_k}{\partial x_i} dx_i dx_k + \frac{\partial u_i}{\partial x_k} \frac{\partial u_k}{\partial x_i} dx_i dx_k \tag{4.4}$$

$$= dl^2 + \sum_{i,k=1}^{3} 2u_{ik} dx_i dx_k. \tag{4.5}$$

Where

$$u_{ik} = \frac{1}{2}\left(\frac{\partial u_i}{\partial x_k} + \frac{\partial u_k}{\partial x_i} + \frac{\partial u_k}{\partial x_i}\frac{\partial u_i}{\partial x_k}\right), \quad \{i, k = 1, 2, 3\} \tag{4.6}$$

is the (symmetrical) *strain tensor.*

If the strain tensor is diagonalized at a given point, the infinitesimal length element becomes

$$dl^2 = \sum_{i=1}^{3}(1 + 2u_{ii}) dx_i^2. \tag{4.7}$$

That is the sum of independent terms (extension or compressions) along the different axes (in fact $dx_i' = (1 + u_{ii})dx_i$). In what follow we shall suppose that all strains are small. The displacement vector u_i however, may sometimes be large, even for small strains. For example let us consider the case a long thin rod. Even for large deflection, in which the ends of the rod move a considerable distance, the extensions and compressions in the rod itself will be small. In almost all cases occurring in practice, anyway, if the strains are small also the displacement vector is small. Furthermore happens that if the deformation of the body is fairly small, it returns to its original undeformed state when the external forces causing the deformation cease to act. Such deformation are said to be *elastic* and if microscopic fractures arise in this regime the fracture is said to be *brittle.* For large deformations the removal of the external forces does not result in the total disappearance of

the deformation, a residual deformation remains, so that the state of the body is not that which existed before the forces where applied. Such deformation are said to be *plastic* and if a microscopic fracture arise in this regime the fracture is said to be *brittle*.

In the elastic regime, apart the previous special cases, the displacement vector for a small deformation is itself small, and we can therefore neglect the last term in eq.(4.5) as being of the second order of smallness.

Thus for small deformation the stress tensor is given by

$$u_{ik} = \frac{1}{2}\left(\frac{\partial u_i}{\partial x_k} + \frac{\partial u_k}{\partial x_i}\right), \quad \{i,k = 1,2,3\}. \tag{4.8}$$

Let us consider an infinitesimal volume element dV, and find its volume dV' after the deformation. To do so, we take the principal axes of the strain tensor, at the point considered, as the co-ordinate axes.

$$dV' = \prod_{i=1}^{3} dx_i' = \prod_{i=1}^{3}(1 + u_{ii})dx_i = dV(1 + Tr(u)). \tag{4.9}$$

As being invariant $Tr(u)$ with respect to the system considered, the above result is valide in any co-ordinate system.

4.2.2 Stress Tensor

In a body that is not deformed the arrangement of the molecules correspond to a state of thermal equilibrium. All parts of the body are in mechanical equilibrium. This means that, if some portion of the body is considered, the resultant of the forces on that portion is zero.

When a deformation occurs the arrangement of the molecules is changed and the body ceases to be in its original state of equilibrium. These internal forces which occur when a body is deformed are called internal stresses. If no deformation occurs, there are no internal stress.

Let us consider the total force on some portion of the body. Firstly, this total force is equal to the sum of all the forces on all the volume elements in that portion of the body, i.e. it can be written as the volume integral $\int_\Omega \vec{F} dV$ where $\vec{F}$ is the force per unit volume and Ω the total volume. The action that various parts of the body act on one another cancels by Newton's third law. The required total force can be regarded as the sum of the forces exerted on the given portion of the body by the portion surrounding it. Thus, for any portion of the body, each of the components $\int_\Omega F_i dV$ of the the resultant of all the internal stresses can be transformed into an integral over the surface. To do that F_i must be the divergence of a tensor of rank two,

$$F_i = \sum_{k=1}^{3} \frac{\partial \sigma_{ik}}{\partial x_k}. \quad \{i = 1,2,3\}. \tag{4.10}$$

Then,

$$\int_\Omega F_i dV = \int_\Omega \sum_{k=1}^{3} \frac{\partial \sigma_{ik}}{\partial x_k} dV = \oint_{\Sigma(\Omega)} \sum_{k=1}^{3} \sigma_{ik} df_k, \quad \{i = 1,2,3\} \tag{4.11}$$

where df_k is the k component of the vector $d\vec{f}$ oriented along the outward normal and $\Sigma(\Omega)$ the surface surrounding Ω.

The tensor σ_{ik} is called the *stress tensor* and represents the i-th component of the force on unit area perpendicular to x_k axis. Computing the force momentum acting on a body it is easy to prove that the stress tensor is symmetrical.

Furthermore using eq.(4.10) one has the equations of equilibrium for a deformed body. In fact the internal stresses in every volume must balance ($\forall i$ $(i = 1, 2, 3)$. $F_i = 0$), and then

$$\forall i \ (i = 1, 2, 3), \sum_{k=1}^{3} \frac{\partial \sigma_{ik}}{\partial x_k} = 0. \tag{4.12}$$

Let $\vec{P}$ be the external force applied on unit area of the surface of the body, so that a force $\vec{P}df$ acts on the surface element df. In equilibrium this must be balanced by the force $-\sigma_{i,k}df_k$ of the internal stress acting on that element. Writing $df_k = n_k df$ it holds:

$$\sum_{k=1}^{3} \sigma_{ik} n_k = P_i, \quad \{i = 1, 2, 3\}. \tag{4.13}$$

With this definition we are able to give an explicit form for the mean value of the stress tensor in a deformed body. In fact, multipling eq.(4.12) by x_k and integrate over the whole volume:

$$\forall i \ \ (i = 1, 2, 3), \int_\Omega \sum_{l=1}^{3} \frac{\partial \sigma_{i,l}}{\partial x_l} x_k dV = \int_\Omega \sum_{l=1}^{3} \frac{\partial (\sigma_{il} x_k)}{\partial x_l} dV - \int_\Omega \sum_{l=1}^{3} \sigma_{il} \frac{\partial x_k}{\partial x_l} x_k dV = 0. \tag{4.14}$$

The first integral at the right can be transformed in a surface integral, while in the second one we put δ_{kl}. Making use of eq.(4.13) we find:

$$\oint_{\Sigma(\Omega)} P_i x_k df = \int_\Omega \sigma_{ik} dV = V \overline{\sigma}_{ik}, \quad \{i, k = 1, 2, 3\} \tag{4.15}$$

where $\overline{\sigma}_{ik}$ is the mean value of the stress tensor. Since $\sigma_{ik} = \sigma_{ki}$ this formula can be written in the symmetrical form:

$$\overline{\sigma}_{ik} = \frac{1}{2} \oint_{\Sigma(\Omega)} (P_i x_k + P_k x_i) df, \quad \{i, k = 1.2, 3\}. \tag{4.16}$$

4.2.3 The Thermodynamics of Deformation

Let us consider some deformed body, and suppose that the deformation is changed in such a way that the displacement vector u_i changes by a small amount δu_i, and let us determine the work done by the internal stress in this change. Multiplying the force $F_i = \sum_{k=1}^{d} \frac{\partial \sigma_{i,k}}{\partial x_k}$ by the displacement δu_i and integrating over the volume of the body, we have

$$\int_\Omega \delta R dV = \int_\Omega \sum_{i,k=1}^{3} \frac{\partial \sigma_{ik}}{\partial x_k} \delta u_i dV \tag{4.17}$$

where δR denotes the work done by the internal stress per unit volume. Integrating by parts we get

$$\int_\Omega \delta R dV = \sum_{i,k=1}^{3} \oint_{\Sigma(\Omega)} \sigma_{ik} \delta u_i df_k - \int_\Omega \sigma_{ik} \frac{\partial \delta u_i}{\partial x_k} dV. \tag{4.18}$$

By considering an infinite medium which is not deformed at infinity, we make the surface of integration of first integral tend to infinity; then $\sigma_{ik} = 0$ on the surface and the integral is zero. Using the symmetry of the tensor σ_{ik} one can write

$$\int_\Omega \delta R dV = -\frac{1}{2} \int_\Omega \sum_{i,k=1}^{3} \sigma_{ik} \left(\frac{\partial \delta u_i}{\partial x_k} + \frac{\partial \delta u_k}{\partial x_i} \right) dV \tag{4.19}$$

$$= -\frac{1}{2} \int_\Omega \sum_{i,k=1}^{3} \sigma_{ik} \delta \left(\frac{\partial u_i}{\partial x_k} + \frac{\partial u_k}{\partial x_i} \right) dV \tag{4.20}$$

$$= -\int_\Omega \sum_{i,k=1}^{3} \sigma_{ik} \delta u_{ik}. \tag{4.21}$$

Thus we find

$$\delta R = -\sum_{i,k=1}^{3} \sigma_{ik} \delta u_{ik}. \tag{4.22}$$

In the case of elastic deformations the process can be considered thermodynamically reversible. An infinitesimal change $d\mathcal{E}$ in the *internal energy* is equal to the difference between the heat acquired by the unit volume considered and the work dR done by internal stresses. The amount of heat is, for a reversible process, TdS, where T is the temperature. Thus $d\mathcal{E} = Tds - dR$ with dR given by eq.(4.22)

$$d\mathcal{E} = Tds + \sum_{i,k=1}^{3} \sigma_{ik} du_{ik}. \tag{4.23}$$

This is the fundamental thermodynamic relation for deformed bodies.

Introducing the *free energy* of the body $F = \mathcal{E} - TS$ we find the form

$$dF = -SdT + \sum_{i,k=1}^{3} \sigma_{ik} du_{ik}. \tag{4.24}$$

The component of the stress tensor can be obtained by differentiating $\mathcal{E}$ or F with respect to the components of the strain tensor.

$$\sigma_{ik} = \left(\frac{d\mathcal{E}}{u_{ik}} \right)_S = \left(\frac{dF}{u_{ik}} \right)_T, \quad \{i,k = 1,2,3\}. \tag{4.25}$$

4.2.4 Hooke's law

In order to be able to apply the general formulae of thermodynamics to any particular case, we must know the free energy F of the body as a function of the strain tensor. This expression is

easily obtained by using the fact that the deformation is small and expanding the free energy in power of u_{ik}.

Without external force $\sigma_{ik} = 0$ and then using eq.(4.25) $\frac{\partial F}{\partial u_{ik}} = 0$. It follows that there is no linear term in the expansion of F in powers of u_{ik}.

Next since the free energy is a scalar, each term in its expansion must be a scalar also. Two independent scalar of the second degree can be formed from the components of the the symmetrical tensor $u_{i,k}$: they can be taken as the squared sum of the diagonal components ($\sum_{i=1}^{3} u_{ii}^2$) and the sum of the square values of all the components ($\sum_{i,k=1}^{3} u_{ik}$). Expanding F in power of u_{ik}, we therefore have as far as terms of the second order

$$F = \frac{1}{2}\lambda \sum_{i=1}^{3} u_{ii}^2 + \mu \sum_{i,k=1}^{3} u_{ik}^2.^{1} \tag{4.26}$$

This is the general expression for the free energy of a deformed isotropic body. The quantities λ, and μ are called *Lamé coefficients.*

- The change in volume in the deformation is given by $\sum_{i=1}^{3} u_{ii}$. If the sum is zero, then the volume of the body is unchanged only the shape is altered. Such a deformation is a *pure shear.*

- The opposite case is that of a deformation which causes a change in the volume of the body but no change in its shape. The stress tensor of such a deformation is $u_{ik} = \text{constant} \times \delta_{ik}$. Such a deformation is called an *hydrostatic compression.*

Any deformation can be represented as the sum of a pure shear and an hydrostatic compression using the identity

$$u_{ik} = (u_{ik} - \frac{1}{3}\delta_{ik} \sum_{l=1}^{3} u_{ll}) + \frac{1}{3}\delta_{ik} \sum_{l=1}^{3} u_{ll}, \quad \{i,k = 1,2,3\}. \tag{4.27}$$

The first term on the right is evidently a pure shear, The second one an hydrostatic compression. Using this decomposition F becomes

$$F = \mu \sum_{i,k=1}^{3} (u_{ik} - \frac{1}{3}\delta_{ik} \sum_{l=1}^{3} u_{ll})^2 + \frac{1}{2}K \sum_{l=1}^{3} u_{ll}^2) \tag{4.28}$$

where K is the *bulk modulus* while μ takes here the name of *shear modulus.*

Differentiating eq.(4.28) with respect to u_{ik} one obtains the expression of the stress tensor in function of the strain tensor:

$$\sigma_{ik} = K\delta_{ik} \sum_{l=1}^{3} u_{ll} + 2\mu(\sum_{i,k=1}^{3} u_{ik} - \frac{1}{3}\delta_{ik} \sum_{l=1}^{3} u_{ll}). \quad \{i,k = 1,2,3\}. \tag{4.29}$$

[1] we have here omit the constant term F_0 in this expansion because it is of no interest

It is easy to invert the previous relation and find

$$u_{ik} = \frac{1}{9K}\delta_{ik}\sum_{l=1}^{3}\sigma_{ll} + \frac{1}{2\mu}\sum_{i,k=1}^{3}(\sigma_{ik} - \frac{1}{3}\delta_{ik}\sum_{l=1}^{3}\sigma_{ll}), \quad \{i,k=1,2,3\}. \tag{4.30}$$

The stress tensor u_{ik} is a linear function of the strain tensor σ_{ik}. That is deformation is proportional to the applied forces.

This law valid for small deformations is called *Hooke's law.*

4.3 The Standard Born Model

As shown in the previous section the energy of a deformed body can be calculated considering the contributions from shear deformation and from pure compressions. To study with computer simulations how fractures propagates in the media one needs of a model of the material that can be described using discrete quantities, i.e. it is defined on a lattice.

In the following we shall use a discrete mesoscopic model that reproduces the behavior of an elastic medium and preserve the theoretical essential feature of elasticity here presented. This model is known as Born Model (BM) (Yan, Li and Sander (1989)) and it is a generalization of a Hookean network of springs (de Arcangelis, Hansen, Roux and Herrmann (1989), Hansen, Roux and Herrmann (1989)). The fractal and topological properties of such a model has been extensively studied in the past (Caldarelli, Castellano and Vespignani (1994), Caldarelli, Vespignani and Pietronero 1995).

The medium is described by a set of springs interacting one each other (in the sense that in the rest position the extreme of two neighbors springs share the same position) with an internal energy of the form of eq.(4.28).

In this case to simplify the expression of the energy for the whole system the shear and compression for one spring are expressed as function of the displacement vector u_i. That is the energy V is the sum of the spring energy

$$V = \frac{1}{2}\sum_{i,j} V_{ij} = \frac{1}{2}(\alpha - \beta)\sum_{i,j}[(\vec{u}_i - \vec{u}_j)\cdot\hat{r}_{ij}]^2 + \frac{1}{2}\beta\sum_{i,j}[\vec{u}_i - \vec{u}_j]^2 \tag{4.31}$$

where

- $\vec{u}_i$ is the displacement vector of site i,
- $\hat{r}_{ij}$ is the unit vector between i and j,
- α and β are force constants
- and the sum runs over nearest neighbors sites.

In the first term the scalar product ensures us that the only deformation considered are hydrostatic compressions, while in the second term one deals also with shear deformations. Minimizing the expression of eq.(4.31) with respect to the displacement vectors one is able to compute the rest position.

The main difference with respect to eq.(4.28) is that in this case the interaction is between spring nearest neighbors, while discretizing the continuum equation one obtains also terms involving next nearest neighbors. In the above hypothesis of elasticity regime and small values of displacement vector field, it turns out that these last terms can be neglected.

The next problem is now to assign to this system the dynamical rules to study an evolution like the case of the fractures.

The standard choices inspired to corrosion dynamics are the following.

We want a probabilistic formation of cracks and we can obtain it through an iterative addition of broken lattice bonds to the fracture already grown. At every step the new broken bond is chosen as follows:

- given the crack pattern, one calculates the displacement field of the sites by minimizing the energy of the lattice, i.e. eq. (4.31);

- a new broken bond is randomly chosen among those contiguous to the crack pattern. The probability for every bond is:

$$p_{ij} = \frac{V_{ij}^{\frac{\eta}{2}}}{\sum_{ij} V_{ij}^{\frac{\eta}{2}}} \tag{4.32}$$

  where η is a free parameter of the model. This choice corresponds to assign a breaking probability function of the elongation. Namely, when $\alpha = \beta$, $V_{ij} i^{1/2} = |\vec{u}_i - \vec{u}_j|$ is the usual elongation;

- The new broken bond added to the pattern modifies the boundary conditions for the displacement field.

In the Born Model the energy of the network depends on two parameters, α and β, weighting the contribution of shear and compression forces. Because we are only interested in the energy minimum, only the ratio $\frac{\beta}{\alpha}$ is relevant and we can tune the value of β keeping α fixed ($\alpha = 1$). Numerical and topological studies of the patterns obtained with these rules are extensively studies in the past. In the next section we show how with simple modifications of this dynamic rules it is possible to describe process like the acoustic emission.

4.4 Acoustic Emission and Annealed Disorder

Our purpose is to show that the onset of long range correlation in AE can be related to microscopical processes similar to those of simple SOC automata models(Caldarelli, Di Tolla, F. D. and Petri (1996)). Specifically a *necessary condition* for the AE power law behavior turns out to be the presence of *annealed disorder* in the system. Extensive numerical simulations are realized in the $\beta = 0$ case, and some results for the $\beta \neq 0$ are reported. We recover qualitatively the experimental AE behavior *only when short range correlation between breaking thresholds, i.e. annealed disorder, is considered.* The annealing acts on the neighbors of the broken springs lowering the rupture threshold of the springs nearest neighbors. This means that one rupture weakens the set of bonds around simulating corrosion behavior or damage spreading.

To describe this process we have modified the Born Model introducing the presence of disorder. We start by considering a triangular lattice of sites in which each pair of sites i, j is connected by an elastic (brittle) spring to which is assigned an elongation threshold $R_{i,j}$. The value to be compared with $R_{i,j}$ is the generalized "elongation" $V(i,j)$ (in fact when $\alpha = \beta$, $|\vec{u}(i) - \vec{u}_j|$ is the usual elongation).

The breaking process is inspired to the rules of the simplest automata models prototypes of SOC. A flowchart schematizing the dynamics steps is in FIG. 4.1.

1. We apply an external stress to the sample, by stretching the boundaries of an infinitesimal amount Δl and keeping them fixed in the next relaxations.
2. We then compute the minimum energy of eq.(4.31) to find the displacement vector field at rest.
3. We now compute the energies $V_{i,j}$ for each spring
4. If the "elongation" $V_{i,j}^{1/2}$ is greater than the threshold $R_{i,j}$ the spring is broken and disappears from the expression of eq.(4.31). *Furthermore the thresholds of springs nearest neighbors are lowered to mimick a progressive weakening.* Now the step 2 is repeated, if new spring are eligible for fracture this process repeats. Otherwise the external stress is increased.
5. When the sample is broken in two parts the simulation ends.

Steps from 2 to 4 are performed again over the springs that had their threshold updated, in order to break them if their energy is found to be above the new threshold. If this is the case, more springs are broken and a new *toppling* occurs. One says than an "avalanche" is observed if one or more springs are broken in the system between two consecutive stretches. Hence we assign to each avalanche: a size, an energy, and a duration. The size is taken as the total number of broken springs between two consecutive elongations. The corresponding energy is computed summing up the energy carried by these springs before their breakdown. The duration is determined as the

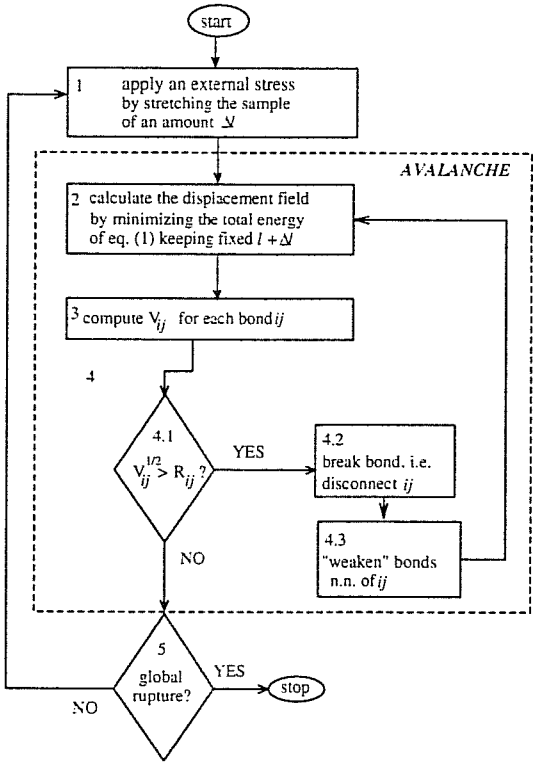

Figure 4.1: Flow-chart of the algorithm used in the simulations. The loop over steps from 2 to 4 is repeated as long as new bonds are broken, and is what we define as an avalanche. The simulation ends when the sample is broken in two pieces.

number of consecutive relaxations (number of loops over steps 2-4) which the systems undergoes before to be further stretched (step 1). The whole sequence of previous steps is repeated until the sample is totally broken. According with the above rules, the energy of the system is stored in the springs and it is released with their rupture. To model the fracturing process, we start the simulations with a defect-free sample. We assign to each spring a failure threshold, uniformly distributed between 0 and a maximum value related to the total stress amount. In this work the behavior of the system is investigated in the limit of a vanishing stress rate for each step (0.5% of the total stress). In this way the dynamics of the lattice becomes very similar to the one investigated in ref. (de Arcangelis et al. (1989)).

In original sandpile models of SOC (Bak et al. (1987)), sand grains are added on the top of a sandpile, causing instability. Every now and then a sand avalanche starts, and restores equilibrium. As a consequence, the system is kept at criticality: the average slope or height do not change, but a small perturbation (added grain) may generate events of any extension in size and time (avalanches). The system stores locally (rigidity) potential energy of the incoming flux of sand, and loses it releasing sand from the boundary. Similarly, in the case of elasticity, the applied stress strains the system, and more and more energy is stored in the springs. This energy is then released through the onset of cracks and in AE. The equilibrium is restored through the relaxation. We compute crack-avalanche statistics by recording the number of broken springs (the size of an avalanche), its duration, and its energy, i.e. the energy lost by the broken springs. We try to interpret this energy as the one released via AE. In real experiments this is measured outside the sample and it is found to display similar power law distributions in many different materials and experimental situations (Petri et al. (1994), Kramer and Lobkovsky (1995)).

We find that when only *quenched disorder* is considered, no avalanche behavior is observed. This can be understood by noting that in the limit $\Delta l \to 0$, only one spring at time breaks, the weakest. This continues up to the breakdown of the system. This situation is analogous to that of the model for hydraulic fracturing investigated in (Tzschichholz and Herrmann (1995)). In fact, in that model no power law is found in the avalanche statistics. In this situation the system resembles a known scenario (Duxbury and Leath (1994)). In fact when stress is applied, the failure instability initiates in an especially weak part of the material and the network stabilizes with a flaw population generated by the failure process. If the external stress increases by successive composition of infinitesimal amounts, one reaches (breaking one spring at time) the critical stress for which the system undergoes complete failure.

Instead when *annealed disorder* is introduced, the situation changes drastically. The frequency distribution of crack sizes turns into a power law, reflecting the self organization of R_{ij} around the local stress values.

The numerical data will be discussed in the next section.

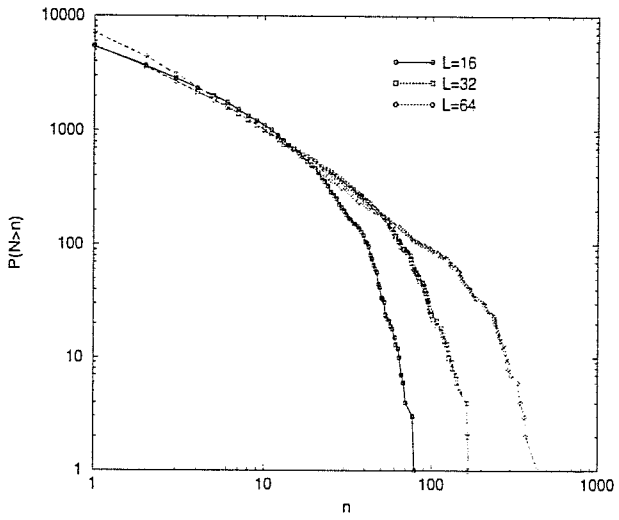

Figure 4.2: Cumulated frequency distribution of the number of broken springs during an avalanche for different lattice sizes: 200 simulations for a 16 × 16 sites lattice; 100 simulations for a 32 × 32 sites lattice; 100 simulations for a 64 × 64 sites lattice.

4.5 Numerical Data

FIG. 4.2 shows the integrated distribution $P(N > n)$ of the number N of broken springs to be greater than n, for lattices of different size. These data are fitted with a law $P(N > n) = An^{-\tau+1}+B$ with an exponent $\tau = 2.00 \pm 0.05$. The annealed situation turns to be close to the one described in ref. (Bernardes and Moreira (1994)), in which a model for the fracture of fibrous material is studied. In that model, a critical behavior is found when the influence of thermal fluctuations is comparable with the disorder due to the interaction among fibers.

Our interpretation of this different behavior with respect to the randomness distribution is that the breakdown threshold and the annealed disorder respectively play the role of the local rigidity and of the short-range couplings that, as pointed out in ref. (Cafiero et al. (1995)), are essential ingredients of SOC behavior. In fact, in our case the breakdown threshold acts as the local rigidity (allowing local accumulation of stress), while the annealed disorder mimics the toppling process in sandpiles (short range distribution of the stress), making the bonds closer to the breakdown value. If one of these ingredients is absent, systems behave in a diffusive way relaxing energies at the boundaries. More specifically, it is the presence of annealed disorder that allows the system to visit different metastable states, in which it stops because of the presence of rigidity. Otherwise, a situation similar to the one of refs. (de Arcangelis et al. (1989), Tzschichholz and Herrmann (1995), Duxbury and Leath (1994)) would take place, where dynamics is ruled by extreme values in the probability distribution of breaking thresholds.

One can assume to have AE proportional to the energy of the springs broken during the crack

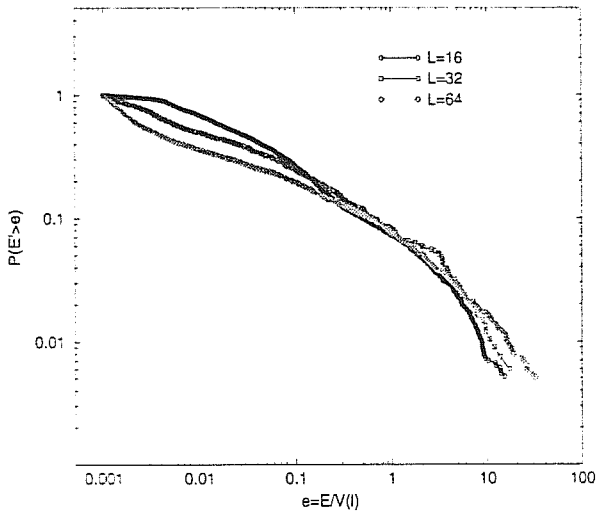

Figure 4.3: Cumulated frequency distribution of the normalized energy lost during avalanches for the simulations of FIG. 4.2.

evolution. By measuring the behavior of this quantity we do not obtain the power law behaviors experimentally observed (Petri et al. (1994)). In fact, one has to note that our finite system accumulates more and more energy in the springs not yet broken. This implies that AE is a function of time in this limit. Instead in our model, breaking processes involving a given number of springs will contribute in the same way to the avalanche size statistics, independently from the different moment of the system evolution at which they happen. On the other hand, they will have a different weight in the statistics of the released energy, due to the fact that the variation of energy they induce is relatively large with respect to the total energy of our sample. Hence with the particular rules chosen for the local correlation, we expect that the system self organizes (i.e. the $R_{i,j}$'s arrange their values around the local stress) in order to maintain a power law only in the number of broken bonds. The energy drift gives rise to a correction term for the AE probability distribution, and it is reasonable that a power law can be recovered in the AE statistics by normalizing the energy of each avalanche to the actual total energy of the lattice at that time. The behavior of cumulated and normalized occurrence frequency, $P(E' > e)$ versus e, is shown in FIG. 4.3. e is the normalized energy defined as $E/V(l)$, $V(l)$ being the total potential energy defined in Eq.(4.31) at lattice elongation l, and E being the sum of the $V_{i,j}$ for each bond i,j broken. It is seen that, according to the above reasoning, the three curves relative to different lattice sizes collapse to a similar distribution. The fitting function $P(E' > e) = Ae^{-\gamma+1} + B$ gives $\gamma \approx 1.2 \div 1.3$. Assuming that $e \sim n^{\rho}$,where n stands for the number of broken bonds, a simple scaling relation yields $\rho = \frac{(1-\tau)}{(1-\gamma)}$. With the previous values this brings to $E \approx V(l)\, n^4$ for the energy released. Then a power law distribution can be observed when the potential energy stored in the system does not vary too much during the AE process. This seems reasonable for most of real systems, where AE starts when approaching the plastic regime.

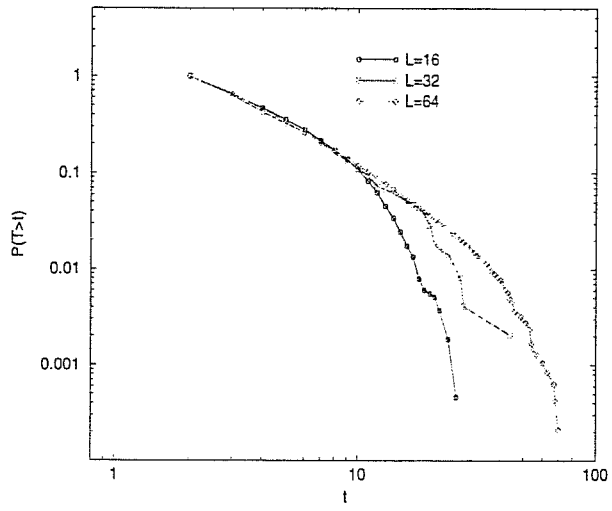

Figure 4.4: Frequency distribution for the duration time of the avalanches for the simulations of FIG. 4.2

Finally, we report the statistics of duration t of crack avalanches, FIG. 4.4. A critical behavior $P(T > t) \sim t^{-\delta+1}$ is again observed, with an exponent $\delta = \tau = 2.00 \pm 0.05$. We have performed simulations also for the cases $\beta = 0.5$ and $\beta = 1$. In our preliminary results we find the same exponents for size and duration of avalanches, i.e. $\tau = \delta = 2$, whereas AE seems to be characterized by a little smaller exponent $\gamma \approx 1.1$.

4.6 Results

Our principal results are:
a) scale invariance arises when correlation (*annealing*) between the breaking of one bond and the bonds nearest neighbors is considered. The resulting competition with quenched disorder is closely related to SOC in automata model, in which short range coupling and rigidity are necessary ingredients to set the system at some point of marginal stability. This is responsible for the critical behavior, as opposed to the extreme value statistics, typical of quenched disordered systems;
b) due to the particular chosen rules, critical behavior is displayed in the avalanche size statistics, and not in AE. However, a self-similar probability distribution for this latter quantity is recovered when the ratio of the released energy to the total lattice energy (which sensibly increases with time in our model) is considered. This shows that a critical behavior of AE is compatible with systems where the elastic energy does not increase too much while straining. This is the situation of most of real systems undergoing external macroscopic strains in the vicinity of the plastic regime;
c) The above point allows us to relate these peculiar scaling processes to "slowly" developing fractures.

We remark that a more complete understanding of these process is relevant not only for a more

complete knowledge of the behavior of large statistical systems, but also from a technological point of view.

5 Landscape Evolution in River Networks

5.1 Introduction

Similarities are observed among all kinds of river basins (see FIG. 5.1), nevertheless since some years ago, the nature of the above patterns, as well as the features of the individual components of the general structure were traditionally described through a framework basically dependent on the existence of fundamental scales. This type of description changed dramatically after the introduction of *fractal geometry* by B. Mandelbrot (Mandelbrot (1982)). *Fractals* brought into the analysis of river basins a completely new and different perspective. New relationships were found, both in the planar and altitude dimension which spanned through a wide range of scales in the form of power–laws.

Spatial and temporal scale–free behaviors are the fingerprints of both fractal structures and critical processes. Their abundance in Nature indicates a universal tendency of large, driven dynamical systems to self–organize into a critical state far away from equilibrium.

The above arguments led us to believe that fractal river basins are best studied within this framework. the theory, and its extension, provide many of the needed tools to firmly link fractal growth and processes for river basins, as we shall discuss in this chapter.

Through experimental studies, it has become evident in the past few years that the geometrical and topological structures of river basins are characterized by the absence of a single well-defined length scale. This is reflected in the appearance of power laws in the distribution of several quantities, chiefly total contributing area at a point (Rodriguez-Iturbe, Ijjasz-Vasquez, Bras and Tarboton (1992)) and stream lengths (Tarboton, Bras and Rodriguez-Iturbe (1988)): (Rigon, Rodriguez-Iturbe, Giacometti, Maritan, Tarboton and Rinaldo (1993)), and by the clear experimental assessment of scaling properties (yielding either self-similarity or self-affinity (Feder (1988))) for many geometrical descriptors of the river basin (Mandelbrot (1982), Maritan, Rinaldo, Giacometti and Rodriguez-Iturbe (1996), Rodriguez-Iturbe and Rinaldo in press (1996)) The discovery of the general underlying mechanisms yielding scale-free features is the present theoretical challenge.

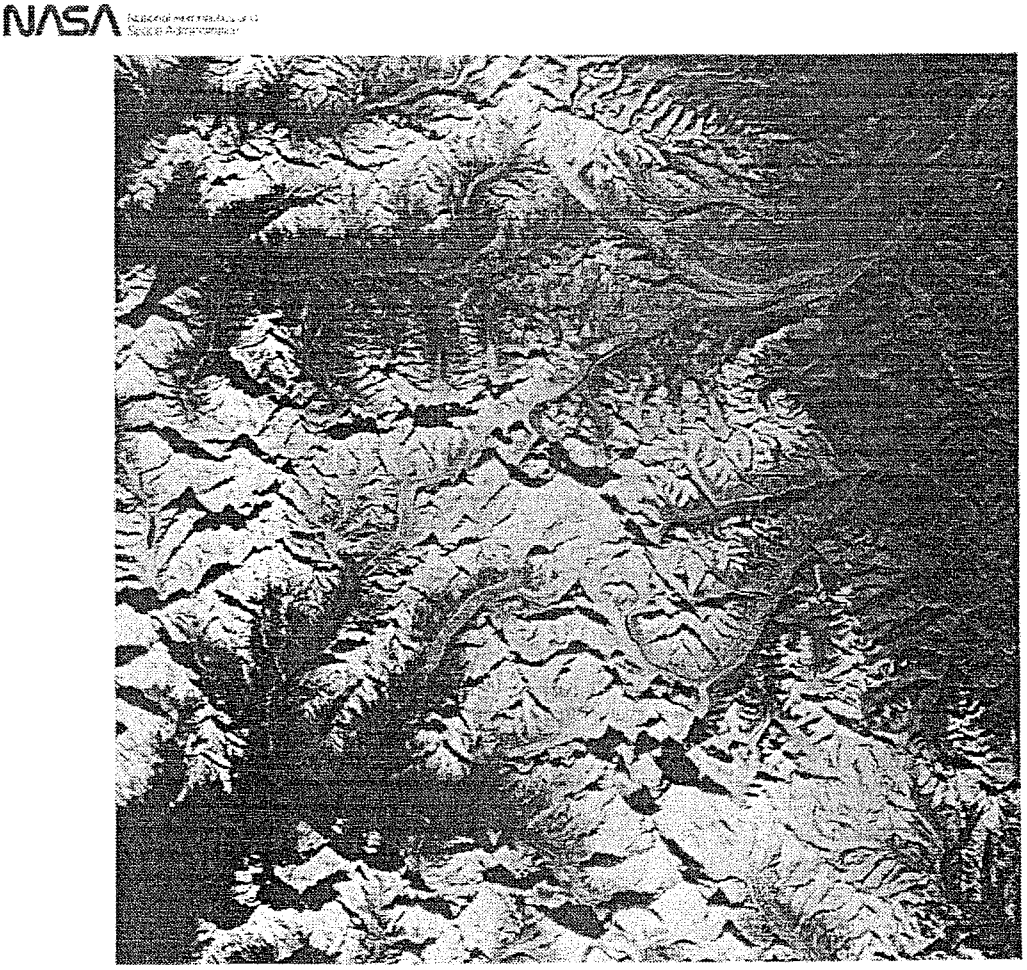

Figure 5.1: Satellite Image of Everest and Cho Oyu, November 3^{rd}1994 (courtesy of NASA).

Much interest has been recently attracted by landscape evolution models. Chief among those are the detailed deterministic models which address the description of the detailed dynamics acting on the landscapes (Howard (1994)). The reductionist approach, where a precise description of the details of the dynamics is sought, is successful, and much interesting, in the pursuit of the description and the classification of landforms. Nevertheless, as standard in critical phenomena, the mechanism producing scale-free structures is expected to depend only on a few key features common to all the networks rather than on the details of the particular system under study. Hence in this work, centered on the dynamic origin of fractal river networks, we follow a nonreductionist approach based on the simplest possible, parameter-free models capable of allowing the emergence of complexity.

In the following sections a brief introduction of river network phenomenology is presented. After that we will introduce our original work. A cellular model recently introduced for the evolution of the fluvial landscape is revisited using extensive numerical and scaling analyses. The relevance of the model, a crucially simple scheme of fluvial erosion which purposedly addresses a single transport process, is related to the speculation that other competing landforming processes are essentially irrelevant to the evolution of the main features of the planar morphology of the network. The basic network shapes and their recurrence especially in the aggregation structure are then addressed. The roles of boundary and initial conditions are carefully analyzed as well as the key effect of quenched disorder embedded in random pinning of the landscape surface. It is found that the above features strongly affect the scaling behavior of key morphological quantities, thereby suggesting new insight into feasible topological optimality and on the complex competition of tectonic and erosional processes. In particular, we conclude that randomly pinned regions (whose structural disorder bears much physical meaning mimicking uneven landscape-forming rainfall events, geological diversity or heterogeneity in surficial properties like vegetation, soil cover or type) play a key role for the robust emergence of aggregation patterns bearing much resemblance to real river networks. The above results, precisely because of the extreme simplicity of the controlled modeling environment, suggest a protocol of relevant factors for all landscape evolutions models ranging from the reductionist approaches to the self-organized ones.

The analogy between sandpiles and rock erosion is here proposed as a possible explanation of the self-similar properties of the drainage basins of rivers. In fact for those systems exist a large number of phenomenological laws that show the long range behavior of the main physical quantities describing the system. Furthermore in this case the self-organization of the system is related to a principle of minimum energy expenditure, that is the model inspired by the sandpile dynamics drives the system towards a global minimum of a state function. The link between global minimization principles and self-organization not only explains in a complete way the river networks evolutions, but it is a promising line of research to fully explain the presence of long range correlations in Nature.

Our main goal is twofold. On one hand we will extend previous investigations both in accuracy

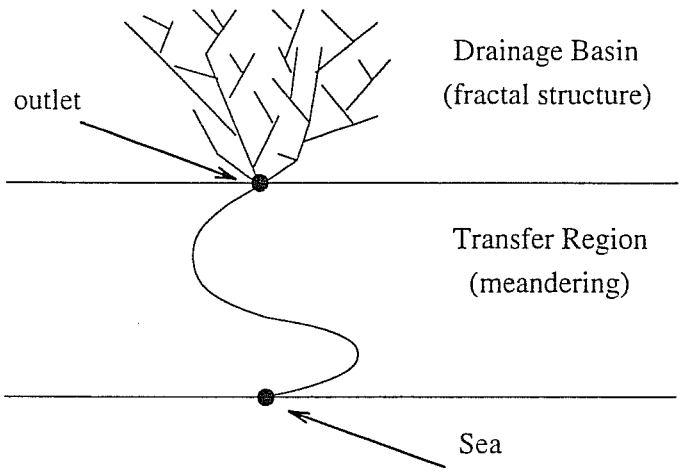

Figure 5.2: Typical structure of a river from mountains to the sea

and in statistics by performing simulations at much larger scales. On the other hand, we will consider important issues such as the effect of the boundaries and of the initial conditions bearing much significance on geologic influences. In particular we will show that both the aforementioned effects play an important role in the results previously obtained. We also study the effects of disorder, say through the presence of small, uncorrelated inhomogeneities in the initial conditions, in particular with regard to the robustness to single/multiple outlet arrangements.

5.2 Geomorphology of River Networks

5.2.1 Basic Phenomenology

Each river can be divided in three different parts (see FIG. 5.2)

- The *drainage basin* whose this work is devoted, in which soil erosion determines formation of fractal structures.
- The transfer region, in which erosion process are rarer and the interplay between the erosion and deposition process gives rise to meandering effects.
- The delta zone, in which the deposition processes take eventually the main place.

In this work we shall consider what is the evolution of the first part of the river, the drainage basin. In this region the space is divided between different separate basins that collect the water flowing over them.

In this region some interesting field observation exists, they are hereafter described to introduce the physical quantities of the phenomenon.

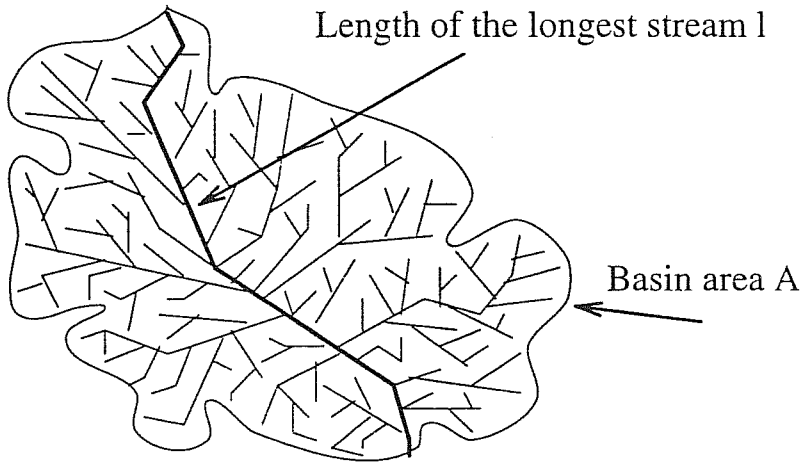

Figure 5.3: Drainage (sub)basin and relative longest stream. The Hack's law states $L \propto A^h$, $h \simeq 0.6$.

5.2.2 Hack's law

The drainage basin of river networks shows a surprisingly universal self-affine nature (see FIG. 5.3)

If one considers the length l of the longest stream in a certain area and the value A of this area, it holds

$$l \propto A^h. \tag{5.1}$$

This is known as *Hack's law* and h is the Hack's exponent (Hack (1957)).

The universality of such law is illustrated in the two following figures: while in FIG. 5.4 only one river (Shenandoah Valley) is studied considering all the possible subbasins, in FIG. 5.5 different rivers in the world are presented with respect to their main basin.

The original work done by Hack was based on fields observations. His conclusion has been verified through the new experimental tool derived from the analysis of satellite photos. This method is call Digital Elevation Map (DEM) and it is introduced hereafter.

5.2.3 Digital Elevation Map Method

The network associated to a given natural terrain pertaining to a river basin can be experimentally analyzed by using the so-called Digital Elevation Map (DEM) technique [e.g. (Band (1986), Tarboton et al. (1988), Rodriguez-Iturbe and Rinaldo in press (1996))] which allows to determine the average height of areas (pixels) of the order 10^{-2}Km^2. Thus a fluvial basin is represented in a objective manner often over 4 log scales of linear size. Lower bounds are imposed by channel initiation processes at $O(10 - 100)$ m. Crossovers of geological nature provide altered aggregation processes and thus an upper cutoff, usually beyond scales of $O(10^5 - 10^6)$ m. Thus the observational evidence

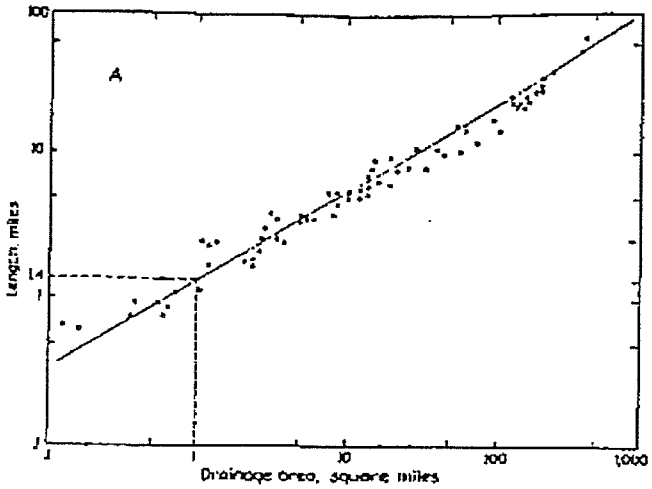

Figure 5.4: Relation between lengths and area of the Shenondah Valley subbasins (courtesy of Rodriguez-Iturbe and Rinaldo).

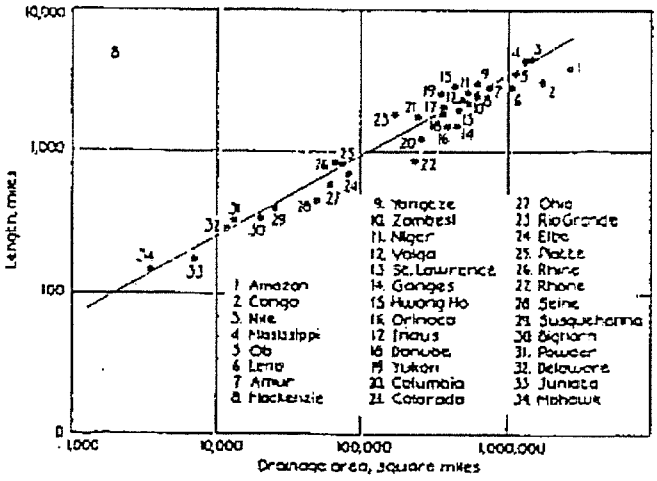

Figure 5.5: Relation between lengths and area of the different rivers in the world (courtesy of Rodriguez-Iturbe and Rinaldo).

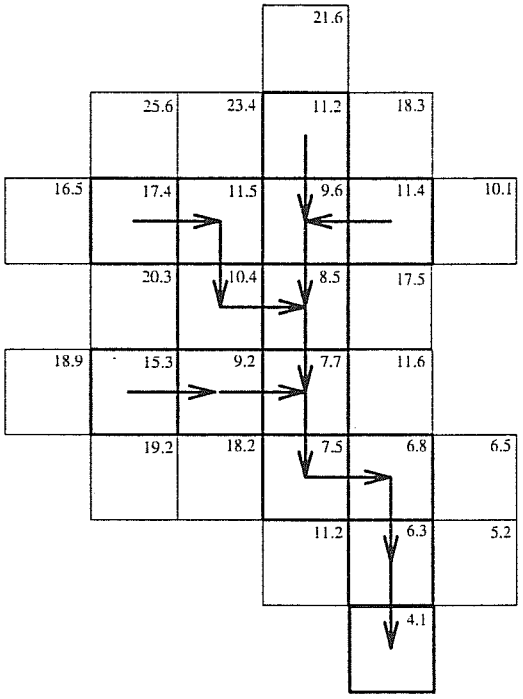

Figure 5.6: An example of the DEM method on a sample elevation map. The mean height of the regions are in fictitious unit length and it is reported in the upper right corner.

yields a much reliable framework over many scales for comparison with dynamical models aimed at the origin of scale-free features.

The method is based on one of the basic principles explained at the beginning that is the water falling from one site follows the steepest descent between those available.

From one satellite photograph the zone is divided into portions of about $10Km^2$ each of these regions will be treated as a point in the following. Then an average height z is assigned to this coarse-grained sites (from satellite it is easy to compute the elevation field of a region).

The network is built using the elevation field and starting from the highest mountain according to the steepest descent rule as depicted in FIG. 5.6. Field observations are then required only to verify the behavior predicted. If one assume that exists uniform flow on the basins, the number of sites *upstream* a certain region can be considered as a measure i of the total water collected.

One typical map of a basin is shown in FIG. 5.7. and it is related to the Fella river in the North of Italy.

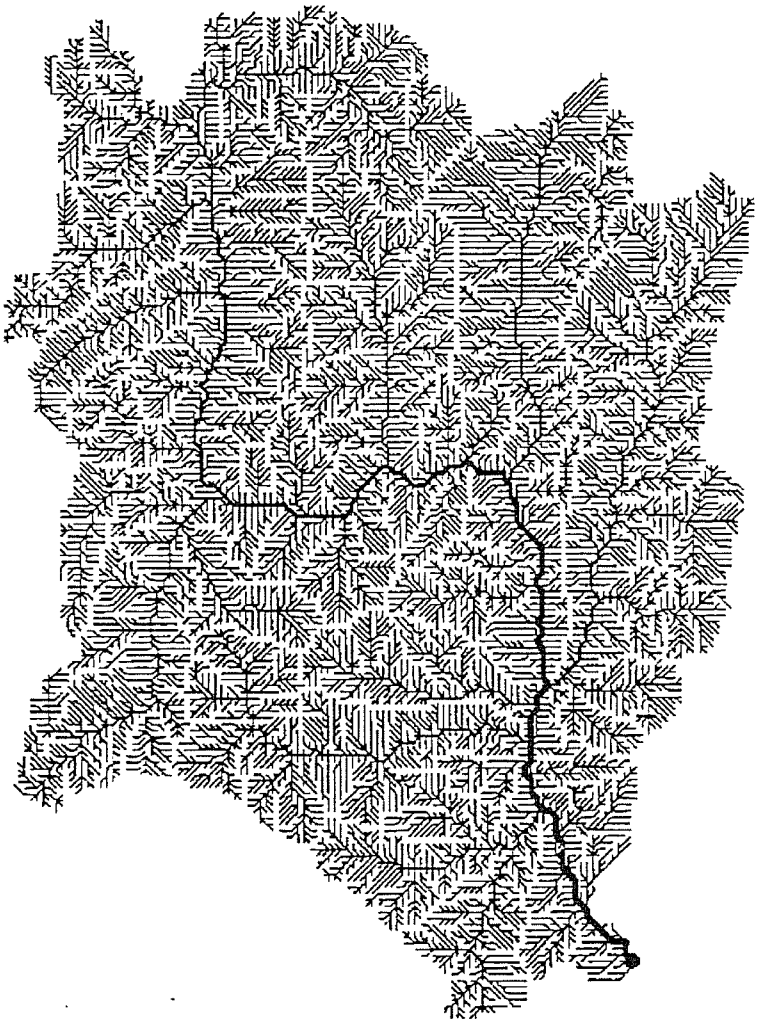

Figure 5.7: An example of the DEM method on a sample elevation map for the Fella river in the North of Italy.

5.2.4 Drainage Area and Threshold Erosion: Feedback between Channelling and Hillslope Evolution

Gilbert (Gilbert (1877)) was the first to enunciate some simple qualitative principles of landscape formation: the law of uniform slope, through which rapid erosion of steeper slopes tends to reduce the landscape to low relief; the divide law, which states that streams steepen toward headwaters; the law of geological structure, which observes that hard rocks erode less and in different time scales and hence "stands out"; and law of the local action. Traditionally, geomorphology of river networks has been divided into the areas of channel network and hillslope geomorphology. The complex interaction between the two regimes and its importance and role have been overlooked for quite a long time(Willgoose, Bras and Rodriguez-Iturbe (1991)). There are significant approaches in the field of hillslope or fluvial evolution by Refs. (Horton (1945), Leopold and Langbein (1962). Culling 1963). These models deal with fluvial or overland flow possibly coupled with erosion, creep, rain splash, and rockfall and debris flow. Altough very different from each other they do not consider the dynamics of landscape evolution and neglect the interplay between fluvial processes and different hillslopes. Aim of this work is to demonstrate that the landscape evolution is ruled by a mechanism similar to those illustrated in the SOC toy models shown in the first chapters. This mechanism links together the two ingredients of fluvial network development and hillslope evolution.

Experimental evidence shows that the topographic threshold associated with channel head locations defines the boundary between essentially smooth and undissected slopes and the valley bottoms towards which they drain. From field obseravtions (Dietrich, Wilson, Montgomery, Kean and Bauer (1992), Dietrich, Wilson, Montgomery and Kean (1993)) show that data from channel heads define a threshold between channelled and unchannelled regions of the landscape.

On the average channels will occurr when the product of powers of the contributing area A and local slope $\vec{\nabla} z$ of the landscape elevation $z(x)$ exceeds a certain critical value. In particular in the following will be adopted the following rule

$$\vec{\nabla} z A^{1/2} \geq \tau \tag{5.2}$$

The above issue were explained by some preliminary models (Rinaldo, Rodriguez-Iturbe, Rigon, Bras and Vasquez (1993), Caldarelli, Maritan, Giacometti, Rodriguez-Iturbe and Rinaldo n.d.a, Caldarelli, Maritan, Giacometti, Rodriguez-Iturbe and Rinaldo n.d.b) where is suggested that the formation process of river networks achieves a steady state upon the attainment of local optimal rules equivalent to a critical erosion parameter and from global rules of minimum energy dissipation equivalent to stable equilibrium.

A flowrate unit is associated with each pixel and the flow contributing to any pixel follows the steepest descent path through drainage directions whose collection defines the planar structure under consideration. The resulting network is therefore the two-dimensional projection of the three-dimensional tree-like structure of the steepest descent paths draining a given basin. The

planar patterns of network aggregation are obtained by employing the original cellular model for the evolution of a fluvial landscape (Rinaldo et al. (1993)). It is aimed at describing in a crucially simple manner the sole fluvial component of landscape evolution. Although such component must be coupled to other - chiefly hillslope - transport processes to yield a comprehensive dynamical description (Willgoose et al. (1991), Dietrich et al. (1993), Howard (1994), Howard, Dietrich and Selby (1994), Rigon, Rinaldo and Rodriguez-Iturbe (1994)), it rules the planar imprinting of the network. Hence the detailed study of the model is deemed significant.

Starting from a three dimensional landscape, evolution occurs according to a threshold dynamics similar to the one proposed in self organized critical (SOC) models The main idea of the erosion dynamics is that whenever the local shear stress exceeds a given threshold, erosion starts an "avalanche" and a related rearrangement of the network patterns takes place. The model of self-organizing fluvial structures may be seen as a modification Of the sandpile model previously introduced, as a paradigm of the dynamics Of open, dissipative systems with many degrees of freedom. It may be thought of as belonging to the set of models in which the threshold for activity, say τ_c, rather than being a constant value, depends on non-local properties of the self-organizing structure. In the fluvial case, the non-local character of the threshold value follows from the fact that the threshold at the arbitrary site equals a shear stress, i.e. $\tau \propto \nabla h\sqrt{a}$, where h is the local landscape elevation and a is total contributing area surrogating total flow collected from a distributed rainfall event. As such, the exceedence of τ_c depends not only on local conditions (i.e., a critical value of ∇h), but also on non-local conditions defined by the contributing area a computed through drainage directions, i.e. it depends on the entire state of the system which is self-organizing. Notice that the physical rationale for the nonlocal dependence lies in the fact that the system is open, i.e. injected from outside, allowing flow rates to be proportional to total contributing drainage area. The long-range nature of the threshold dynamics tends to hide from the observer the temporal fluctuations which take place in the evolutionary time scale. In this sense the above model was classified [*Rinaldo et al., 1993*] as one of spatial self-organized criticality.

Whether or not river self-organization qualifies as a more general framework of self-organized criticality remains to be seen. If SOC must necessarily refer to the occurrence of a critical state in the sense of critical phenomena, where a small local perturbation can cause a significant change in the configuration of the whole system and thus the system shows both spatial and temporal scaling, then the time dynamics should be specifically considered. One way to do this is through the oscillation of the threshold in time, i.e. $\tau_c(t)$, simulating climatic fluctuations (Rinaldo, Dietrich, Vogel, Rigon and Rodriguez-Iturbe (1995))

through which indeed temporal evolution appear, or through perturbations of random location and strength in the evolution of the landscape. This is also true, as we will discuss later, if the landscape-forming rainfall events are described as nonuniform in space, leading to patches of activity randomly scattered spatially (in such a case the outflow response of the system becomes a $1/f$ signal). However, regardless of any additional features, we believe that the central scope of

SOC is the dynamic explanation of the growth of fractal structures of the type appearing in nature, i.e. the physics of fractals. As such we feel that our classification of the model as a particular case of SOC is a suitable one regardless of the description of the embedded temporal activity because the system always reaches a fractal state.

A question, indeed more interesting than the semantics of SOC, is whether the constraints in the model may be relaxed to produce a 'hot' fluvial landscape more closely resembling an ordinary sandpile (Rodriguez-Iturbe and Rinaldo in press (1996)).

5.3 The model

We consider a lattice model of a real landscape. Let h_x be the height of the landscape associated to every site x of a square lattice of size $L \times L$. The lattice is tilted at an angle θ with respect to a given axis to mimic the effects of gravity. Two possibilities will be analyzed:

1 All the sites on the lowest side (kept at height $h = 0$) are possible outlets (i.e. the multiple outlet arrangement) of an ensemble of rivers which are competing to drain the whole $L \times L$ basin;

2 Only one site is kept at $h = 0$ and it is the outlet of a single river in the $L \times L$ basin.

In addition, for both the above cases, two types of initial conditions will be considered: (a) a regular initial landscape, e.g. flat, and (b) an irregular surface obtained by superposing to a smooth sloping surface a suitable noise.

Each site collects an unit amount of water from a distributed injection (here a constant rainfall rate as in the original approach) in addition to the flow which drains into it from the upstream sites. A unit of water mass is assigned to each pixel of drainage area so that the total area drained into a site is also a measure of the total water mass collected at that site. ¿From each site water flows to one of the eight sites, four nearest neighbors and four next nearest neighbors, having the lowest height (i.e. the steepest descent path). We shall indicate all these eight neighboring sites as nearest-neighbors (nn). This construction allows the assignment of drainage directions to an arbitrary landscape. The drained area a_x is associated to each site x according to the equation

$$a_x = \sum_{y(x)} a_y + 1 \tag{5.3}$$

where the sum runs over the subset $y(x) \in nn(x)$ of neighbor sites whose area is actually drained by x. The second term in eq.(5.3) represents the uniform injection.

Also, the (up)stream-length l_x from site x to the source is computed according to the following procedure. At a given site x the areas of all $nn(x)$ of that sites are checked. The nn with largest value leads to the outlet and is defined to be a downstream site. The nn with the second largest

value indicates the longest path toward the source and is defined to be the upstream site. The sum of all the upstream sites from site x to the source is l_x. The downstream length could be defined through an analogous procedure. Experimental measures are available for both a_x and l_x (Rodriguez-Iturbe and Rinaldo in press (1996)).

The time evolution of the model follows the following steps:

1 The shear stress τ_x acting at every site is computed according to

$$\tau_x = \Delta h_x \sqrt{a_x} \tag{5.4}$$

where Δh_x is the local gradient along the drainage direction.

2 If the shear stress at a site exceeds a threshold value, τ_c, then the corresponding height h_x is reduced (i.e. by erosion) in order to decrease the local gradient. The shear stress is set just at the threshold value. This produces a rearrangement of the network followed by a reupdating of the whole pattern as in step 1.

3 When all sites have shear stress below threshold the system is in a dynamically steady state. Since this situation is not necessarily the most stable, a perturbation is applied to the network with the aim of increasing the stability of a new steady state. A site is thus chosen at random and its height is increased in such a way that no lakes, i.e. sites whose height is lower than that of their eight neighbors. are formed. Steps 1 and 2 then follow as before.

After a suitable number of the perturbations (step 3), the system reaches a steady state which is unsensitive to further perturbations and where all statistics of the networks are stable. This resulting state is scale-free, i.e. it is characterized by power-law distributions of the physical quantities of interest.

5.4 Results

5.4.1 Landscape evolutions

Our numerical calculations were carried out on a bidimensional square lattice (where each site has eight nearest-neighbors) for sizes up to $L = 200$ with reflecting boundary conditions in the direction transversal to the flow and open boundary condition in the parallel one. We considered the following initial conditions:

Model A A comb-like structure with a single outlet This was the situation originally studied in (Rinaldo et al. (1993)) and our results are in agreement with theirs.

Model B An inclined plane with all sites at the bottom of the plane allowed to be possible outlets. This choice was selected with the aim of investigating the differences arising when arranging the boundary conditions with multiple outlets versus single outlet. The former allows for competition for drainage area among rivers.

Model C,D The two previously considered situations with the addition of a random, uncorrelated noise (whose strength - i.e. variance - is less than 10% of the average height).

An average over a few (up to five) configurations was taken. This choice, especially when coupled to large sizes of the system, proves sufficient for a statistical descriptions sought in view of the self-averaging nature of the random perturbation.

In FIG.5.8 typical landscapes sculpted by the above dynamical process are shown in four cases (corresponding to models A,B,C and D). The corresponding networks drawn through the steepest descent construction are shown in FIG.re 5.9.

Two features can be grasped from these pictures. First, in the results of both model A and B there is a strong memory of the initial configuration despite the fact that the dynamics of the erosion process was somewhat expected to be sufficiently strong to soon lose the imprinting of its initial condition. Secondly, the single outlet restriction imposed in model A appears to be a severe constraint because it increasingly affects the wandering of the main river towards the lowest part of the basin. Our results suggest that this is indeed the case for flat initial conditions (A and B) while for noisy initial conditions boundary effects are of lesser importance.

5.4.2 Area and length exponents

Let us define $P(a, L)$ and $\Pi(l, L)$ as the exceedence (cumulative) probability distributions of the drainage area a and stream length l respectively arising in a domain of linear size L. The following scaling forms are expected to hold (Maritan et al. (1996)):

$$P(a, L) = a^{1-\tau} F(\frac{a}{L^{1+H}}) \tag{5.5}$$

$$\Pi(l, L) = l^{1-\gamma} G(\frac{l}{L^{d_l}}) \tag{5.6}$$

Here H is the Hurst exponent (Feder (1988)) and d_l is the stream-length (or chemical distance) fractal exponent.

As it was already noted (Maritan et al. (1996)), for self-affine river networks ($H < 1$, $d_l = 1$) the scaling relations relate all exponents in terms of H. For self-similar river networks ($H = 1$, $d_l > 1$), the same happens in terms of d_l.

Another important indicator of basin morphology is the relation between the mean total contributing area $< a >$ and the length of the main stream $l_{\max} \propto L^{d_l}$, which follows the previously

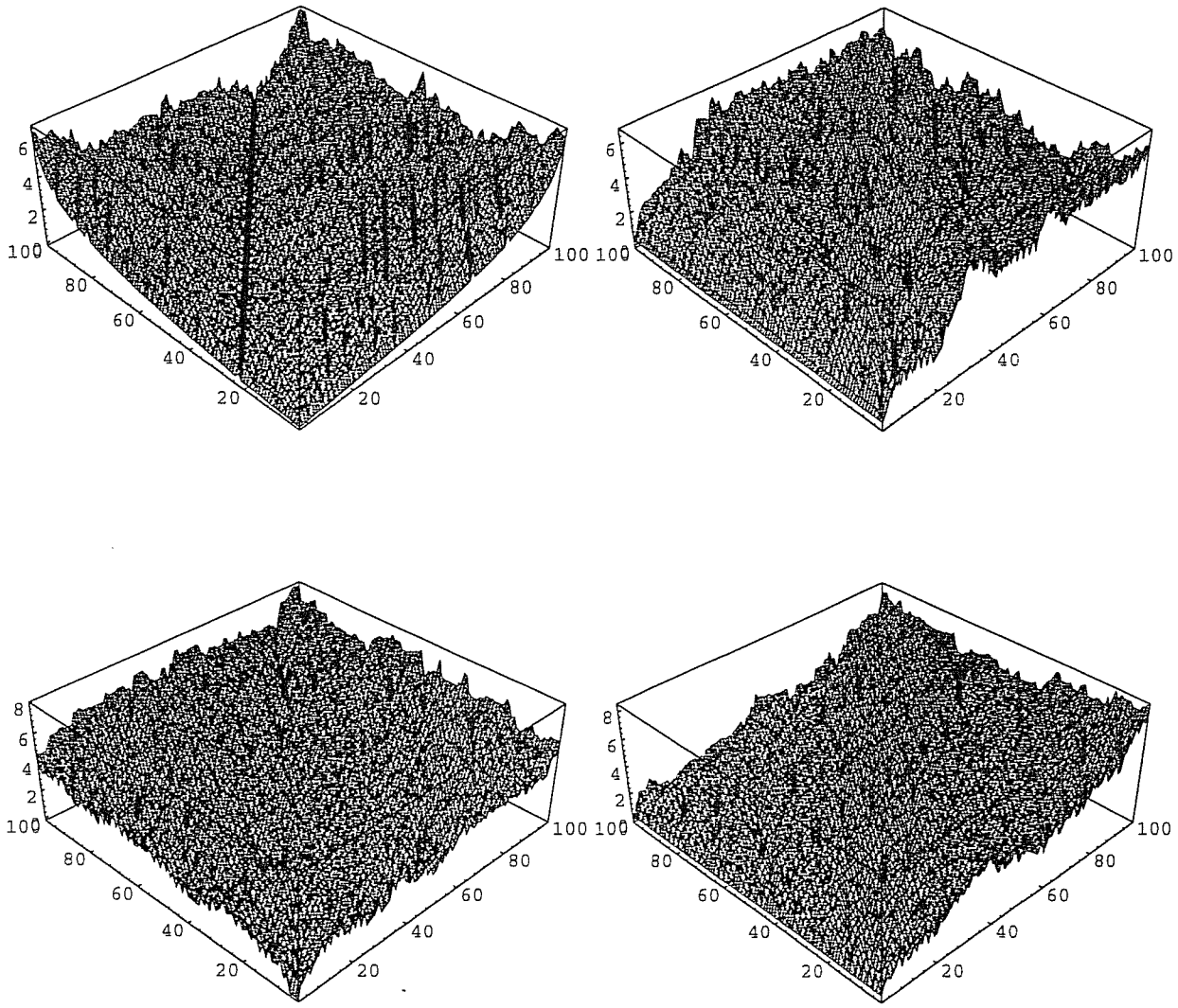

Figure 5.8: In clockwise order a snapshot of the final landscape for Model A, Model B, Model D and Model C. Model A and C have a single outlet, Model B and D have multiple outlets. The initial condition is deterministic for A and B, while C (D) has a small random noise superimpose to A (B).

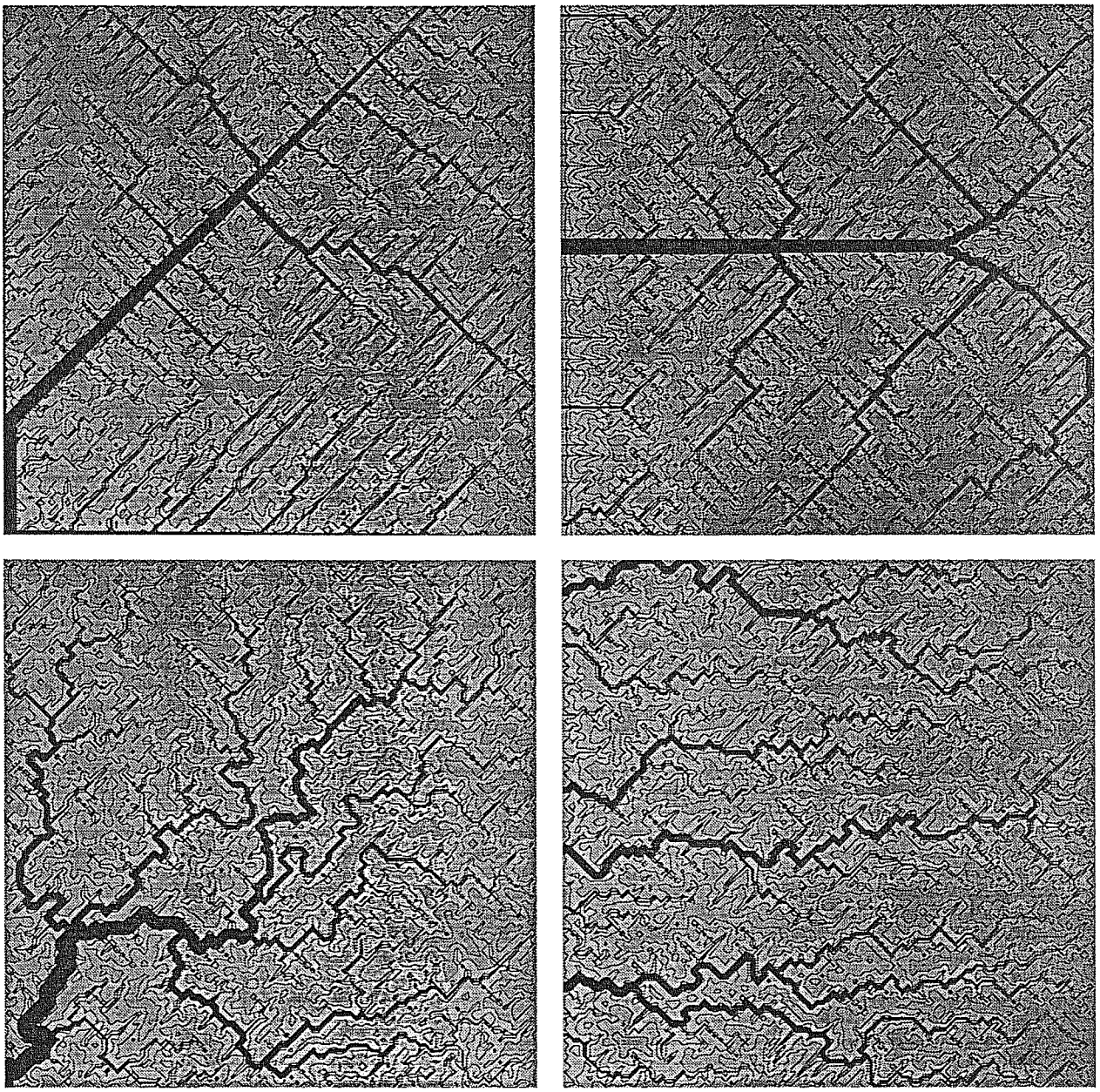

Figure 5.9: The network structure corresponding to the landscapes of the previous figure. Only sites with area ≥ 5 are shown for sake of clarity.

introduced Hack's law (Hack (1957)):

$$< a > \propto l_{max}^{1/h} \propto L^{d_l/h} \tag{5.7}$$

The related exponent has been studied in all simulations. A summary of the scaling relations between the various exponents involved is reported in Table 5.1.

Experimental values of τ and γ are available from earlier analyses of DTMs from basins of different size, geology, exposed lithology, climate and vegetation (Rodriguez-Iturbe and Rinaldo in press (1996)). It was observed that, while a majority of basins tend to seemingly universal values $\tau = 1.43 \pm 0.02$ and $\gamma = 1.8 \pm 0.1$, exceptions are observed where altered values are observed although always in a concerted manner. Since it was suggested that scaling laws for river networks are related, e.g. $\gamma = 1 + (\tau - 1)/h$, it was concluded there that no universal exponents are expected in nature. Rather, the roles of geology and tectonics concert a coordinated scaling structure which strives for fractality yet adapted to its geological environment. The results of the model described here, revisited in the above light, conform to this view.

Our results for model A are in agreement with the results of (Rinaldo et al. (1993)). The results of the four models A,B,C and D for the area distributions are shown in FIG.5.3 It is apparent that, due to the pathological initial conditions, the scaling behavior for models A and B is somewhat more noisy than for models C and D. FIG. 5.11 contains the collapse plot for case C. The case D (not shown) is almost undistinguishable from case C. FIG. 5.12 shows the stream-length distribution for model C for which the same remarks of FIG. 5.3 apply. In FIG. 5.13 we show the collapse plot corresponding to case C.

A summary of the scaling exponents obtained is included in Table 5.2 where we observe a consistent picture of related scaling exponents as theoretically expected - see Table 5.1.

We have also monitored the evolution of total energy dissipation of the system, defined as $E = \sum_x a_x^{0.5}$ (where x spans all sites of the lattice) (Rinaldo, Rodriguez-Iturbe, Rigon, Bras, Vasquez and Marani (1992)).

We observe an almost monotonical decrease of E associated with the dynamical evolutions, and a stabilization on different plateaus of values of E. This fact, also observed in other models bears important consequences in the light of the suggested connection of fractality and optimality.

5.5 Geological constraints and Quenched Random Pinning

This section presents a detailed study on the effects on landscape evolution of quenched randomness, simulated by a random choice of sites unable to evolve regardless of the threshold value developed therein. It is found that this form of disorder tends to favour aggregation patterns characterized by values of $\tau = 1.43 \pm 0.02$ for both models, say, A and B (i.e. with single outlets or open boundary conditions). This results suggests that the origin of the recurrent values observed in nature could

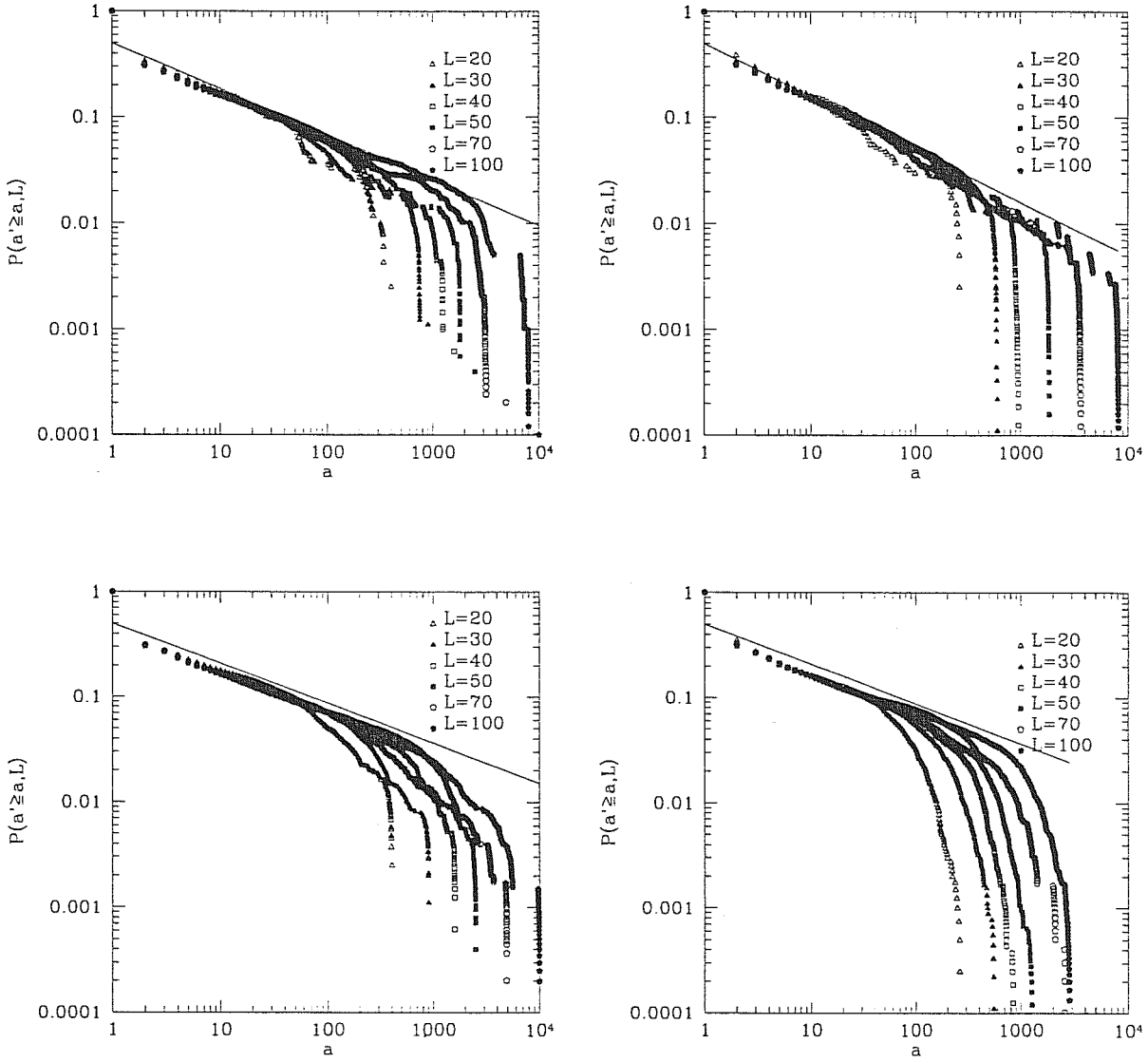

Figure 5.10: Log-Log plot of the area cumulated distribution $P(a, L)$ versus a for model A,B,C and D, in the same order as above. The full line has a slope corresponding to $\tau = 1.43$, $\tau = 1.50$, $\tau = 1.38$ and $\tau = 1.38$ respectively.

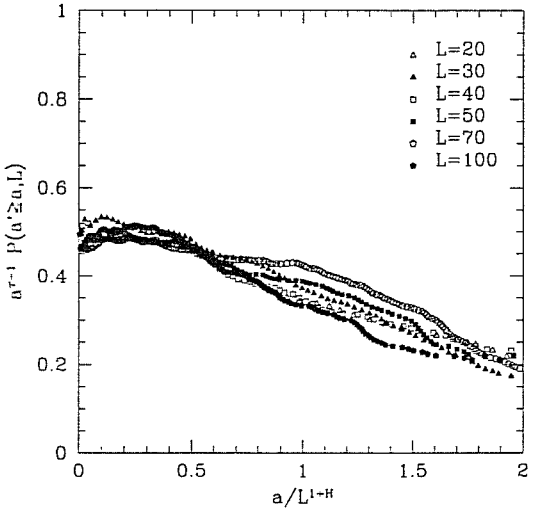

Figure 5.11: Scaling function $a^{1-\tau}P(a, L)$ versus a/L^{1+H} for model C. The used values to obtain the collapse were $\tau = 1.38$ and $H = 0.6$.

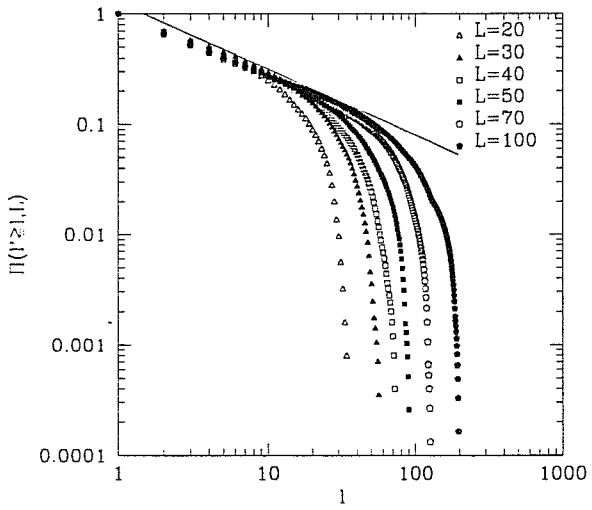

Figure 5.12: Log-Log plot of the upstream cumulated lengths $\Pi(l, L)$ versus l for model C. The full line has a slope corresponding to $\gamma = 1.6$.

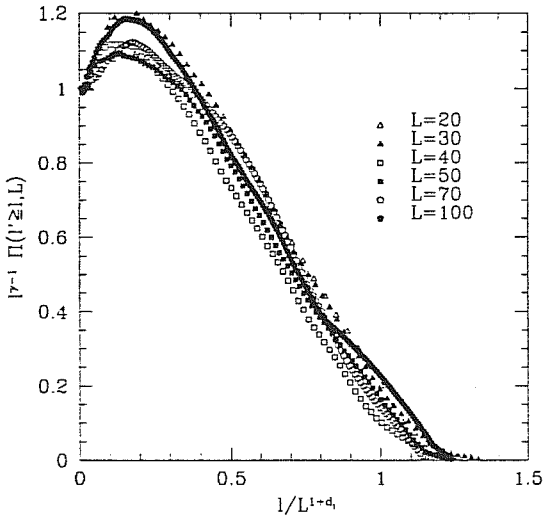

Figure 5.13: Scaling function $l^{1-\gamma}\Pi(l,L)$ versus l/L^{d_l} for model C. The used values to obtain the collapse were $\gamma = 1.6$ and $d_l = 1.0$.

be related to the ubiquity of heterogeneity in surface properties characterizing locally the critical shear threshold.

Within the river basin morphological and geological constraints play a definite role in the dynamical evolution of landforms. The effects of quenched constraints, simulating any heterogeneity is the distribution of surficial properties affecting erosion properties, is to favour some sites for the flowpaths, thus excluding other sites from the capture of the developing network which ultimately shapes the evolution process. In order to mimic such effects we analyzed the effect of a random pinning of a small region of the total surface (typically $5-9\%$) where the evolution is frozen, that is, the height is pinned to its initial value. We find that this constraint tends to favour aggregation even in the presence of random initial conditions.

FIG.5.14 displays the effect of the pinning. FIG.5.14 (a) shows the evolved configuration of a 100 configuration with multiple outlet and random initial noise (model C). FIG. 5.14 (b) shows the same configuration but with a 5% dilution pinning. It is apparent how some of the smaller streams on the left have increased their size thus leading to a bigger aggregation.

In this case we found $\tau = 1.43 \pm 0.02$. Moreover, all the other exponents verify the correct scalings predicted in Table 5.1. Purely for comparison purposes with the prevous results, we also report the plot of the area distribution and the corresponding collapse plot for this case in FIG. 5.15.

We also found that model D reproduces the same results, i.e. $\tau \sim 1.43$ and $\gamma \sim 1.60$, and that these are robust with respect to changes of the pinning dilution (actually we have reached a density

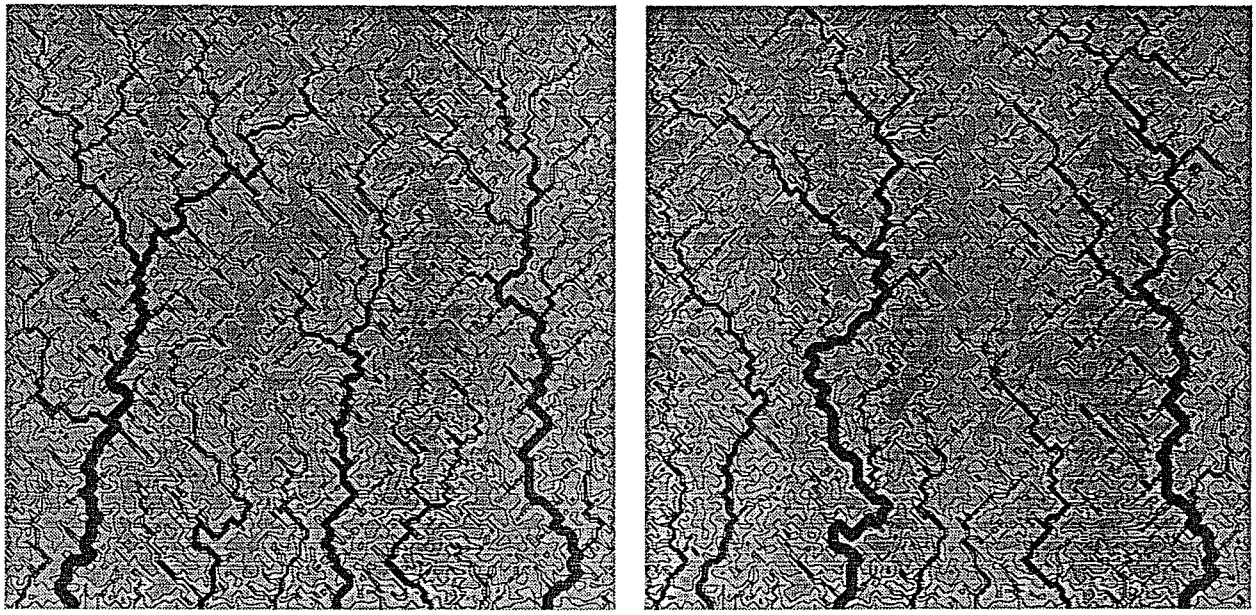

Figure 5.14: Comparision between the evolution of two identical initial configurations of model C with size $L = 100$ without (left) and with pinning (right). The pinning diluition was 5%.

of quenched sites up to 9%). This result suggests that the origin of recurrent values observed in nature could indeed be related to the ubiquity of geological and morphological constraints in the surface properties locally characterizing the critical shear stress.

5.6 Conclusions

In this chapter we revisited the model originally introduced in (Rinaldo et al. (1993)) which we extended both in accuracy and goals. Specifically, we analyzed the stability of the universality class of the original model with respect to the initial conditions and to the change from single to multiple outlets. We found that if one starts with structured initial conditions, critical exponents are sensible to a change from single to multiple outlets. On the other hand, upon starting from disordered initial conditions, we found critical exponents belonging to a new class which appears to be robust to the change from single to multiple outlet. Thus this simple model, under controlled conditions, yields somewhat different yet internally consistent scale-free fluvial landforms depending on the dominant conditions affecting evolution.

The above results conform to the experimental observation suggesting that the relevant scaling exponents for river networks are not universal. Rather, the fractal nature of river networks adjusts to the constraints imposed by the geological environment in a coordinated manner. As such a consistent variation of all scaling exponents is observed, Table 5.1.

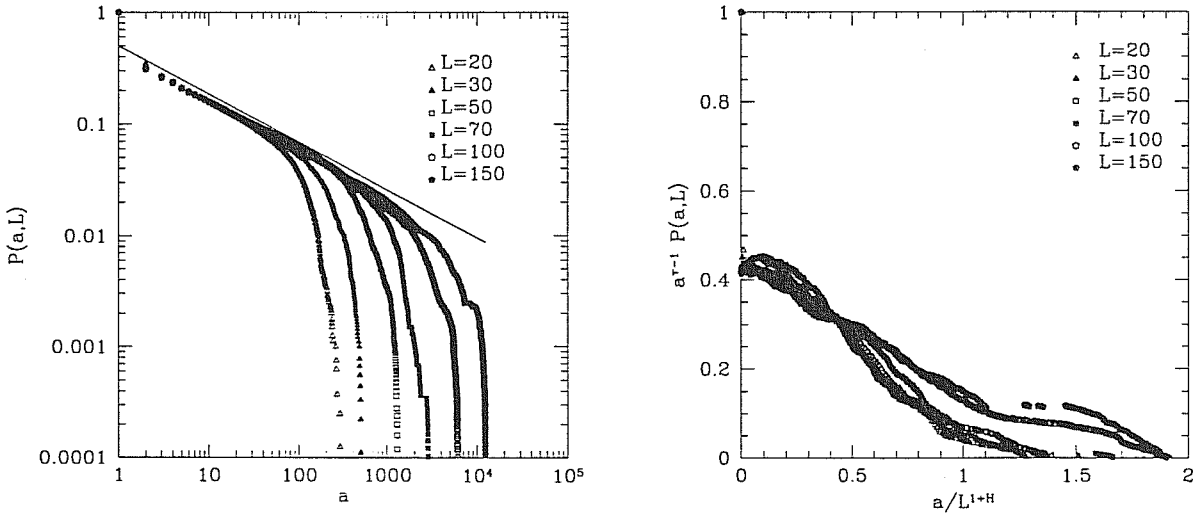

Figure 5.15: Log-Log plot of the area distribution $P(a, L)$ vs. a (left) and corresponding collapse plot (right) for model C with a 5% dilution.

Exponent	Self-Similar	Self-Affine
τ	$2 - d_l$	$(1+2H)/(1+H)$
γ	$2/d_l$	$1+H$
h	$d_l/2$	$1/(1+H)$

Table 5.1: Scaling relations: all the exponents can be determined in terms of d_l in the fractal case and H in the self-affine case.

	Model A	Model B	Model C	Model D
τ	1.43 ± 0.03	1.50 ± 0.03	1.38 ± 0.02	1.38 ± 0.02
γ	1.60 ± 0.05	1.70 ± 0.05	1.60 ± 0.02	1.60 ± 0.02

Table 5.2: Summary of the results for the four models considered in the text. Here we show the sets of critical scaling exponents τ and γ obtained from the various simulations after suitable ensemble averaging.

It is interesting to observe that the final state of all simulation yields indeed fractal structures, as observed in nature, though characterized by different aggregation properties. We suggest that the lack of robustness of the scaling exponents with respect to boundary and initial conditions is related to the non-local character of the shear-based threshold, differently from what is observed in classical sandpile models of self-organized criticality. The intrinsic interest of the different aggregation properties of the steady states of the dynamics is related to their optimality with respect of total energy dissipation. In fact, depending on external conditions, the same dynamical process may indeed get trapped in steady state configurations yielding local minima of the total energy dissipation functional, in what we may define as a feasible optimality process.

Finally, we have found that quenched disorder, modeled by random pinning, has a profound effect on the robustness of the resulting planar patterns by favouring aggregation and by locking the planar landforms into modes quite similar to the ones observed in nature.

The remarkable success obtained by such a simple model in enlightening some crucial features of the real basins is promising for a future success in a general characterization of the dynamics of fractal growth.

Bibliography

Alstrøm, P.: (1988), Mean field exponent for self–organized critical phenomena, *Physical Review A* **38**, 4905–4906.

Bak, P., Chen, K. and Creutz, M.: (1989), Self–organized criticality in the "game of life", *Nature* **342**, 780–782.

Bak, P. and Sneppen, K.: (1993), Punctuated equilibrium and criticality in a simple model of evolution, *Physical Review Letters* **71**, 4083–4086.

Bak, P., Tang, C. and Wiesenfeld, K.: (1987), Self–organized criticality: an explanation of $1/f$ noise, *Physical Review Letters* **59**, 381–384.

Band, L.: (1986), Topographic partition of watersheds with digital elevation model, *Water Resources Research* **22**, 15–24.

Bernardes, A. T. and Moreira, J. G.: (1994), Model for fractures in fibrous material, *Physical Review B* **49**, 15035–15039.

Binder, K.: (1993), *Phase Transitions and Critical Phenomena*, Vol. **8**, London Academic, London.

Boettcher, S. and Paczuski, M.: (1996), Exact results for spatiotemporal correlations in a self organized critical model of punctuated equilibrium, *Physical Review Letters* **76**, 348–351.

Burlando, B.: (1990), *Journal of Theoretical Biology* **146**, 99.

Burlando, B.: (1993), *Journal of Theoretical Biology* **163**, 161.

Cafiero, R., Loreto, V., Pietronero, L., Vespignani, A. and Zapperi, S.: (1995), Local rigidity and self–organized criticality for avalanches, *Europhysics Letters* **29**, 111–116.

Caldarelli, G.: 1996, Mean field theory for ordinary and hot sandpiles.

Caldarelli, G., Castellano, C. and Vespignani, A.: (1994), Fractal and topological properties of directed fractures, *Physical Review E* **49**, 2673–2679.

Caldarelli, G., Di Tolla, F. D. and Petri, A.: (1996), Self–organization and annealed disorder in fracturing processes.

Caldarelli, G., Loreto, V., Ivaskevic, E. and Vespignani, A.: 1996, Renormalization group for hot sandpiles.

Caldarelli, G., Maritan, A., Giacometti, A., Rodriguez-Iturbe, I. and Rinaldo, A.: n.d.a.

Caldarelli, G., Maritan, A., Giacometti, A., Rodriguez-Iturbe, I. and Rinaldo, A.: n.d.b.

Caldarelli, G., Maritan, A. and Vendruscolo, M.: 1996, Hot sandpiles.

Caldarelli, G., Tebaldi, C. and Stella, A. L.: (1996)a, Branching process and life evolution at the end of a food chain, *Physical Review Letters* **76**, 4983–4986.

Caldarelli, G., Tebaldi, C. and Stella, A. L.: 1996b, Renormalization group approach on boundary effects in sandpiles, *in preparation* .

Caldarelli, G., Vespignani, A. and Pietronero, L.: 1995, Fixed scale transformation for fracture growth processes governed by vectorial field, *Physica A* **215**, 223–232.

Carlson, J. M. and Langer, J. S.: (1989), Properties of earthquakes generated by fault dynamics, *Physical Review Letters* **62**, 2632–2635.

Coniglio, A.: (1982), Cluster structure near the percolation threshold, *Journal of Physics A* **15**, 3829. At least in the case of the $q = 1$ Potts model, i. e. percolation, this can be easily verified by considering this derivation of the red bond dimension.

Coniglio, A.: (1989), Fractal structure of Ising and Potts clusters: exact results, *Physical Review Letters* **62**, 3054–3057.

Culling, W.: 1963, Soil creep and the development of hillside slopes, *J. Geol.* **71**, 127–161.

de Arcangelis, L., Hansen, A., Roux, S. and Herrmann, H. J.: (1989), Scaling laws in fracture, *Physical Review B* **40**, 877–880.

de Boer, J., Derrida, B., Flyvberg, H., Jackson, A. D. and Wettig, T.: (1994), Simple model of self–organized biological evolution, *Physical Review Letters* **73**, 906–909.

de Boer, J., Jackson, A. D. and Wettig, T.: (1995), Criticality in a simple model of evolution, *Physical Review E* **51**, 1059–1074.

Dhar, D.: (1990), Self–organized critical state of sandpile automaton models, *Physical Review Letters* **64**, 1613–1616.

Dietrich, W. E., Wilson, C. J., Montgomery, D. R. and Kean, J. M.: (1993), Analysis of erosion thresholds, channel networks and landscape morphology using a digital terrain model, *J. Geol.* **3**, 161–180.

Dietrich, W. E., Wilson, C. J., Montgomery, D. R., Kean, J. M. and Bauer, R.: (1992), Erosion thresholds, and land surface morphology, *J. Geol.* **20**, 675–679.

Duxbury, P. M. and Leath, P. L.: (1994), Failure probability and average strength of disordered systems, *Physical Review Letters* **72**, 2805–2809.

Eldredge, N. and Gould, S.: (1988), Punctuated equilibrium prevails, *Nature (London)* **332**, 211–212.

Feder, J.: (1988), *Fractals*, Plenum, New York.

Feller, W.: (1971), *An Introduction to Probability Theory and its Applications*, Wiley & Sons, New York.

Flyvbjerg, H., Sneppen, K. and Bak, P.: (1993), Mean field theory for a simple model of evolution, *Physical Review Letters* **71**, 4087–4091.

Frette, V., Christensen, K., Malthe-Sørensen, A., Feder, J., Jøssang, T. and Meakin, P.: (1996), Avalanche dynamics in a pile of rice, *Nature* **379**, 49–52.

Gilbert, G. K.: (1877), *Report on the geology of the Henry Mountains*, Vol. U.S. Geological Survey of the Rocky Mt. Rg.

Gould, S. and Eldredge, N.: (1977), *Paleobiology* **3**, 114.

Gould, S. and Eldredge, N.: (1993), Punctuated equilibrium comes of age, *Nature* **366**, 223–227.

Grassberger, P. and Manna, S. S.: (1990), Some more sandpiles, *Journal de Physique* **51**, 1077–1098.

Hack, J. T.: (1957), Studies of longitudinal profiles in virginia and maryland, *U. S. Geological Survey Prof. Paper* **294-B**, 1.

Hansen, A., Roux, S. and Herrmann, H. J.: (1989), *Journal de Physique* **50**, 733.

Harris, A. B. and Lubensky, T. C.: (1981), Generalized percolation, *Physical Review B* **24**, 2656–2670.

Harris, T.: (1963), *Theory of Branching Processes*, Springer & Verlag, Berlin.

Horton, R. E.: (1945), Erosional development of streams and their drainage basins: Hydrophysical approach to quantitative morphology, *Geological Society American Bullettin* **56**, 275–30.

Howard, A. D.: (1994), A detachment-limited model of drainage basin evolution, *Water Resource Research* **30**, 2261–2285.

Howard, A., Dietrich, W. and Selby, M.: (1994), Modelling fluvial erosion on regional to continental scales, *Journal of Geophysical Research* **99**, 13971–13986.

Hwa, T. and Kardar, M.: (1992), Avalanches hydrodynamics and discharge events in models of sandpiles, *Physical Review A* **45**, 7002–7023.

Kramer, E. M. and Lobkovsky, A.: (1995).

Landau, L. D. and Lifshitz, E. M.: (1970), *Theory of Elasticity*, Pergamon Press, Oxford.

Leopold, L. B. and Langbein, W. B.: (1962), The concept of entropy in landscape evolution, *U. S. Geological Survey Prof. Pap.* **500 A.**

Majumdar, S. N. and Dhar, D.: (1992), Equivalence between the Abelian sandpile model and the $q \to 0$ limit of the Potts model, *Physica A* **185**, 129–145.

Mandelbrot, B.: (1982), *The Fractal Geometry of Nature*, W. H. Freeman, S. Francisco.

Manna, S. S.: (1990), Large scale simulation of avalanche cluster distribution in sand pile model, *Journal of Statistical Physics* **59**, 509–521.

Manna, S. S.: (1991), Critical exponents of sand pile models in $2d$, *Physica A* **179**, 249–268.

Maritan, A., Rinaldo, A., Giacometti, A. and Rodriguez-Iturbe, I.: (1996), Scaling laws for river networks, *Physical Review E* **53**, 1510–1515.

Maslow, S., Paczuski, M. and Bak, P.: (1994), Avalanches and $1/f$ noise in evolution and growth models, *Physical Review Letters* **73**, 2162–2165.

Olami, Z., Feder, H. J. S. and Christensen, K.: (1992), Self–organized crticality in a continuous nonconservative cellular automata modelling earthquakes, *Physical Review Letters* **68**, 1244–1247.

Petri, A., Paparo, G., Vespignani, A., Alippi, A. and Costantini, M.: (1994), Experimental evidence of critical dynamics in microfracturing processes, *Physical Review Letters* **73**, 3423–3426.

Pietronero, L., Vespignani, A. and Zapperi, S.: (1994), Renormalization scheme for self–organized criticality in sandpiles models, *Physical Review Letters* **72**, 1690–1693.

Raup, D. M.: (1986), Biological extinction in earth history, *Science* **231**, 1528–1533.

Rigon, R., Rinaldo, A. and Rodriguez-Iturbe, I.: (1994), On landscape self-organization, *Journal of Geophysical Research* **99**, 11971–11993.

Rigon, R., Rodriguez-Iturbe, I., Giacometti, A., Maritan, A., Tarboton, D. and Rinaldo, A.: (1993), On hack's law.

Rinaldo, A., Dietrich, W. E., Vogel, G. K., Rigon, R. and Rodriguez-Iturbe, I.: (1995), Geomorphological signatures of varying climate, *Nature* **374**, 632–636.

Rinaldo, A., Rodriguez-Iturbe, I., Rigon, R., Bras, R. L. and Vasquez, E. I.: (1993), Self–organized fractal river networks, *Physical Review Letters* **70**, 822–825.

Rinaldo, A., Rodriguez-Iturbe, I., Rigon, R., Bras, R. L., Vasquez, E. I. and Marani, A.: (1992), Minimum energy and fractal structures of drainage networks, *Water Resource Research* **28**, 2183–2190.

Rodriguez-Iturbe, I., Ijjasz-Vasquez, E., Bras, R. L. and Tarboton, D. G.: (1992), Power law distribution of mass and energy in river basin, *Water Resource Research* **28**, 1095–1103.

Rodriguez-Iturbe, I. and Rinaldo, A.: in press (1996), Fractal river basins, chance and self-organization.

Scheidegger, A. E.: (1967), *Bull. Assoc. Sci. Hydrol.* **65**, 15.

Stella, A. L., Tebaldi, C. and Caldarelli, G.: (1995), Self–organized critical scaling at surfaces, *Physical Review E* **52**, 72–75.

Tang, C. and Bak, P.: (1988)a, Critical exponent and scaling relations for self–organized critical phenomena, *Physical Review Letters* **60**, 2347–2350.

Tang, C. and Bak, P.: (1988)b, Mean field theory of self–organized critical phenomena, *Journal of Statistical Physics* **51**, 797–802. Notice that in this and the following reference the τ definition differs from that adopted here. Our τ must be increased by 1 in order to match with their definition.

Tarboton, D., Bras, R. L. and Rodriguez-Iturbe, I.: (1988), The fractal nature of river networks, *Water Resource Research* **24**, 1317–1322.

Tzschichholz, F. and Herrmann, H. J.: (1995), Simulation of pressure fluctuations and acoustic emission in hydraulic fracturing, *Physical Review E* **51**, 1961–1970.

Vergeles, M.: (1995), Self–organization at non zero temperatures, *Physical Review Letters* **75**, 1969–1972.

Vespignani, A. and Zapperi, S.: n.d., personal communication.

Vespignani, A., Zapperi, S. and Loreto, V.: 1996, Dynamically driven renormalization group, *submitted to Journal of Statistical Physics* . babbage preprint COND-MAT 9603052.

Vespignani, A., Zapperi, S. and Pietronero, L.: (1995), Renormalization approach to the self–organized critical behaviour of sandpile models, *Physical Review E* **51**, 1711–1724.

Willgoose, G. R., Bras, R. L. and Rodriguez-Iturbe, I.: (1991), A coupled channel network growth and hillslope evolution model, *Water Resource Research* **27**, 1671–1702.

Yan, H., Li, G. and Sander, L. M.: (1989), *Europhysics Letters* **10**, 7.